CONTROLLED DELIVERY OF BIOACTIVE FACTORS FOR TISSUE REGENERATION

by

Noah Ray Johnson

Bachelor of Science, The Pennsylvania State University, 2010

Submitted to the Graduate Faculty of

Swanson School of Engineering in partial fulfillment

of the requirements for the degree of

Ph.D. in Bioengineering

University of Pittsburgh

2014

UNIVERSITY OF PITTSBURGH

SWANSON SCHOOL OF ENGINEERING

This dissertation was presented

by

Noah Ray Johnson

It was defended on

November 25, 2014

and approved by

William J. Federspiel, Ph.D., Professor, Department of Bioengineering

Patricia A. Hebda, Ph.D., Professor, Departments of Otolaryngology and Pathology

Alan Wells, M.D., DMSc, Professor, Department of Pathology

Dissertation Director: Yadong Wang, Ph.D., Professor, Department of Bioengineering

CONTROLLED DELIVERY OF BIOACTIVE FACTORS FOR TISSUE REGENERATION

Noah Ray Johnson, Ph.D.

University of Pittsburgh, 2014

Growth factors have enormous clinical potential as they orchestrate all repair and regenerative processes in the body. However, their half-lives in vivo when applied alone are very short, on the order of minutes to hours. Therefore, large doses and multiple applications are necessary which is expensive and raises safety concerns considering their potency. To address this issue we developed a coacervate delivery system which protects growth factors from degradation and sustains and localizes their release at the site of injection. By imitating the native signaling environment involving ligands, proteoglycans, and cell receptors our delivery vehicle also enhances growth factor bioactivity, enabling the use of minute and clinically-safe dosages. This dissertation describes the translational potential of this growth factor therapy to address three significant clinical needs: 1) Diabetic wound healing, 2) Cardiac repair following myocardial infarction, 3) Bone regeneration for congenital defects and trauma.

TABLE OF CONTENTS

LIST OF FIGURES

1.0 INTRODUCTION

1.1 REGENERATIVE THERAPIES: INSIGHTS AND CHALLENGES

Regenerative therapies all consist of three components: cells, scaffolds, and signals (**Fig. 1**). Cells can be derived from many different sources and some examples include mesenchymal stem cells (MSCs), embryonic stem cells (ESCs), iPSC (induced pluripotent stem cells), and mature cells such as fibroblasts, myocytes, or osteoblasts, to name a few. We are able to synthesize scaffolds using a plethora of materials, both natural and synthetic. Finally, signals are incoporated in the form of growth factors, nucleic acids, or small molecules, among many others. These are the building blocks we have at our disposal, and in some cases we will combine all three of these components for application; in some cases, however, we can rely on the body to contribute one or more of these, depending on its capability. One thing often overlooked though is the importance of the extracellular matrix (ECM) which integrates these three components, and this will be a critical theme of this dissertation.

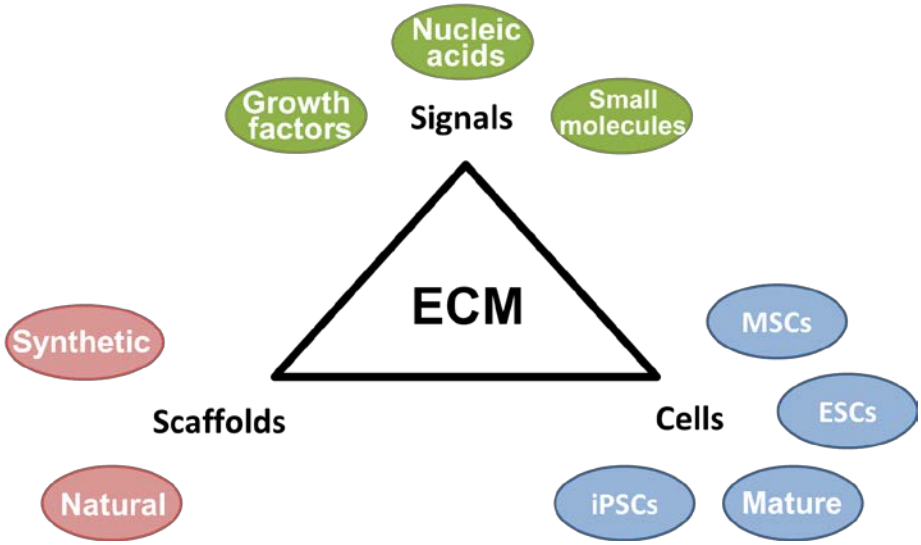

Figure 1. Components of regenerative therapies.

The research presented here focuses on growth factors as the signal components because they are the natural biomolecules that control all repair and regenerative processes in the human body. When injury occurs, growth factors are released from nearby cells and they bind to cell receptors on the same cell or different cells, activate an intracellular cascade, and eventually results in some functional output of the cell such as proliferation, migration, survival, or secretion of more signaling molecules. This occurs on a massive scale with the ultimate goal of repairing or regenerating that injured tissue. In theory, we should able to accelerate this process by strategic application of growth factors; furthermore, for some chronic conditions, we should also be able to stimulate healing that would otherwise never occur naturally.

Growth factors have one key limitation for regenerative therapies; they are highly unstable in the body when applied alone, with half-lives on the order of minutes to hours. This is due to proteolytic degradation and rapid dilution and systemic uptake and removal from where they are applied. Therefore a delivery vehicle is imperative to: 1) Protect the growth factors from

degradation, 2) Localize them to the site where they are needed, and 3) Slowly release them over time thereby extending their bioactivity.

1.2 CONTROLLED PROTEIN DELIVERY

Numerous delivery systems have been developed for growth factors. Naturally-derived materials including collagen and fibrin were proposed for growth factor delivery more than 20 years ago.[1] Since then other materials including polysaccharides such as CMC, chitosan, and alginate and synthetic polymers including poly(lactic-co-glycolic acid) (PLGA) blends and polyethylene glycol (PEG) have also been utilized.[2-4] However, it was quickly realized that simple sponges and gels do not provide adequate exposure time of growth factors to cells within the target tissue. To extend release, groups have employed various cross-linking techniques[5] or directly fused binding sites with affinity for the scaffold onto the growth factors of interest.[6, 7] Microparticles have also become a highly studied group of controlled release vehicles.[8] However, these delivery strategies all overlook the essential role of the extracellular matrix in protection and translocation of growth factors within the tissue. Heparin-based delivery systems advantageously imitate the native signaling environment involving ECM proteoglycans, ligands and cell receptors.[9-12] Heparin has been incorporated into particle [13, 14] and gel-based delivery systems previously,[15-17] however none have proven safe and efficacious to be used clinically. Additionally, these classical delivery systems often require harsh organic solvents or toxic cross-linking agents to prepare which significantly reduce growth factor bioactivity.[18, 19] Circumventing this drawback, we developed a coacervate which could be formed and injected in aqueous solution, fully protecting protein activity.[20] Furthermore, heparin-based

coacervate delivery enhances the bioactivity of released growth factors,[21] significantly reducing the dosage necessary to achieve therapeutic efficacy. This potentiation is owed to imitation of the natural signaling environment, as described above.

1.3 DRUG DELIVERY SYSTEMS FOR WOUND HEALING

Wound healing is a highly coordinated process which relies on precise spatiotemporal presentation of signals to succeed. Significant progress has been made in identifying these signaling molecules and their mechanisms of action in both healthy and diseased states [22-26]. Consequently, there has also been great interest in applying these signals therapeutically to accelerate healing, or enable healing which will otherwise never occur naturally. The current limitation for therapies involving proteins, genes, and small molecule drugs has been a delivery system which can effectively enable their full therapeutic benefit. Namely, a delivery system in the context of wound healing should do the following for its cargo: 1) Maintain its bioactivity through protection from proteolysis in the wound bed, 2) Localize its bioavailability by preventing rapid dilution in wound fluid and systemic uptake and distribution, 3) Facilitate its release or presentation within the wound at a physiologically relevant rate and duration. If these goals are achieved, a successful delivery system will also minimize the dosage and application frequency necessary for efficacy.

Here we aim to highlight recent advances in delivery systems for wound healing applications. As the topic has been thoroughly reviewed several times in the past [27-29], we place particular emphasis on those systems developed in recent years. We identify 5 vehicle types which include hydrogels, scaffolds, particles, complexes, and coacervates (**Fig. 2**) and

provide numerous examples to discuss their advantages and potential drawbacks. In effort to provide adequate depth, we limit our scope to biomaterial-based delivery systems for proteins and small molecule drugs with demonstrated efficacy for skin wound healing but not bone, muscle, or other epithelial defects such as those of the cornea. We include several systems for sustained release of genes and plasmids but not trans-membrane vehicles for gene transfer as these have a separate set of criteria and limitations [30, 31]. We also exclude biomaterial scaffolds for delivering cells in the classical tissue engineering paradigm, as well as therapies which have already received FDA approval as these have been reviewed extensively [32-34].

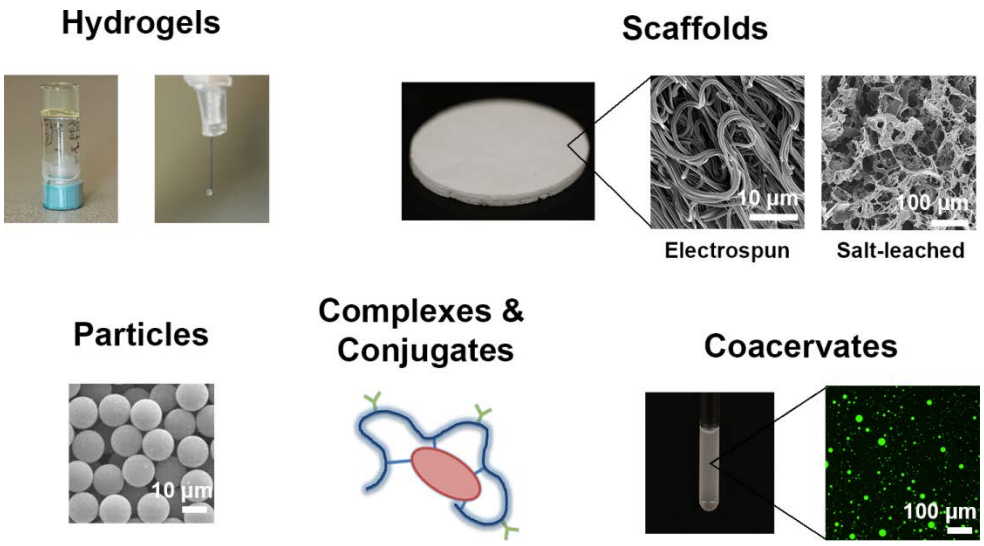

Figure 2. Five types of delivery systems.

1.3.1 Hydrogels

Hydrogels are one of the most highly utilized delivery vehicles. They are versatile, able to form from nearly any water-soluble polymer. They also feature a number of tunable parameters such as porosity, swelling ratio, and cross-link density to offer some control over release rate. A final advantage is that to an extent, they may mimic the mechanical properties of the granulation tissue and maintain a moist wound environment [27, 35].

Hydrogels are often formed from naturally occurring materials because of their abundance and good biocompatibility. Chitosan is one such natural hydrogel commonly employed in controlled release vehicles, appealing in part for its inherent benefits in the wound healing process [36]. Chitosan membranes have been used to cover a wound and slowly release antibiotics such as silver sulfadiazine as they swell. These membranes can be single layer [37] or bilayer [38], and their release may be tuned by variable addition of a second component such as alginate [39]. Chitosan sponges have also been described for controlled release of several different antibiotics to prevent microorganism infection [40-43] and have been evaluated *in vivo* [44]. Chitosan hydrogels delivering fibroblast growth factor-2 (FGF-2) have proved successful in extending the protein's bioactivity and improving wound repair in diabetic mice [45, 46]. Another major advantage of hydrogels for wound healing applications is that they may be designed to polymerize on demand and thereby conform to the defect space. For example, chitosan hydrogels, designed to polymerize by enzyme-catalyzed cross-linking as injected into the defect, and were used to delivery rutin, a flavonol glycoside with healing properties [47]. Similarly, photo-cross-linkable chitosan hydrogels have been developed to polymerize in the wound after 20s of exposure to UV light [48].

Fibrin is another naturally derived material often used in wound healing applications, owed to its involvement in wound hemostasis [49]. In one intriguing study, fibrin was tethered to plasmid hypoxia-inducible factor-1α (HIF-1α) via a peptide linker which resulted in a robust angiogenic response within the wound bed [50]. In another case, fibrin was employed as a carrier for adenovirus-mediated endothelial nitric oxide synthase (eNOS) gene transfer which up-regulated wound nitric oxide (NO) levels [51]. Interestingly, the release mechanism of adenovirus in this approach is through fibrinolysis, initiated by local cells which are then promptly transfected [52]. This therapy was then advanced to co-deliver plasmid eNOS with the Rab18 gene which regulates inflammatory cytokine and proteolytic enzyme secretion. This unique approach targeting angiogenesis, inflammation, and proteolysis was tested in a hyperglycemic ulcer model using rabbits and led to numerous positive healing measures [53]. Growth factors have also been delivered using fibrin gel. For example, delivered keratinocyte growth factor (KGF) successfully stimulated healing in a skin-grafted humanized mouse model [6]. Likewise, fibroblast growth factor-1 (FGF-1) delivered by a modified fibrin gel resulted in angiogenesis and may potentially be used to treat chronic wounds [54, 55].

A common strategy to facilitate delivery vehicle loading is to conjugate heparin or other glycosaminoglycans with affinity to growth factors, cytokines and morphogens [56]. Heparin-conjugated fibrin was developed to sequester heparin-binding factors from platelet-rich plasma (PRP) including vascular endothelial growth factor (VEGF), platelet-derived growth factor (PDGF), and FGF-2, and provide their sustained release. When applied to full-thickness mouse wounds, healing measures such as epithelialization and angiogenesis were enhanced compared with PRP alone or unmodified fibrin [57]. These results demonstrate the importance of protein loading and stabilization in development of delivery systems, particularly those for proteins with

short half-lives. Drawing too from this concept, synthetic extracellular matrix (ECM) films were formed by cross-linking chondroitin sulfate and heparan sulfate and loaded with FGF-2. When applied to large excisional wounds on genetically diabetic *db/db* mice, the films induced dramatically faster wound closure by mimicking native ECM function in the wound bed [58].

In another utilization of natural materials, gelatin-hyaluronate sponges were loaded with epidermal growth factor (EGF) and silver sulfadiazine. In rat excisional wounds, the two molecules acted synergistically to significantly reduce inflammation and increase cell proliferation in the early stages of healing [59]. A hydrogel of pure alginate was developed for the targeted, short term release of SDF-1α protein which improved healing of incisional wounds in pigs [60] and excisional wounds in mice [61]. Finally, combining these materials in a composite matrix of gelatin and oxidized alginate allowed the slow release of a cyclic adenosine monophosphate (cAMP) analog which influenced keratinocyte proliferation and migration, ultimately accelerating re-epithelialization of full-thickness wounds in rats [62, 63].

Synthetic polymers, while lacking the inherent biocompatibility of natural materials, do feature highly controllable and reproducible material properties [64]. Polyethylene glycol (PEG) is one of the most widely utilized hydrophilic polymers for drug delivery and is known for its good biocompatibility [65]. A disulfide cross-linked PEG hydrogel was developed for the sustained release of doxycycline for wound healing. This vehicle was evaluated in an interesting mouse model of chemical warfare wounds. Skin permeation of doxycycline was enhanced by the hydrogel which correlated to better wound healing measures [66]. PEG was also combined with another common synthetic polymer, poly(ε-caprolactone) (PCL), in a hydrogel for sustained release of micelles containing curcumin, a natural drug derived from the turmeric plant which

has healing properties. Curcumin-delivering hydrogels successfully enhanced healing of both incisional and excisional wounds on rats [67].

Although hydrogels have been used successfully in numerous pre-clinical wound models, they do suffer one significant drawback as delivery vehicles. The nature of their formation and composition leads to a large burst release due to partial non-loading of the drug or its rapid efflux from the gel as it swells [68]. This can be particularly dangerous because systemic drug levels may become elevated and lead to unwanted side effects at distal locations. Regranex®, an FDA-approved carboxymethylcellulose hydrogel containing PDGF and indicated for diabetic ulcers, serves as an unfortunate example. A retrospective study found that it led to increased risk of cancer mortality and resulted in a black box warning issued by the FDA in 2008 [69].

1.3.2 Scaffolds

Scaffold is a general term, so in this section we will specifically discuss porous scaffolds which are implanted rather than injected or polymerized *in situ* as is possible with hydrogels. This is usually not a drawback for wound healing applications as most wounds are superficial and relatively easy to access for manipulation. In fact, a scaffold may be the best choice when good mechanical properties or a long degradation time are desired. Their 3-D structure also encourages cell infiltration and enables strategic patterning of stimuli to precisely direct tissue regeneration [35].

Natural materials are often utilized in scaffolds similar as hydrogels, though they need not necessarily be hydrophilic. Collagen is most common and there are well-established methods for reducing its antigenicity and applying cross-links for long-term mechanical stability [70]. In one example, curcumin-incorporated collagen matrices (CICM) were developed to improve full-

thickness wound healing in rats [71]. The same collagen scaffold was used to release Glycyl-histidyl-lysine (GHK), a matrikine with numerous healing properties such as angiogenesis and growth factor activation [72, 73]. Interestingly, the group has also investigated the sustained release of both reactive oxygen species (ROS) [74], and antioxidants [75] into the wound bed. FGF-2 impregnated pure gelatin sheets were also demonstrated to improve the granulation region thickness and collagen density in diabetic rat wounds [76]. These sheets also demonstrated efficacy in several patients with chronic non-healing wounds, however a randomized controlled clinical trial is necessary to conclusively assess the benefit of this therapy. An advanced wound dressing was formed from chitosan cross-linked collagen loaded with FGF-1 and demonstrated accelerated healing of diabetic rat wounds [77]. FGF-2 was also delivered by a collagen-gelatin scaffold and tested in normal wounds [78], and furthermore in a diabetic pressure ulcer model using mice [79]. In another study, the release of platelet lysate from the same scaffold was evaluated and a dose-dependent response of lysate concentration on wound healing outcomes was observed [80]. A “gene-activated” bilayer dermal equivalent (BDE) was constructed from a collagen-chitosan sponge and contained plasmid DNA encoding for VEGF complexed with a non-viral gene delivery vector. The BDE enhanced vessel density and overall tensile strength of newly formed dermal tissue in both full-thickness excisional wounds [81] and burn wounds [82] in pigs.

Drug loading of scaffolds is often by adsorption or entrapment and is therefore poor for some non-ideal drug-scaffold combinations. One method of improving loading efficiency is by modifying the therapeutic protein itself. In one instance, VEGF was modified with a collagen-binding domain which enhanced its affinity to the endogenous ECM and retention in the granulation tissue 7 days after application to rat wounds [83]. The fusion protein was then loaded

into a collagen scaffold with enhanced efficiency and greatly improved vascularization in diabetic rats, also reducing VEGF levels in the serum compared to the native protein [84]. A similar approach was used to modify neuronal growth factor (NGF) and demonstrated accelerated re-epithelialization in a rabbit ischemic ulcer model [85].

Another natural material, hyaluronic acid (HA), was used to form sponges for the sustained release of EGF and arginine, which accelerated epithelialization of diabetic rat wounds by inducing moderate inflammation in the early stage of healing [86]. Similar sponges also containing collagen were found to induce better neovascularization in a genetically type 2 diabetic mouse model compared to a commercial artificial skin [87].

Scaffolds developed using synthetic polymers often employ the fabrication technique of electrospinning. Electrospun scaffolds offer advantages of high surface area and tunable fiber diameter which may closely match those of native ECM proteins, promoting cell adhesion [88]. Core-sheath type electrospun poly(ethylene glycol)-poly(D,L-lactide) (PELA) nanofiber mats containing FGF-2 were implanted into diabetic rat wounds where they enhanced angiogenesis after 2 weeks and the scaffolds degraded completely within 4 weeks [89]. The large surface area and porosity of electrospun scaffolds allows for rapid hydrolytic degradation of polymer fibers. Similar scaffolds were also developed to provide controlled release of plasmid FGF-2. When implanted into skin defects of diabetic rats they led to improvements in numerous healing measures [90]. PEG/PCL block copolymer nanofibers have also been synthesized with chemically-immobilized EGF on their surface [91]. These scaffolds had some moderate effects on the healing of normal mouse wounds, but the results were greatly enhanced by the addition of FGF-2 within the core of co-axial fibers [92]. Likewise, curcumin has also been delivered using

electrospun nanofiber mats of PEG/PCL or PCL alone, which were shown to accelerate wound healing of normal rats and diabetic mice, respectively [93, 94].

Natural polymers are often difficult to electrospin on their own and are therefore blended with synthetic polymers. One group investigated chitosan and poly(ethylene oxide) (PEO) co-electrospun with PRP as a growth factor source. The bioactivity of the proteins was demonstrated to withstand the electrospinning process with *in vitro* assays, however this therapy still requires *in vivo* validation [95]. In at least one report, chitosan scaffolds providing sustained release of EGF showed no significant benefit over unloaded scaffolds towards the healing of excisional porcine wounds [96]. These data highlight the importance of *in vivo* testing, as *in vitro* assays cannot fully recapitulate the complex environment of a wound.

Not all scaffolds are formed by electrospinning. Modified chitosan was also used to synthesize porous foam dressings for release of neurotensin (NT) to modulate the inflammatory stage in diabetic wounds. The chitosan scaffolds delivering NT increased early wound closure dramatically compared to unloaded scaffolds by mitigating the acute inflammatory response and increasing collagen deposition by dermal fibroblasts [97].

1.3.3 Particles

Nano- and microparticles are another highly studied type of drug delivery system which hold certain advantages over hydrogels and scaffolds. With respect to wound healing applications, particles may by injected by fine-gauge needle into the healthy tissue surrounding the wound so as not to complicate healing within the wound bed. They may also be tuned through numerous parameters to have complex release profiles unobtainable with gels and scaffolds [98, 99].

Poly(lactic-co-glycolic acid) (PLGA) is the most common polymer used to synthesize particles for controlled delivery. One rationale is that the lactic acid produced as the PLGA degrades may actively participate in the healing process, stimulating collagen synthesis and angiogenesis [100]. PLGA nanoparticles were developed to protect the activity of curcumin and release it over 8 days. When evaluated in full-thickness splinted excisional wounds in mice the combined effect of lactate and curucmin reduced the inflammatory response and enhanced angiogenesis and granulation tissue formation [101]. Similar nanoparticles were also used to release EGF albeit much more quickly, lasting only a day. Still, when applied to excisional wounds in diabetic rats the therapy induced the greatest number of proliferating cells and slightly accelerated wound closure compared to free EGF solution [102].

Particles have also been developed to deliver genes or plasmids. One example are biodegradable poly(β-amino esters) (PBAE) nanoparticles used to deliver plasmid Sonic hedgehog, a morphogen known to play multiple roles in tissue regeneration. After intradermal injection of the particles at the periphery of mouse wounds, upregulation of multiple growth factors and greater neovascularization in the wounds was observed [103].

In a unique and interesting approach, nanoparticles of a silica, PEG, and chitosan composite were used to provide slow and sustained release of NO to wounds. NO is known to have both immunoregulatory and wound healing properties. The nanoparticles applied topically accelerated healing of both infected and uninfected mouse wounds [104, 105]. Furthermore they were directly compared to the common NO-donor, diethylenetriamine (DETA NONOate) and showed superior results in a mouse wound model of diabetes combined with immunodeficiency, which has significant clinical relevance [106].

Nanoparticles need not necessarily be polymeric; in fact, lipids hold an advantage of rapid self-assembly without requiring organic solvents. One group developed two types, solid lipid nanoparticles (SLNs) and nanostructured lipid carriers (NLCs) for delivery of EGF. The loading efficiency of NLCs was greater than that of SLNs, as is common with encapsulating cargo within a shell versus entrapping it in a matrix. Both types of lipid particles delivering EGF significantly accelerated healing of full-thickness wounds in *db/db* mice, however four applications were necessary, possibly due to the inability of the vehicle to adequately sustain release [107].

Particles are also easily incorporated within other carrier systems to augment their functionality. They may be used to extend release if the inherent rate is too quick, or to provide biphasic release kinetics. For example, a polyurethane scaffold embedded with gelatin-coated PLGA microparticles, each releasing PDGF, produced a quick burst followed by slow prolonged release [14]. Likewise, distinct release kinetics for multiple factors will be very important for certain applications [108]. Nanofiber composite scaffolds of chitosan and PEO were synthesized for fast release of VEGF and combined with nanoparticles providing slow sustained release of PDGF. Dual release resulted in fast closure of full-thickness wounds in rats, driven by an enhanced angiogenic response [109].

In one notably elaborate delivery vehicle, VEGF and PDGF were placed in gelatin nanoparticles and combined with FGF-2 and EGF embedded in electrospun collagen and HA nanofibers for sustained release of 4 factors at once. Accelerated wound closure, increased collagen deposition and improved angiogenesis were all observed when the scaffolds were implanted in excisional wounds on diabetic rats [110]. Complex scaffolds with their own functionality have also been developed to compliment the delivery of a single factor. For

example, an inner gelatin hydrogel layer for maintenance of a moist wound environment and containing FGF-2 microspheres was layered below an outer polyurethane membrane to protect the wound. This bi-layer scaffold proved effective at healing porcine full-thickness wounds [111].

Gelatin microparticles delivering FGF-2 suspended in a gelatin hydrogel showed good results in a porcine pressure-induced decubiticus ulcer model [112]. In another approach, gelatin microspheres were conjugated to a catechol-type protease inhibitor, loaded with doxycycline, and incorporated into a collagen dressing [113]. Their ability to reduce MMP levels in the wound bed and prevent infection was evaluated in a bacteria-challenged excisional wound model in rats [114]. Finally, gelatin microparticles delivering FGF-2 were dispersed within a collagen sponge and enhanced angiogenesis and cell proliferation in a mouse model of pressure ulcers [115].

One group loaded chitosan microparticles with EGF and VEGF and suspended them in a dextran hydrogel for application to burn wounds. The therapy did show a beneficial effect in a rat burn wound model, however weekly applications were necessary, indicating that the release duration was too short [116]. Another group suspended PLGA nanoparticles delivering VEGF and FGF-2 in a composite hydrogel and applied it to full-thickness wounds on diabetic mice. This combined therapy led to improved wound closure compared to control scaffolds but not compared to the scaffold with free growth factors [117]. These results highlight some potential drawbacks of particulate delivery systems. Most require organic solvents which can reduce the bioactivity of fragile protein drugs significantly. Additionally, constant release rate is difficult to achieve because they inherently follow first-order kinetics due to changing surface area as the particles degrade [98].

1.3.4 Complexes and Conjugates

A fourth type of delivery system comprises complexes and conjugates. Conjugates are typically formed by chemical bonds while complexes are typically formed by physical interactions. Both approaches seek to sequester soluble drugs in order to stabilize and extend their half-life or to provide targeting and facilitate their interactions with cell receptors. In one of the simplest examples of conjugation, PEG was attached to FGF-1 to improve its thermal and structural stability *in vivo*. In diabetic rat wounds, PEGylated FGF-1 led to complete wound closure 4 days faster than free FGF-1 and 7 days faster than control [118]. Complexes may also be used to improve skin permeation, of interest for wounds which have formed a protective scab or to treat deep tissue injury preceding a pressure ulcer. A low molecular weight version of protamine, a cation-rich nuclear protein, was developed to complex with the N-terminus of EGF. Protamine-EGF complexes showed 11-fold greater transdermal penetration than free EGF and demonstrated efficacy in healing full-thickness wounds on both normal and diabetic mice [119] and in a mouse burn wound model [120].

Another very interesting approach involves engineering ECM mimetics, considering its significance in orchestrating the regenerative process [56, 121, 122]. One such approach is a synthetic peptide fragment of fibronectin containing its growth factor binding domain for protein loading, an integrin-binding domain to localize the complex to cells, and a factor XIIIa sequence for cross-linking to form a matrix to facilitate injection. The multi-functional recombinant fibronectin was applied for co-delivery of VEGF and PDGF to diabetic mouse wounds, where it induced angiogenesis and accelerated wound closure [123]. The same group used a similar approach to deliver the cytokine CXCL11 which, synergistic with fibronectin, promoted diabetic wound healing in *db/db* mice [124]. Along similar lines, vitronectin complexes with insulin-like

growth factors (IGFs) can enhance keratinocyte migration and protein synthesis [125], and similar effects were observed with EGF and FGF-2 [126]. In their first pre-clinical evaluation, vitronectin complexes of IGFs and EGF accelerated healing of partial-thickness burn wounds in pigs, although this approach did require multiple administrations per week [127]. To improve the clinical usefulness, HA was then added as a carrier system for vitronectin:GF complexes [128]. In a clinical pilot study, this therapy demonstrated convincing efficacy at re-epithelializing venous leg ulcers, and also showed promise for treating other types of chronic wounds [129]. These results provide strong evidence for consideration of the role of the ECM in growth factor signal transduction when designing controlled delivery vehicles.

Another group designed polymer-growth factor conjugates using a "Polymer Masking-UnMasking-Protein Therapy (PUMPT)". They demonstrated that succinoylated dextrin conjugated to EGF can stabilize the protein until the polymer degrades at the target site and "unmasks" its bioactivity [130, 131]. The group went on to evaluate dextrin-EGF in full-thickness diabetic mouse wounds and the therapy had marked success [132]. In another unique approach *S*-nitrosothiols (RNSOs) were grafted onto a polymer backbone and then interpolymer complexes were created to form a cross-linked polymer network. This vehicle provided sustained release of NO for at least 10 days and accelerated healing of excisional wounds in diabetic rats, although the mechanistic benefits were not explored [133].

The specificity of complexes and conjugates may be seen as a disadvantage because many cannot be used as a platform for delivery of different types of molecules. Because they are designed with a specific target in mind, the synthesis and optimization process can become time-consuming. On the other hand, a specialized delivery vehicle will often lead to better outcomes compared to delivery with a generalized release platform.

1.3.5 Coacervates

Coacervates are an interesting new class of drug delivery vehicles developed only recently for controlled release of proteins and small molecule drugs. Coacervates are nanometer-sized liquid droplets, held together and apart from their environment by hydrophobic forces [134]. As delivery vehicles, they feature rapid preparation by self-assembly not requiring organic solvents, and high loading capacity [135]. Preparation in aqueous solution is convenient and circumvents the risk of protein denaturation or residual organic solvents in conventional particle synthesis. Coacervates are also distinct from polymeric particles in their mechanical properties; they are soft and deformable which is particularly amenable to a wound environment where they may reside without impeding the massive influx of cells. This deformable nature allows for quick adsorption and spreading to coat polymeric scaffolds and provide drug release for tissue engineering applications [136]. Although they are a relatively young technology with just a decade's worth of experimental validation, the advantages several coacervate systems have shown over conventional delivery methods bears much promise for their utility in the future [137].

One well-described coacervate system is elastin-like peptides (ELPs). These are recombinant proteins which resemble the hydrophobic regions of tropoelastin which undergo spontaneous coacervation above a tunable transition temperature [138]. Fusion proteins containing ELPs and KGF were developed and self-assembled into coacervate particles at body temperature. A chronic wound model was performed using an insulin-resistant diabetic mouse strain, and the fusion peptide led to markedly enhanced granulation and re-epithelialization [139].

A second coacervate system is a polycation:heparin complex which was developed specifically for the controlled delivery of heparin-binding growth factors [21, 140]. The growth factor is pre-bound to heparin, then a synthetic polycation is added which instantly forms liquid coacervate droplets by charge-based complexation. Within the coacervate the growth factor is protected from the proteolytic wound environment and its bioactivity upon release is enhanced by heparan sulfate preotoglycan-like interactions. This coacervate was utilized to sustain the release of heparin-binding epidermal growth factor (HB-EGF) with near zero-order release kinetics for at least 10 days. A single application of the HB-EGF coacervate to full-thickness excisional mouse wounds accelerated wound closure by enhancing wound granulation, re-epithelialization, keratinocyte proliferation, and angiogenesis [141].

One drawback of coacervates is their relative instability in the body. They are held together by relatively weak interactions which may dissociate by large environmental changes in pH or ionic strength. However, these are typically stable within a particular tissue in the body. On the other hand, this responsiveness may also be used to build in stimuli-responsive specificity.

1.3.6 Future goals

A wide variety of biomaterial-based delivery systems exist for proteins, genes, and small molecule drugs with wound healing applications. Hydrogels, scaffolds, particles, complexes, and coacervates have each demonstrated success in numerous *in vivo* models and each may be optimal for a particular application or circumstance. However, wound healing is an extremely complex process and it is important to understand the etiology of each wound type and develop similarly complex delivery systems for individualized treatment. Towards this goal, it will be

necessary to combine different types of biomaterials to develop composite systems capable of delivering multiple factors with precise release kinetics.

1.4 THE POTENTIAL OF COACERVATE SYSTEMS IN DRUG DELIVERY

A complex coacervate is a liquid-liquid separation formed by electrostatic interactions between two polymers of opposite charge. Coacervates exist as spherical liquid droplets, often on the nanometer or micron scale in diameter, resembling an emulsion except that they do not necessarily contain stabilizing molecules such as surfactants. Coacervates have been investigated since the mid-20th century mostly within the context of food science research [134]. With the advancement in drug delivery, the use of coacervates as controlled delivery vehicles has started only recently. One particularly attractive feature of coacervates for drug delivery is their high loading capacity and the fact that they form by self-assembly in an aqueous medium [135]. Once encapsulated within the coacervate phase, labile proteins or drugs are separated and protected from the surrounding environment, thereby preserving their bioactivity. Compared to other common vehicles such as hydrogels and microparticles, coacervates form quickly and do not require organic solvents which could reduce protein drug retention and bioactivity. Finally, their size often enables coacervates to be applied via fine gauge needles, important for minimizing damage associated with injection.

Several themes have become apparent among complex coacervates developed for drug delivery. One major theme is the incorporation of native extracellular matrix (ECM) proteins such as heparin, elastin, hyaluronic acid, and chondroitin sulfate. These approaches strategically employ the body's own charged molecules as one or both components of the coacervate, most

commonly the polyanion. Secondly is the slow and sustained manner of release of loaded cargos, avoiding burst release experienced with many other types of delivery systems. Thirdly, due to their reliance on charge-based interactions coacervates exist in dynamic equilibrium with their environment. They are therefore susceptible to disaggregation in response to increasing ionic concentrations of their environment which interfere with these interactions. The consequences of these characteristics are well understood and can therefore be anticipated and even exploited to engineer coacervate drug carriers with precise design requirements.

Below we exhibit several coacervate systems which have been developed for the delivery of small molecule drugs and proteins. Despite their apparent similarity with coacervate, charge-based polyplexes for nucleic acid delivery [142] and lipid-based emulsion delivery systems [143] are thoroughly reviewed elsewhere and will therefore not be described here.

1.4.1 Elastin-like peptides

Elastin-like peptides (ELPs) were developed in the late 20th century [144], then further explored as drug delivery vehicles more recently [138]. ELPs are recombinant proteins designed to mimic the hydrophobic regions of tropoelastin. They consist of simple pentapeptide repeats, most commonly VPGXG, where X represents any amino acid except proline, termed the "guest residue". ELPs exhibit an inverse temperature phase transition, aggregating to form a coacervate above their transition temperature (T_t) which is tunable based on the guest residue and ELP chain length [145].

Drug delivery using ELPs has been focused on targeting and abolition of solid tumors [146]. One approach is local injection of ELPs with a T_t between room and body temperature, enabling *in situ* coacervation to form drug depots which slowly release their cargo. After intra-

tumoral injection of radionuclide-conjugated ELPs, tumor regression was observed in more than two-thirds of the mice treated and the therapeutic effects lasted for at least 2 months [147]. A second approach is systemic injection of ELPs with a T_t between body temperature and 42 ˚C in combination with mild hyperthermia at the target tumor site. Local heating of the tumor, achieved clinically by methods such as ultrasound, increases extravasation of the ELPs and induces *in situ* coacervation. This method resulted in two-fold higher accumulation of doxorubicin-conjugated ELPs at the tumor site compared to non-heated tumors and even greater accumulation if multiple thermal cycles were applied [148, 149]. ELP coacervate has also demonstrated usefulness in tissue engineering applications as a viscous medium for delivery and differentiation of chondrocytes or progenitor cells [150, 151].

1.4.2 Carboxymethyl chitosan-based coacervates

Carboxymethylation increases the water solubility of chitosan and the resulting carboxymethyl chitosan (CMC) has become a commonly studied polymer with a variety of applications, including drug delivery. The polyanionic nature of CMC enables its coacervation with positively-charged molecules via electrostatic interactions. This method was employed using unmodified chitosan as the polycation to deliver doxorubicin in an oral formulation that slowly released it within the GI tract, significantly increasing its intestinal absorption and bioavailability in the blood [152]. The group went on to encapsulate the coacervate beads within sodium alginate shells for further stabilization and protection in the low pH gastric environment [153].

1.4.3 Mussel adhesive proteins

Another common coacervate system exploits the unique properties of charged proteins secreted by marine organisms such as tubeworms and mussels. These polyelectrolyte proteins undergo complex coacervation to produce a robust underwater adhesive which facilitates anchoring to a surface or cementing together sand and shell fragments. Recombinant mimics of these mussel adhesive proteins (MAPs) have been characterized and evaluated for numerous applications [154]. Of particular importance for drug delivery, coacervation of recombinant hybrid MAPs with hyaluronic acid (HA) creates micron-sized droplets that are stable for at least 8 days in phosphate-buffered saline [155]. Recombinant MAPs also retain their adhesive qualities after coacervation with HA, allowing their use as a device coating or easy integration into tissue engineered scaffolds [156]. Although these systems have yet to be used in a drug delivery setting, these explorations are anticipated in the near future.

1.4.4 The future of coacervate delivery vehicles

Compared with other drug delivery vehicles including micro- and nano-particles, liposomes, hydrogels and dendrimers, coacervate is a very recent development, with just over a decade of history. Despite the short history, coacervate delivery vehicle as a class has already shown that: (1) it forms rapidly in water by self-assembly, (2) it can substantially improve the bioactivity of proteins *in vitro* and *in vivo*, (3) it readily coats a biomaterial surface either alone or combined with other molecules, (4) it can increase the efficacy of cell therapy, and (5) targeting is feasible. Self-assembly in water and affinity to proteins that significantly reduce protein denaturation and burst release make coacervate a rational choice for controlled release of proteins and peptides.

Ionic coacervates can be less stable compared with conventional drug delivery vehicles in biological fluids because of their ionic nature, and this needs to be addressed for a systemic delivery route when the coacervate will be carried by blood. To this end, much can be borrowed from strategies for stabilization of liposomes. Furthermore, active targeting of a specific tissue or pathology (e.g. cancer, infarction, or inflammation) will greatly expand the utility of this new class of drug delivery vehicles. Other future growth areas are "control" over release kinetics including stimulus-responsive release and external guidance of the coacervate post-injection. In all, we anticipate that coacervate will evolve into a versatile tool for controlled drug delivery in the near future and a likely catalyst for the "big bang" of this field will be a successful clinical translation of any coacervate vehicle.

1.5 A POLYCATION:HEPARIN COACERVATE DELIVERY VEHICLE

Our lab previously developed a coacervate delivery system which utilizes heparin to first bind one or more heparin-binding proteins, including numerous growth factors, cytokines, and morphogens [157]. A synthetic polycation containing arginine [158] as the positive charge-bearer is then introduced to interact with the highly-sulfated heparin by polyvalent charge attraction. A complex coacervate instantly forms with droplet sizes range from 0.1-10 μm in diameter, dependent on the loaded protein and the ionic environment. The strong, specific interaction between heparin and heparin-binding proteins results in very high loading efficiency of this coacervate, often greater than 99%. The release rate is influenced by multiple factors, including the heparin-binding affinity of the protein of interest, the net charge of the coacervate, and the polycation molecular weight, charge density, and biodegradation rate [21, 159].

One significant advantage of this coacervate system is owed to pre-conjugation of the growth factors to heparin which potentiates their bioactivities by mimicking the way that ECM proteoglycans present these factors to cell receptors [21, 159]. In one instance, a single injection of heparin-based coacervate delivering fibroblast growth factor-2 (FGF-2) induced stable angiogenesis subcutaneously [20]; a similar benefit was observed after injection into the infarcted myocardium which resulted in improved cardiac function [160]. Another advantage of this controlled release system is its simple incorporation into tissue engineering scaffolds by adsorption. This technique was recently employed to recruit progenitor cells into a porous polymer graft by slowly releasing the stem cell trafficking chemokine, stromal cell-derived factor-1α (SDF-1 α) [136].

1.6 SPECIFIC AIMS

The central hypothesis of this research is that controlled growth factor delivery with a polycation:heparin coacervate can stimulate tissue regeneration in the clinically-relevant context of skin wound healing, cardiac repair, and bone regeneration. Our preliminary results and the current literature on growth factor signaling pathways supports the use of the following growth factors for respective indications: Heparin-binding EGF-like growth factor (HB-EGF) for skin wound healing [141, 161, 162], Sonic hedgehog (Shh) morphogen for cardiac repair [163-166], and bone morphogenetic protein-2 (BMP-2) for stimulation of muscle-derived stem cells (MDSCs) to regenerate bone defects [167-169]. Towards our central hypothesis, I tested the efficacy of coacervate-based controlled delivery of each of these factors in a clinically-relevant animal model, outlined in the following four Specific Aims:

Specific Aim 1: **Develop a coacervate delivery vehicle with tunable release kinetics.** A lysine-based polycation was designed to interact with heparin and self-assemble to a coacervate structure. The cytocompatibility of the polycation was evaluated and its loading efficiency and tunable release rate described. Finally, it was demonstrated that the coacervate may be adsorbed onto polymeric scaffolds to provide integration of controlled release with tissue engineering scaffolds.

Specific Aim 2: **Evaluate the efficacy of controlled delivery of HB-EGF to accelerate dermal wound healing.** Growth factor therapy has the potential to accelerate the healing of acute wounds such as surgical incisions, and chronic wounds such as diabetic ulcers. The stimulatory effects of HB-EGF coacervate on the proliferation and migration processes of human dermal cells were first evaluated using *in vitro* assays. Full-thickness skin wounds were then created on both normal and genetically-diabetic mice to test the *in vivo* efficacy of this therapy and elucidate the mechanisms of improved healing.

Specific Aim 3: **Investigate the controlled delivery of Shh morphogen to promote cardiac repair following myocardial infarction.** Heart failure resulting from myocardial infarction is a leading cause of death and morbidity worldwide [170]. Shh morphogen activates multiple pro-regenerative processes, which were first studied *in vitro* using cardiac myocytes and fibroblasts. The Shh coacervate was then loaded into a polyethylene glycol (PEG) hydrogel to prevent its leakage following injection into the pulsating heart muscle. Myocardial infarction was induced in rats by ligation of the coronary artery and the hydrogel was injected within the ischemic zone and evaluated over 4 weeks.

Specific Aim 4: **Assess the contribution of controlled delivery of BMP-2 towards improving MDSC therapy for bone defect regeneration.** Congenital or trauma-induced bone

injuries currently lack a good clinical solution [171]. We utilize BMP-2 delivered by the coacervate to stimulate the osteogenic differentiation of MDSCs *in situ*. We first tested the *in vitro* cytotoxicity and bioactivity of the BMP2 coacervate on MDSCs. Next we elucidated the potential of this co-therapy to form ectopic bone by injection into the mouse quadriceps muscle pocket where the signals to produce bone are absent. Finally, to evaluate the translational potential of this therapy we used human MDSCs in a critical-sized cranial defect model using immunodeficient mice and directly compared to a gene therapy approach.

2.0 DEVELOPMENT OF A POLYCATION:HEPARIN VEHICLE WITH TUNABLE RELEASE KINETICS

Polycations have high potential as carriers of proteins and genetic material. However, poor control over release rate and safety issues currently limit their use as delivery vehicles. Here we introduce a new lysine-based polycation, poly(ethylene lysinylaspartate diglyceride) (PELD) which exhibits high cytocompatibility. PELD self-assembles with the biological polyanion heparin into a coacervate that incorporates proteins with high loading efficiency. Coacervates of varying surface charge were obtained by simple alteration of the PELD:heparin ratio and resulted in diverse release profiles of the model protein bovine serum albumin. Therefore, coacervate charge represents a direct means of control over release rate and duration. The PELD coacervate also rapidly adsorbed onto a porous polymeric scaffold, demonstrating potential use in tissue engineering applications. This coacervate represents a safe and tunable protein delivery system for biomedical applications.

2.1 INTRODUCTION

Polycations have high potential as carriers of proteins and genetic material. Chitosan and polyethylenimine (PEI) are two polycations commonly used in biomedical applications including non-viral gene delivery [172-175], vaccine administration [176, 177], and delivery of peptides

[178, 179]. However, safety risks associated with cytotoxicity and the accumulation of nanoparticles following delivery seriously limit their potential [180, 181]. Poly(L-lysine) (PLL) has also been widely investigated as a delivery vehicle for proteins and DNA [182-185], however PLL has similar biocompatibility issues as PEI [186, 187]. A synthetic polycation with good biocompatibility and controllable release rate would be highly beneficial for biomedical applications involving protein or gene therapy.

We have previously reported the synthesis of an arginine-based polycation, poly(ethylene argininylaspartate diglyceride) (PEAD), designed to complex with heparin to form a delivery matrix for heparin-binding growth factors [158]. PEAD:heparin self-assembles to form a coacervate, an assortment of organic molecules held together by polyvalent charge attraction and separated from the aqueous phase. We have demonstrated the use of this coacervate to deliver several factors for stimulating angiogenesis [20], accelerating cutaneous wound-healing [141], and improving heart function post-myocardial infarction [160, 166]. In all cases the coacervate showed high loading efficiency, protection from degradation, sustained release over time, and enhanced bioactivity compared to the growth factor in free-form. Having demonstrated that the coacervate satisfies the necessary functions of a delivery vehicle, we now address controllability of release rate by modification of the polycation and the coacervate composition.

The polyvalent and ionic nature of the coacervate makes modification of the charge density of the polycation one of the simplest ways to control release rate. Adjusting the polycation:heparin ratio in the coacervate is another simple way. The polycation and growth factor compete for ionic interaction with heparin; thus a coacervate with greater polycation content will compete more, resulting in faster growth factor release, while lower polycation content will slow release. We first attempted to control growth factor release using this approach

with PEAD, however the charge density of this polycation was too large. A very small decrease in the PEAD:heparin mass ratio led to such a large drop in the overall coacervate charge that the growth factor did not release (**Fig. 3**). Therefore our rationale for the development of a new polycation was that a polycation of slightly weaker charge density may allow for improved control over release rate.

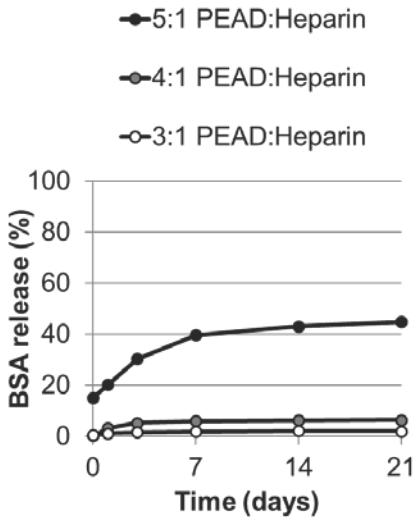

Figure 3. Effect of PEAD:heparin on BSA release. The PEAD:heparin mass ratio was varied and the release of bovine serum albumin (BSA) tracked over 21 days.

Here we report a new polycation, poly(ethylene lysinylaspartate diglyceride) (PELD), with lysine as the source of positive charge instead of arginine. PEAD has high biocompatibility [158], and here we demonstrate that the same design principle applies to lysine, thus PELD also

has excellent biocompatibility. We describe the synthesis and characterization of PELD and its usefulness for controlled release.

2.2 MATERIALS AND METHODS

2.2.1 Materials

Ethylene glycol diglycidyl ether (EGDE) and trifluoroacetic acid (TFA) (TCI America, Portland, OR), t-BOC aspartic acid (BOC-Asp-OH) and t-BOC lysine (BOC-Lys) (Bachem, Torrence, CA), dimethylforamide (DMF), dichloromethane (DCM) and tetra-*n*-butylammonium bromide (TBAB) (Acros Organics, Geel, Belgium), dicyclohexylcarbodiimide (DCC) and *N*-hydroxysuccinimide (NHS) (Alfa Aesar, Ward Hill, MA), 4-dimethylaminopyridine (DMAP) (Avocado Research Chemicals, Lancaster, UK), and polyethleneimine (PEI; MW=50-100 kDa) (MP Biomedicals, Santa Ana, CA) were used as received. Heparin Sodium USP (MW=16 kDa; Scientific Protein Labs, Waunakee, WI), fluorescein (Aldrich Chemical Co, Milwaukee, WI), bovine serum albumin (BSA) (Millipore, Billerica, MA), and poly(D,L-lactide-co-glycolide) 50:50 (PLGA) (Lakeshore Biomaterials, Birmingham, AL) were also used as received.

2.2.2 Synthesis of PELD

The intermediate, poly(ethylene aspartate diglyceride) (PED) was synthesized as previously described [158]. Briefly, EGDE (1.00 g) was combined with BOC-Asp-OH (1.34 g) and TBAB (5 mg) and dissolved in 0.6 ml DMF. The mixture was maintained at 120°C under N_2 for 20 m in

a microwave synthesizer (Biotage, Uppsala, Sweden). DMF was evaporated under reduced pressure and TBAB was removed by multiple precipitations in diethyl ether. t-BOC was removed by stirring product in 4:1 DCM:TFA for 2 h. t-BOC lysine was conjugated to PED by DCC/NHS coupling. Briefly, BOC-Lys (0.692 g), NHS (0.323 g), DCC (0.753 g), and DMAP (5 mg) were dissolved in 5 ml DMF. PED (0.864 g) was dissolved in 5 ml DMF in a separate vial. The two vials were then combined and stirred under N_2 for 24 h. An insoluble dicyclohexylurea byproduct formed and was removed by filtration at 0.22 μm. Finally, t-BOC was removed by stirring in pure TFA for 2 h and the product was purified by multiple precipitations in diethyl ether and then ethyl acetate.

2.2.3 Characterization of PELD

^{1}H NMR was performed with a Biospin Avance NMR spectrometer (Bruker, Billerica, MA) using deuterium oxide (D_2O) solvent. The Fourier transformed infrared (FTIR) spectrum was recorded using a Nicolet IR-100 spectrometer (Thermo, Waltham, MA). Differential scanning calorimetry (DSC) was performed under nitrogen gas at a heating rate of 10°C/min using a Q200 DSC (TA Instruments, New Castle, DE). Glass transition temperature (T_g) was determined using Universal Analysis 2000 software (TA Instruments) as the middle of the glass transition. Gel permeation chromatography (GPC) was performed on a Viscotek VE2001 system equipped with a 270 Dual Detector (differential refractive index and right angle light scattering) (Malvern Instruments, Westborough, MA). Two GRAM columns of 30 Å and 1,000 Å porosities (PSS, Warwick, RI) and dimethylacetamide containing 3 g/L lithium bromide and 6 ml/L acetic acid were used as the stationary and mobile phases, respectively, and results were compared to polystyrene standards for calibration.

2.2.4 Preparation of polycation:heparin coacervates

PEAD, PELD and heparin were each dissolved in 0.9 % saline and 0.22 μm filter-sterilized. Addition of either polycation to heparin immediately induced self-assembly of the coacervate, causing the complex to phase separate, visible as a turbid solution.

2.2.5 Zeta potential and dynamic light scattering (DLS) measurements

PELD and heparin were dissolved in DI water at 10 mg/ml and 1 mg/ml, respectively, then combined at PELD:heparin mass ratios of 2.5, 5, 7.5, 10, 12.5, and 15. Each coacervate solution was diluted to a 1 ml total volume with DI water. Zeta potential and particle size (hydrodynamic diameter) were both measured using a Zetasizer Nano ZS (Malvern, Westborough, MA).10-20 readings were taken for each mass ratio and averaged.

2.2.6 Fluorescent imaging of PELD coacervates

PELD and heparin were dissolved in DI water at 10 mg/ml and fluorescein at 10 μg/ml. 10 μl fluorescein was mixed with heparin first and then PELD was added to form coacervates with PELD:heparin mass ratios of 5, 10, and 15. The total mass of coacervate ($m_{PELD}+m_{heparin}$) was 1 mg for each, prepared in 0.1 ml water. The coacervates were added to a 96-well plate and imaged immediately using a Nikon Eclipse Ti fluorescent microscope (Nikon Instruments, Melville, NY).

2.2.7 Cytotoxicity assay

PEAD was synthesized as previously described [158]. $5x10^4$ NIH 3T3 fibroblasts were seeded per well in a 96-well plate and cultured for 12 h at 37°C/ 5% CO_2 in DMEM containing 10% FBS and 1% penicillin/streptomycin. Media was then removed and culture media containing PEAD, PELD or PEI at various concentrations (10, 1, 0.1, 0.01 mg/ml) was added to 4 wells per group. After 24 h cells were washed once with DPBS and cell viability was assessed using Live/Dead Assay (Molecular Probes, Eugene, OR) following manufacturer's instructions. Results were normalized and compared to a control group which was not exposed to a polycation.

2.2.8 BSA release assay

PELD and heparin were each dissolved in 0.9% saline at 10 mg/ml. Heparin was initially combined with 500 μg BSA, then PELD was added to form mass ratios of 6, 8, and 10, corresponding to zeta potentials of approximately -10, -5, and 0 mV, respectively. Tubes were stored at 37°C under shaking conditions and after 0, 1, 3, 7, 14, and 21 days, tubes were centrifuged at 12,000 x g for 5 min and the supernatant removed and frozen at -20C. After all timepoints were collected, BSA concentration was determined using the Pierce 660 nm Protein Assay (Thermo). In order to account for protein content of the polycations and heparin in the release fractions, results were normalized to an assay performed identically but without BSA.

2.2.9 Coacervate adsorption to polymer scaffolds

Porous PLGA scaffolds prepared by salt-leaching technique were synthesized as previously described [188]. The scaffolds were 1 mm thick and 5 mm in diameter with a 75-150 μm pore size. PELD and heparin were dissolved in deionized water at 5 mg/ml and combined at a 10:1 PELD:heparin mass ratio for maximal turbidity at charge neutrality. 1.2 ml coacervate was added to a glass vial and stirred to prevent settling of the coacervate by gravity. 50 μl coacervate was removed to a cuvette and optical density was read using a spectrophotometer (Biotek, Winooski, VT). PLGA scaffolds were then added to three separate vials and the coacervate was sampled and optical density read in similar fashion every 5 min. Three vials that did not receive any scaffold were used as the control. Digital images of the PELD coacervate-coated PLGA scaffold were taken at the endpoint, next to a bare PLGA scaffold.

2.2.10 Scanning electron microscopy

PELD and heparin were dissolved in deionized water at 10 mg/ml and combined at a 10:1 PELD:heparin mass ratio to form the coacervate. For coacervate imaging alone 500 μl coacervate was pipetted directly onto an aluminum stub. For PLGA scaffold coating, scaffolds were submerged in 1 ml coacervate and soaked for 5 min, then mounted on aluminum stubs. Uncoated scaffolds from the same batch were also prepared. All samples were frozen and lyophilized overnight. Samples were sputter coated with gold at a 3.5 nm thickness and imaged using a JEOL JSM-633 OF scanning electron microscope (JEOL USA, Peabody, MA).

2.2.11 Statistical analysis

Statistical analysis was performed using SPSS 16.0 software (SPSS Inc, Chicago, IL). Data was tested for normality and equal variance before analysis. Statistical differences were calculated using one-way analysis of variance (ANOVA) followed by Tukey's post-hoc testing.

2.3 RESULTS AND DISCUSSION

2.3.1 PELD synthesis and characterization

The intermediate involved in PELD synthesis, PED, is also used in PEAD synthesis, as previously reported [158]. Briefly, PED is formed by polycondensation of a 1:1 molar ratio of t-BOC aspartic acid and EGDE, followed by removal of the BOC protecting group (**Fig. 4a**). t-BOC lysine is then conjugated and subsequently de-protected to form the final product. During the conjugation step, t-BOC lysine is activated by DCC and may then react intermolecularly as its contains one unprotected primary amine. PED is added immediately following activation to limit the amount of poly-lysine that forms before conjugation. This appears to have little effect on the functionality of the polycation for complexation with heparin; however, lysine with both amine groups protected may be used in the future for a more homogeneous product. Purification by repeated precipitations removes solvents and byproducts until no impurity peaks are observed on the ^{1}H NMR spectrum. PELD was analyzed by ^{1}H NMR for chemical shifts distinctive of its structure (**Fig. 4b**). Protons in the ethylene glycol backbone produced shifts at δ4.1 and 4.4 and a multiplet between δ3.4 and 3.9. Shifts between δ1.2 and 1.8 correspond to the aliphatic tail of

lysine. FTIR analysis of PELD shows absorbance around 1665 cm^{-1} resulting from ester bonds and in the 3000-3500 cm^{-1} range due to amide bonds and free hydroxyl groups (**Fig. 4c**). PELD had a T_g of 51.92 °C, and no crystallization was observed between -50 °C and 150 °C (**Fig. 4d**). GPC analysis indicated that PELD had a molecular weight (M_p) of approximately 3.5 kDa.

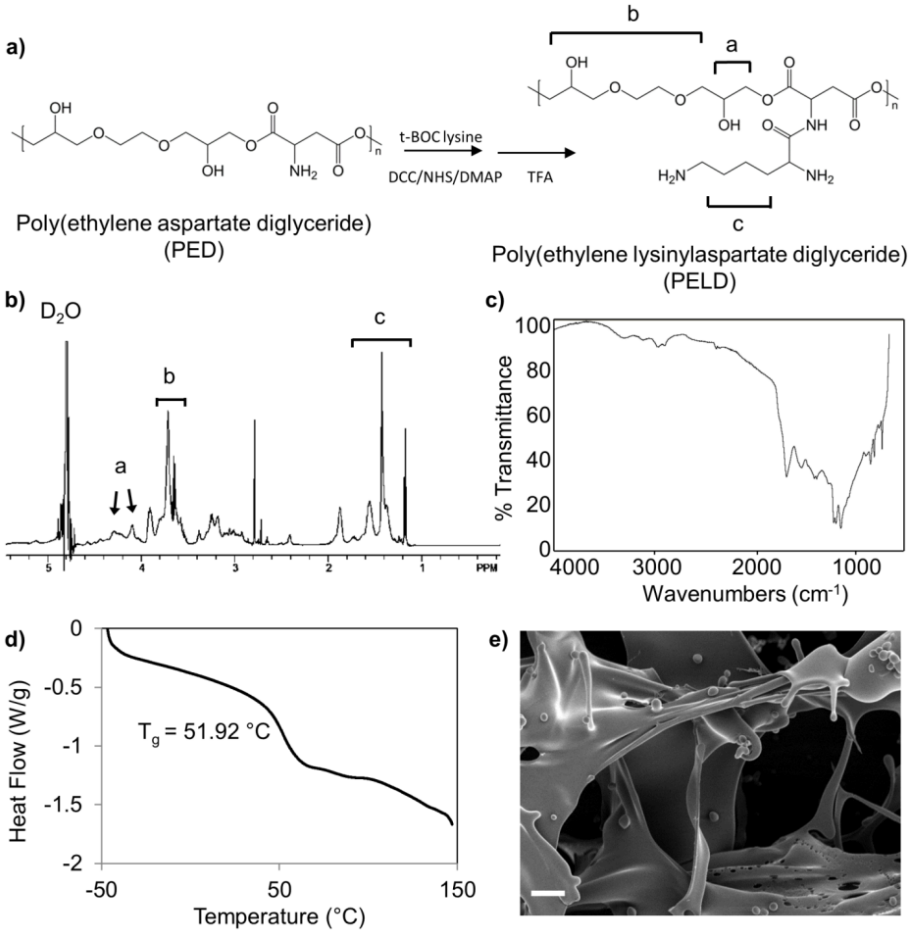

Figure 4. Synthesis and characterization of PELD and PELD:heparin coacervate a) The intermediate PED was synthesized by polycondensation of EGDE and aspartic acid. PELD was formed by conjugation of t-BOC lysine to aspartic acid in PED. Groups producing characteristic chemical shifts in the ^1H NMR spectrum are indicated. b) ^1H NMR spectrum of PELD shows signals characteristic of lysine and the backbone comprised of glycerol and aspartic acid. The D_2O is observed at δ4.8. c) FTIR spectrum of PELD shows ester stretches at 1665

cm^{-1} and weak amide and hydroxyl stretches near 3000 cm^{-1}. d) DSC thermogram indicates a glass transition temperature of 51.92°C. e) Scanning electron micrograph of lyophilized PELD:heparin coacervate displaying both ribbon-like sheets and globular domains. Scale bar = 10μm.

2.3.2 Characterization of PELD:heparin coacervates When combined with polyanions such as heparin, PELD self-assembles into a coacervate. Coacervation is a liquid-liquid phase separation analogous to an emulsion except that the coacervate phase still contains water [135]. The PELD:heparin coacervate is visible as a turbid solution. The morphology of the PELD coacervate was observed by scanning electron microscopy (**Fig. 2e**) and reveals both ribbon-like sheets and fibers, and globular structures. The ribbon-like structures are on the micron scale and highly variable in size, while most globular beads are 1-5 μm. A number of different PELD:heparin mass ratios ranging from 2.5 to 15 were further characterized. Zeta potential, a measure of the surface charge on a colloidal system, was analyzed first. As expected, a low PELD:heparin ratio yielded an overall negative surface charge, indicating an excess of anionic heparin (**Fig. 5a**). As the mass ratio increased, so did the zeta potential, reaching an overall neutral charge at a mass ratio of approximately 10. This indicates that heparin, the most negatively charged biomolecule, has approximately 10-fold greater charge density per unit mass compared to PELD. At mass ratios above 10, excess PELD molecules exist and create a positive surface charge. Zeta potential is also commonly used to estimate the stability of a colloidal system. Large positive or negative zeta potentials (generally +30 or -30 mV) indicate that the particles will tend to repel each other, while particles with low zeta potentials have little force to prevent aggregation.

The hydrodynamic diameter, or particle size, was also observed using dynamic light scattering (DLS) to assess how the PELD:heparin mass ratio and resultant surface charge affects the coacervate droplet size. The smallest droplet size was observed was 214 nm at a mass ratio of 2.5 and the largest was 1208 nm at a mass ratio of 7.5 (**Fig. 5b**). In general, large droplet sizes were observed around a mass ratio of 10, where the charge of the coacervate was near its isoelectric

point. As the mass ratio was adjusted, and the zeta potential deviated from zero, the droplet size decreased. This is likely an effect of coacervate aggregation, further elucidated by polydispersity measurements.

Polydispersity index (PDI) in DLS measurements is calculated from the cumulants analysis of the DLS intensity autocorrelation function. It is arbitrarily scaled to a maximum value of 1 and values less than 0.2 are typically considered monodisperse while values greater than 0.7 are considered highly polydisperse. Coacervates bearing the highest surface charge (mass ratios of 2.5 and 15) were monodisperse (**Fig. 5b**). However, as surface charge approaches neutrality the repulsion force between coacervate droplets decrease and aggregations form more readily. We also expect the size of aggregations to vary, thereby increasing the PDI. Indeed, we observed that PDI tended to increase as the coacervate surface charge approached neutrality with a maximal PDI of 1 at a mass ratio of 10.

a)

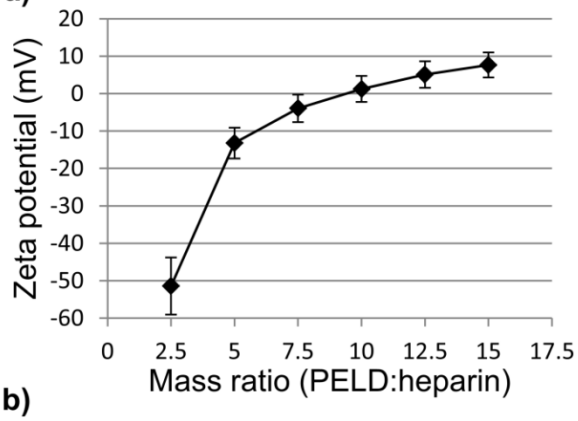

b)

PELD:heparin mass ratio	Hydrodynamic diameter (nm)	PDI
2.5	214.0	0.017
5	727.0	0.261
7.5	1208.0	0.278
10	1131.8	1.000
12.5	722.0	0.336
15	642.0	0.163

Figure 5. Zeta potential and hydrodynamic diameter of PELD:heparin coacervates PELD was combined with heparin at different mass ratios to form coacervates. a) Zeta potential measurements reveal surface charge of coacervates, with an isoelectric point (charge neutrality) at a mass ratio of 10. b) DLS measurements of hydrodynamic diameter and polydispersity of the coacervates. Hydrodynamic diameter represents the average size of the coacervate droplets in water. Polydispersity index (PDI) is arbitrarily limited to a maximum value of 1 with values ≤ 0.2 being considered monodisperse and values ≥ 0.7 indicating high polydispersity.

Mass ratios of 5 (negative), 10 (neutral), and 15 (positive) were selected for fluorescent imaging. Fluorescein, a small, charged dye, was added to the heparin solution and became incorporated into the coacervate upon addition of PELD. Droplets ranging from < 1 μm to approximately 5 μm in diameter were observed in the negatively- and positively-charged coacervates, which appeared similar in size and distribution (**Fig. 6**). This correlates well with our DLS results with the droplets > 1 μm representing aggregates which lead to the recorded

polydispersity. The neutral coacervate had droplets ranging from 1-10 μm and was very polydisperse, as observed with DLS. Images were taken immediately after coacervation, therefore aggregation likely occurs more quickly in neutral coacervates.

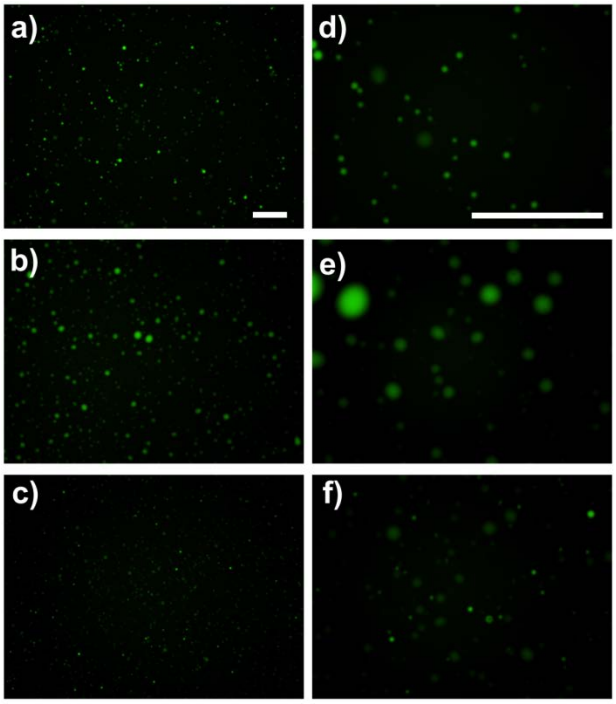

Figure 6. Fluorescent imaging of coacervates. Fluorescein, a charged fluorescent dye was incorporated into the coacervate to enable imaging by fluorescent microscopy. 10x magnification images of coacervates with PELD:heparin mass ratios of a) 5, b) 10, and c) 15. d-f) High magnification (40x) images of a-c, respectively. Scale bars=100 μm.

2.3.3 PELD cytocompatibility

Polycations typically carry high cytotoxicity, making them unsuitable in many translational applications.[189] Development of a biocompatible polycation which can deliver growth factors

without affecting cell response itself is of high importance. We tested the cytocompatibility of PELD using an established method for polycations with the fibroblast cell line, NIH 3T3.[190, 191] We compared PELD to polyethyleneimine (PEI), a common polycation used in cell culture and as a polymer transfectant for non-viral gene delivery [192, 193]. We also used PEAD as a positive control as we have previously shown it to be highly biocompatible both *in vitro* and *in vivo* [158]. At concentrations up to 10 mg/ml PELD had no effect on cell viability compared to PEAD (**Fig. 7**). Conversely, PEI induced a significant reduction in fibroblast viability at all concentrations, even as low as 0.01 mg/ml, compared to both PEAD and PELD. This toxicity of PEI has been well documented previously and exemplifies a major limitation of many polycations in scientific research [182]. These results indicate that PELD displays no *in vitro* cytotoxicity issues in a range of concentrations that are physiologically relevant, considering the dilution when applied in the body. Considering the biocompatibility of PEAD [158] it is unsurprising that utilizing the same design principle for lysine results in a lysine-based polycation that also has excellent biocompatibility.

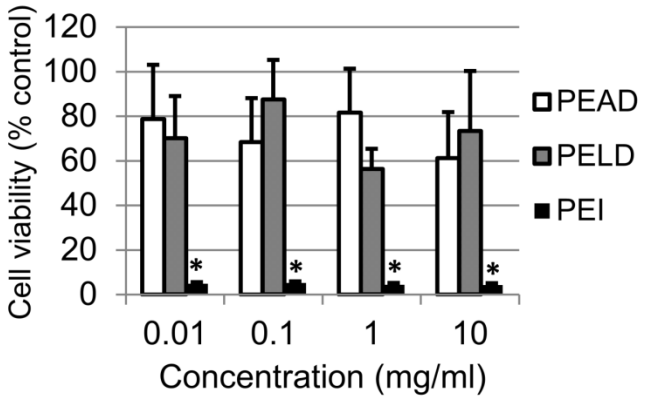

Figure 7. Polycation cytotoxicity. NIH3T3 fibroblasts were exposed to PEAD, PELD, or PEI dissolved in culture media at 0.01, 0.1, 1, or 10 mg/ml. Cell viability was measured after 24 hours by Live/Dead assay. *p<0.01 compared to both PEAD and PELD groups.

2.3.4 Controlled release from PELD coacervates

The high cytocompatibility of PELD warranted further investigation of its suitability for controlled release of biomolecules. Heparin-binding sites often contain multiple cationic amino acids, rendering high positive charge density which interacts with the many sulfate groups of heparin.[194] Therefore PELD competes with growth factors and other proteins for binding to heparin, and thus positively-charged coacervates exhibit poor loading efficiency (data not shown). Only coacervates with negative zeta potential were investigated for release characteristics. We tested the loading and release of bovine serum albumin (BSA) from PELD:heparin coacervates of three different mass ratios over 21 days. BSA is commonly used as a model protein in drug delivery research and it also binds to heparin with a k_d of 4.3 µM [195]. Observations common among all coacervates were high loading efficiencies of greater than 95%, low initial burst release, and sustained release thereafter through the end of the experiment (**Figure 8**). A direct relationship between charge and release rate was observed with a more

negative charge inducing a slower release of BSA from the coacervate. Total release after 21 days ranged from 17.4% to 58.8% for the -10 mV and 0 mV coacervates, respectively, with the -5 mV coacervate displaying an intermediate total release. We expect that multiple mechanisms play a role in the release of biomolecules: degradation of the polycation, as has been demonstrated with PEAD and similar polycations [158, 159], dissociation of the coacervate in an ionic environment, and competition for heparin between the polycation and heparin-binding proteins. The dependence of release on charge supports the participation of the last mechanism. These data demonstrate that a high degree of control over release can be obtained by simply altering the PELD:heparin mass ratio of the coacervate.

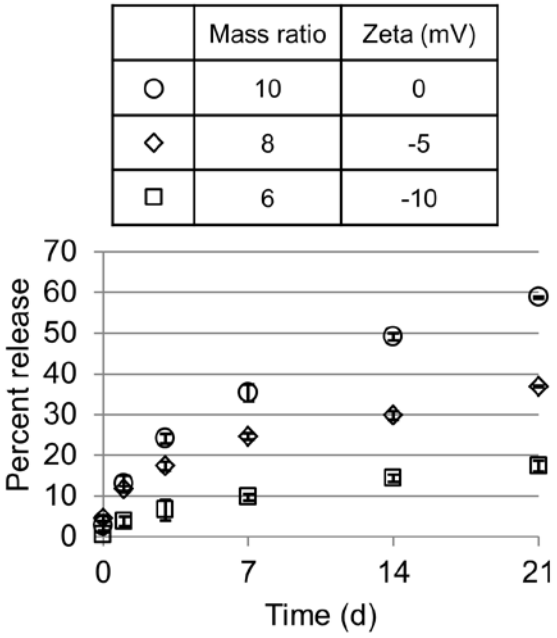

Figure 8. BSA release from coacervates. PELD:heparin mass ratios of 10, 8, and 6 were used which correspond to zeta potentials of approximately 0, -5, and -10 mV, respectively. Each coacervate was loaded with 500 μg BSA and release was quantified on days 0, 1, 3, 7, 14, and 21 by total protein assay.

2.3.5 Coacervate coating of polymeric scaffolds

The value of a controlled release vehicle for many tissue engineering approaches will hinge on its ability to coat a polymeric scaffold. The coacervate is highly charged and therefore interacts by Coulombic forces with polymers bearing surface charge. It also contains many functional groups such as hydroxyl groups on PEAD which may form hydrogen bonds with polarized materials. Finally, the coacervate may participate in hydrophobic interactions with non-wetting surfaces as it is phase-separated from water.

We next tested the ability of the coacervate to adsorb to a porous poly(lactic-co-glycolic acid) (PLGA) disk as a model polymeric scaffold. When the turbid coacervate solution was exposed to the disk the optical density dropped rapidly (**Fig. 9a**). The change in optical density was directly proportional to the fraction of coacervate removed from the solution and adsorbed to the scaffold. The coacervate adsorbed rapidly and after 15 minutes reached a plateau at maximal fractional adsorption. Coacervate alone with no scaffold served as a control, and showed no significant change in optical density throughout the course of the experiment. After 30 minutes, coacervate-coated scaffolds were a yellow-orange color, similar to the color of PELD (**Fig. 9b**).

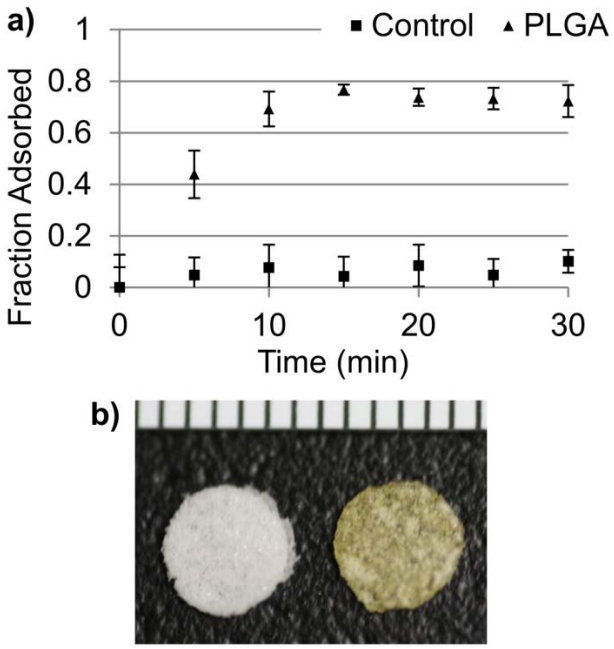

Figure 9. Adsorption of PELD coacervate to polymer scaffolds. PELD coacervate was prepared in water and then porous PLGA scaffolds were added. **a**) Coacervate adsorption to the scaffold was measured as a fractional change in optical density. A control coacervate solution did not receive a scaffold. **b**) PELD coacervate-coated scaffold (right) next to a bare PLGA scaffold (left) at the endpoint of the experiment. Ruler units are 1mm.

Coated and uncoated PLGA scaffolds were further analyzed by scanning electron microscopy. The coacervate was clearly observable as a thin network which covered the surface of the PLGA material and also spanned some pores with spider web-like morphology (**Fig. 10**). However, the coating does not occlude the pores, allowing space for cells to infiltrate the scaffold. There is also coacervate clearly visible within the pores of the scaffold, indicating that coacervate penetrated beyond the scaffold outer surface. This may be important for forming a chemokine gradient which extends into the scaffold for recruitment of cells. These data suggest that the coacervate delivery vehicle can be quickly and easily adsorbed onto polymeric tissue

engineering scaffolds in aqueous solution to provide sustained release of heparin-binding growth factors or cytokines.

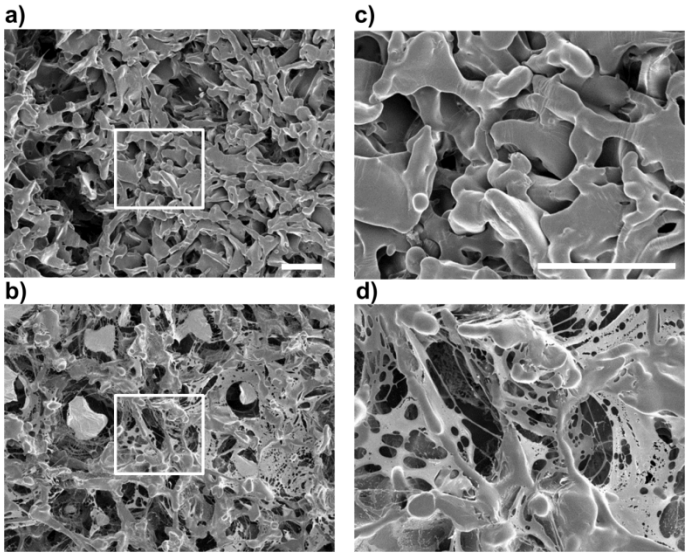

Figure 10. Scanning electron micrographs of PELD coacervate adsorbed to scaffolds. PLGA scaffolds with a 75-150 μm pore size were prepared by salt-leaching method and imaged by SEM. **a)** Uncoated PLGA scaffold (150x magnification). **b)** Coated PLGA scaffold, submerged in PELD coacervate solution in water for 5 minutes, then lyophilized and imaged (150x magnification). **c-d)** High magnification (500x) SEM images of the indicated areas of a and b, respectively. All scale bars = 100μm.

2.4 CONCLUSIONS

We designed a lysine-based polycation to interact polyvalently with intact heparin and spontaneously form a coacervate in aqueous solutions. Compared to the commonly used polycation PEI, PELD displayed significantly better cytocompatibility. Loading and release of

BSA was tunable based on the PELD:heparin ratio of the coacervate. Finally, rapid adsorption of the coacervate onto polymeric scaffolds in water provides a simple means to integrate controlled release of biomolecules with tissue engineering scaffolds. These results suggest wide applicability of this polycation for controlled and sustained delivery of heparin-binding proteins. In the future, release rate and duration may be selected for specific growth factors on an application-specific basis.

3.0 CONTROLLED DELIVERY OF HB-EGF TO ACCELERATE DERMAL WOUND HEALING

3.1 INTRODUCTION – NORMAL WOUND HEALING

Dermal injury remains one of the most prevalent and economically burdensome healthcare issues in the world. In the US alone there are more than 100 million acute wounds annually, including surgical incisions, trauma, and burns [196]. Current wound management requires frequent dressing changes and patients are at constant risk of infection until the skin regains its barrier function. In chronic wounds, a variety of underlying detriments, including pressure, insufficient blood flow, and edema, prevents healing from occurring without proactive treatment [197]. Current treatment options are limited, costly, and inefficient. As a result, the development of new therapeutics is necessary to satisfy the clinical need.

Growth factor therapies hold tremendous potential to address the shortcomings of current wound care modalities [198, 199]. Growth factors act as critical extracellular cues that orchestrate the wound healing process; supply of exogenous growth factors may therefore induce faster re-epithelialization, leading to reduced risk of infection and shorter inpatient stays. In cases of chronic wounds, growth factors may provide the necessary stimuli to induce wound closure

that is otherwise unlikely to occur [200]. Several important growth factors involved in the wound healing process are from the epidermal growth factor (EGF), platelet-derived growth factor (PDGF), and transforming growth factor-β (TGF-β) families. Heparin-binding EGF-like growth factor (HB-EGF), although less studied, is present in both human and porcine wound fluid [201, 202], and is a potent stimulator of keratinocyte proliferation and migration [203, 204]. HB-EGF has been shown to have mitogenic effects on fibroblasts [201, 205], and may therefore be involved in the formation of granulation tissues. Lastly, HB-EGF also plays a role in angiogenesis during wound healing [206, 207]. Clearly, HB-EGF acts as a versatile regulator of wound healing and would be highly beneficial as a regenerative therapeutic.

Provision of exogenous growth factors can accelerate wound healing; however they must be applied in a sustained and localized fashion to be effective. This is due to short growth factor half-lives, rapid dilution in the body, and undesirable effects at high systemic levels [208]. Our group has developed a controlled delivery system based on intact heparin, a highly-sulfated glycosaminoglycan with similar functionality to the extracellular matrix (ECM)-derived proteoglycan, heparan sulfate. Heparin and heparan sulfate bind many growth factors with high affinity, extend their half-lives by protection from proteolytic degradation, and increase their bioactivity [209, 210]. To keep the water-soluble heparin:growth factor complex localized to the site of application, a synthetic polycation, poly(ethylene argininylaspartate diglyceride) (PEAD), was designed to interact with heparin through polyvalent charge attraction, forming a growth factor-containing coacervate [21]. In this simple delivery system, incorporated growth factors are separated from the aqueous environment in the oil phase of the coacervate, further protecting them from degradation. This delivery platform is capable of controlling the release of heparin-binding growth factors and has been used to successfully deliver FGF2 to stimulate therapeutic

angiogenesis [211]. Here we report the utility of this platform in controlled delivery of HB-EGF for wound healing.

3.2 MATERIALS AND METHODS – NORMAL WOUND HEALING

3.2.1 HB-EGF coacervate preparation

PEAD was synthesized as previously described [212, 213]. Heparin USP from porcine intestine (Scientific Protein Labs, Waunakee, WI) and PEAD were each dissolved at 10 mg ml^{-1} in sterile saline and 0.22 μm filter-sterilized. Heparin was initially combined with recombinant human HB-EGF (R&D Systems, Minneapolis, MN). PEAD was then added (50:10:1 mass ratio of PEAD:heparin:HB-EGF) which immediately precipitated the complex out of solution to form the HB-EGF coacervate, visible as a turbid solution.

3.2.2 Fluorescent imaging of the coacervate

A minimal amount of heparin (less than 1% by weight) in the coacervate was replaced with fluorescein (Aldrich Chemicals, Milwaukee, WI) by dissolving it in the heparin solution. The coacervate was centrifuged at 12,100 g for 10 min and the supernatant with unbound fluorescein was aspirated and replaced with deionized water. The coacervate was loaded to a glass chamber slide and imaged by an Olympus Fluoview FV100 confocal microscope (Olympus, Tokyo, Japan).

3.2.3 HB-EGF release profile

200µl HB-EGF coacervate containing 1 µg HB-EGF was pelleted by centrifugation at 12,100 g for 10 min and placed at 37 ^{0}C. On day 0, 1, 4, 7, and 10 the supernatant was aspirated and stored at -80 ^{0}C, and 200µl fresh saline was replaced to cover the pellet. The amount of released HB-EGF in three separate fractions per timepoint was determined by ELISA (R&D Systems, Minneapolis, MN).

3.2.4 *In vitro* scratch wound assay with primary human keratinocytes

1x10^{6} normal human epidermal keratinocytes (NHEK, Lonza, Basel, Switzerland) at passage 3 were seeded per well in a 24-well plate and cultured in full keratinocyte growth media, KGM-Gold (Lonza, Basel, Switzerland), until confluency. A 10 µl pipette tip was used to scratch the cell layer and wells were washed once with DPBS to remove debris. Cells were cultured at 37 ^{0}C in KGM-Gold, without bovine pituitary extract (BPE) or epidermal growth factor (EGF) supplements, containing 100 ng ml^{-1} free HB-EGF or HB-EGF coacervate, or no HB-EGF as control. Photographs were taken of *in vitro* wounds in three wells per group with an Eclipse Ti inverted microscope (Nikon, Tokyo, Japan) at the beginning of the experiment and every 6 hours for one day. Scratch width was measured using NIS Elements Analysis software (Nikon, Tokyo, Japan).

3.2.5 *In vitro* proliferation of primary human keratinocytes

$2x10^5$ passage 3 NHEK were seeded per well in a 24-well plate and cultured at 37 ^{0}C in KGM-Gold media, without BPE or EGF supplements, containing either 10 ng ml^{-1} or 1 ng ml^{-1} free HB-EGF or HB-EGF coacervate, or no HB-EGF as control. After 4 days cell lysates were prepared by the addition of 0.1 % Triton X-100 (Sigma, St. Louis, MO) followed by 3 freeze-thaw cycles. Double-stranded DNA (dsDNA) content of cell lysates was measured by Quant-iT dsDNA high-sensitivity assay kit (Invitrogen, Carlsbad, CA).

3.2.6 Murine wound model and wound closure analysis

6-7 week old C57BL6/J mice (Jackson Labs, Bar Harbor, ME) were anesthesized with isoflurane and the dorsal area was shaved. Two 0.5 mm-thick silicone donut-shaped splints (OD=16 mm, ID=8 mm) were fixed on either side of the dorsal midline, approximately 2.5 cm from the ears, with 6-0 Prolene suture. Identical full-thickness wounds were made using a 5 mm round skin biopsy punch, centered within each splint. 1 μg free HB-EGF, as an HB-EGF coacervate, vehicle alone, or saline was applied to wounds (n=7 animals/ 14 wounds per group) by sterile pipet as a 10 μl solution. Two wounds were made on each mouse to increase sample size and both wounds received the same treatment to avoid cross-contamination. Polyskin II sterile hydrocolloid bandages (Tyco Healthcare, Mansfield, MA) were applied followed by Coban self-adhesive wrap (3M, St. Paul, MN) around the midsection to deter chewing of the splints. On days 7, 10, 14, and 17 only the wrap was removed and wounds were digitally photographed through the clear hydrocolloid bandage. Wound area was measured by blinded operator using a fine-resolution computer mouse to trace the wound margin in MetaMorph Image Analysis Software

(Molecular Devices, Sunnyvale, CA). Suture and wraps were replaced as necessary to keep the splints fixed. On day 7, two animals per group were sacrificed and wounds and surrounding were tissue collected for histological evaluation. Remaining animals were sacrificed on day 17. University of Pittsburgh Institutional Animal Care and Use Committee (IACUC) approval was obtained prior to beginning all animal studies.

3.2.7 Histological analysis

Wound and surrounding tissue was collected using a 7 mm skin biopsy punch and then bisected through the midline of the wound using a razor blade. Both halves were immediately embedded in optimal cutting temperature (OCT) medium (Sakura Finetek, Torrance, CA), frozen, and sequentially sectioned at 5 μm using a MICROM HM525 cryomicrotome (Thermo Fisher Scientific, Waltham, MA). Only sections from the same area of the wound were compared histologically. Skin sections were stained with hematoxylin and eosin (H&E) for standard evaluation and with Masson's trichrome staining (MTS) for evaluation of collagen content, counterstained with hematoxylin.

3.2.8 Immunohistochemical analysis

Wound sections were fixed and stained using a rabbit polyclonal anti-wide spectrum cytokeratin antibody (1:75, Abcam, Cambridge, MA) with an IHC staining kit (Santa Cruz Biotech, Santa Cruz, CA), then counterstained with hematoxylin. Day 7 sections were dual-stained using rabbit polyclonal anti-Ki-67 (1:500, Abcam, Cambridge, MA) and rabbit anti-integrin β4 (1:200, Abcam, Cambridge, MA) followed by goat anti-rabbit IgG Alexa Fluor 488 and Alexa Fluor

594-conjugated secondary antibodies (1:200, Invitrogen, Carlsbad, CA), respectively, and counterstained with DAPI. Day 17 skin sections were dual-stained with purified anti-mouse CD31 (1:50, BioLegend, San Diego, CA) followed by Alexa Fluor 588-conjugated secondary antibody (1:200, Invitrogen, Carlsbad, CA), and FITC-conjugated mouse anti-α-smooth muscle actin (α-SMA, 1:500, Sigma, St. Louis, MI). All images were taken using an Eclipse Ti inverted microscope (Nikon, Tokyo, Japan).

3.2.9 Statistical analysis

Statistical analysis was performed using SPSS 16.0 software (SPSS Inc, Chicago, IL). Statistical differences were detected using analysis of variance (ANOVA) followed by Bonferroni correction as post-hoc testing. Differences were considered significant at $P<0.05$.

3.3 RESULTS – NORMAL WOUND HEALING

3.3.1 Characterization of HB-EGF coacervate

PEAD contains two functional groups per repeating unit that carry positive charge (**Fig. 11a**). The coacervate forms immediately upon addition of PEAD to the heparin:HB-EGF complex in PBS, visible macroscopically as a turbid solution. Fluorescein carries negative charges and integrates into the coacervate via Coulombic forces. Fluorescent imaging of the coacervate with embedded fluorescein revealed spherical droplet with diameters ranging from 10-500 nm (**Fig. 11b**). The release kinetics of HB-EGF from the coacervate were determined *in vitro*. Less than

8% HB-EGF was detected in the supernatant after pelleting the coacervate (day 0 of release assay), indicating a loading efficiency of greater than 92%. No initial burst release of HB-EGF was observed on day 1, and release thereafter was approximately linear at 15 ng day^{-1} (**Fig. 11c**).

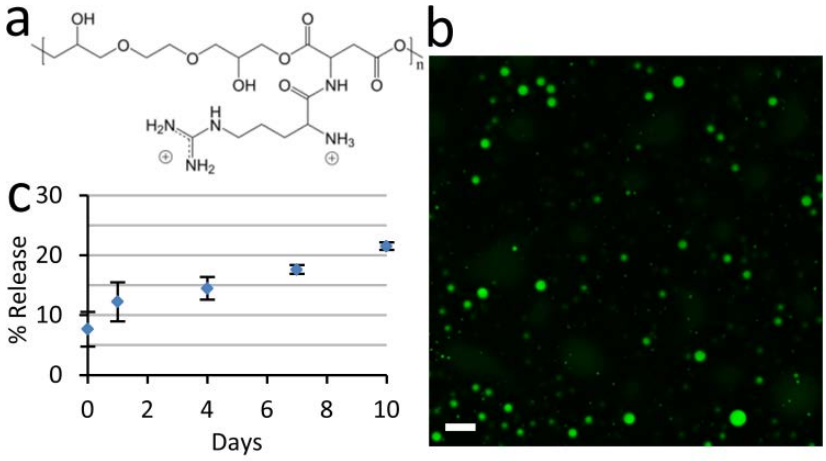

Figure 11. The coacervate controls the release of HB-EGF in a steady fashion. (a) Chemical structure of the PEAD. The backbone of PEAD contains aspartic acid and ethylene glycol diglyceride, connected by biodegradable ester bonds. Arginine is conjugated to provide two cationic charges per repeating unit, giving PEAD strong affinity for polyanions. (b) Confocal fluorescent imaging of fluorescein-labeled coacervate shows spherical morphology with droplet diameters of 10-500 nm. Bar = 1 μm. (c) *In vitro* release profile of HB-EGF from the coacervate into saline over 10 days. Bars indicate means ± SD.

3.3.2 HB-EGF stimulates keratinocyte migration

The effect of free and coacervate HB-EGF on the migratory capacity of primary human keratinocytes was determined by their ability to induce *in vitro* wound closure in a scratch assay. The closure of wounds made in confluent cell monolayers was tracked over 24 hours (**Fig. 12a**).

It is important to mention that cell proliferation may also affect closure rate in this assay, but the short timeframe limits its contribution. Though not statistically significant, the effect of bolus addition of free HB-EGF is evident 6 hours after wounding (**Fig. 12b**). By 12 hours post-wounding, free HB-EGF significantly improved closure of scratch wounds compared to the control. Beginning 18 hours post-wounding, HB-EGF coacervate also significantly improved closure compared to the control. Scratch wound closure in free and coacervate HB-EGF groups was statistically the same at all timepoints. It is important to note that although the same amount of HB-EGF was added to both groups (100 ng ml^{-1}), in the controlled delivery case it is mostly incorporated in the coacervate so the concentration of free growth factor in the medium is much lower.

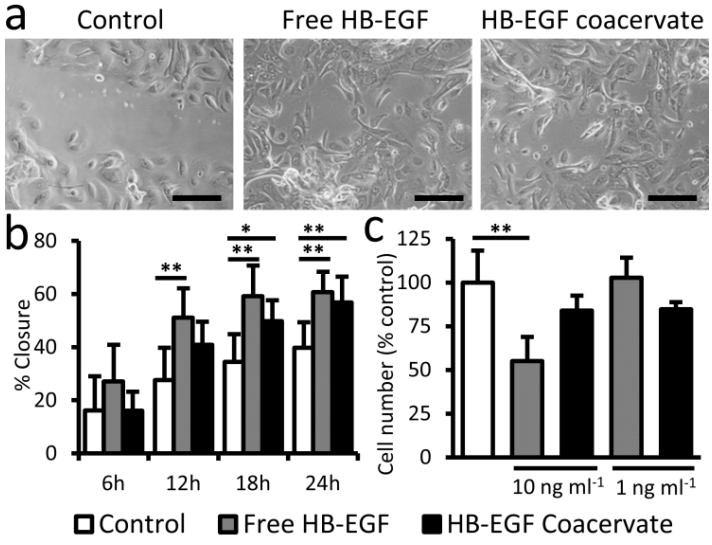

Figure 12. HB-EGF coacervate stimulates primary human keratinocytes. (a) Representative images of scratch wounds on confluent keratinocyte monolayers after 24 h of culture in media supplemented with saline (Control), 100 ng ml^{-1} HB-EGF free or in the coacervate. Bars = 200 μm. (b) Quantification of percent closure of scratch wounds over time. Bars indicate means ± SD. **P*<0.05; ***P*<0.01. (c) Quantification of cell number after 4d

culture of keratinocytes in media supplemented with saline (Control), 1 ng ml^{-1} or 10 ng ml^{-1} HB-EGF free or in the coacervate. Bars indicate means ± SD. $^{**}P<0.01$.

3.3.3 Controlled release of HB-EGF from the coacervate does not inhibit keratinocyte proliferation

Primary human keratinocytes were cultured in the presence of free or coacervate HB-EGF in the culture media. Cell proliferation over 4 days culture was analyzed by DNA quantification. At high HB-EGF concentration (10 ng ml^{-1}), free growth factor reduced cell proliferation compared to control while cell proliferation in the presence of coacervate with the same amount of growth factor had no statistically significant change (**Fig. 12c**). This is consistent with the premise of controlled release reducing the burst effect. At lower concentration (1 ng ml^{-1}) however, neither free nor coacervate HB-EGF had any significant effect on cell number.

3.3.4 HB-EGF coacervate accelerates mouse wound closure

The effects of free and coacervate HB-EGF on wound closure were examined in a splinted mouse full-thickness excisional wound model. A modified skin biopsy punch wounding procedure led to a more uniform wound size than procedures requiring scissors. To mimic human healing, splints were used to avoid skin contraction, thus making re-epithelialization the major factor in wound healing. The wounds were treated immediately with saline, vehicle (PEAD:heparin complex), 1µg HB-EGF free or in the coacervate (**Fig. 13a**). Wound area was tracked over 17 days and animals were sacrificed on days 7 and 17 for histological analysis.

Accelerated closure of wounds treated with HB-EGF coacervate was evident by day 7 and continued throughout the test period compared to all other groups (**Fig. 13b-c**). Only this treatment induced complete wound closure by day 17. No significant difference existed between the other three groups at any time point. Histological analysis after 7 days showed a thick cell-rich granulation region in HB-EGF coacervate-treated wounds with high ECM content, revealed by Masson's trichrome staining (MTS) (**Fig. 14**). Immunohistochemical detection of cytokeratin shows a thick stratum corneum on day 7 that was remodeled to identical structure to the surrounding normal epidermis by day 17 (**Fig. 14**). Signs of returning dermal appendages were also observed by day 17 in HB-EGF coacervate-treated wounds. Other groups showed thin and inconsistent granulation regions which stained less strongly with MTS. Positive cytokeratin staining was observed in all groups in dermal appendages such as hair follicles and sebaceous glands where epithelial cells also reside [214].

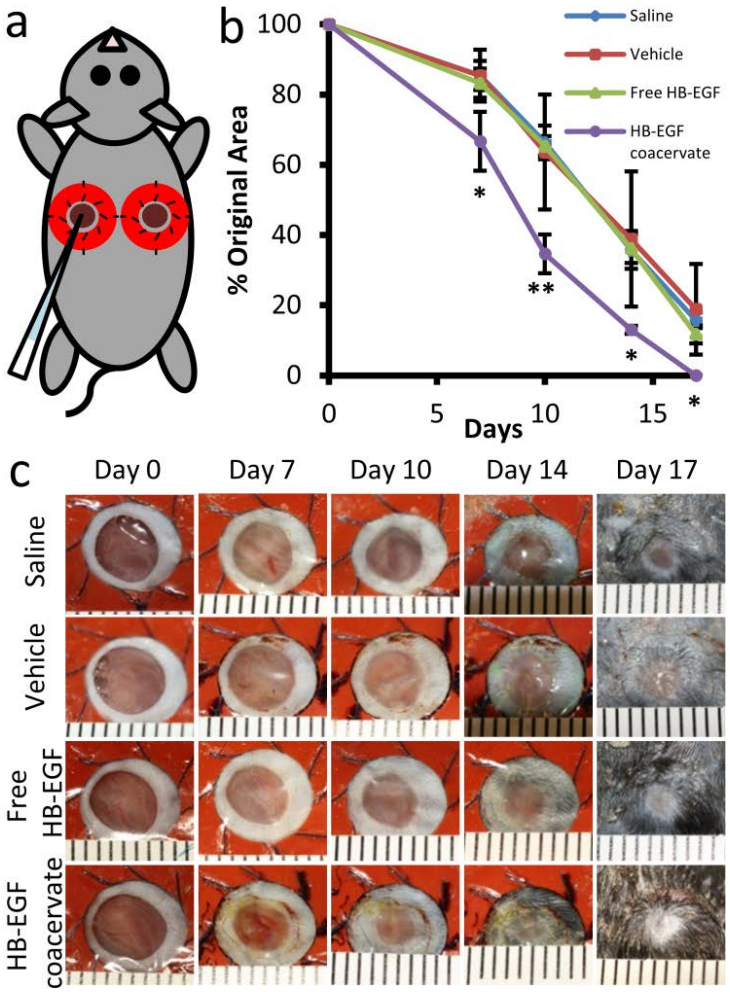

Figure 13. HB-EGF coacervate accelerates healing of full-thickness wounds. (a) Silicone donut-shaped splints, fixed with suture, surrounded the wounds and forced healing to occur by re-epithelialization. Wounds were treated immediately with 10 µl of group-specific solution by sterile pipet. (b) Wound closure over time, measured as percent of original area. Fourteen wounds were averaged for day 7 timepoint after which two animals were sacrificed per group for histology; the remaining 10 wounds per group were photographed until sacrifice on day 17. Bars indicate means ± SD. **P*<0.05; ***P*<0.01. (c) Representative photographs of wounds treated with saline, vehicle (PEAD:heparin complex), 1 µg HB-EGF free or in the coacervate. Ruler units are mm.

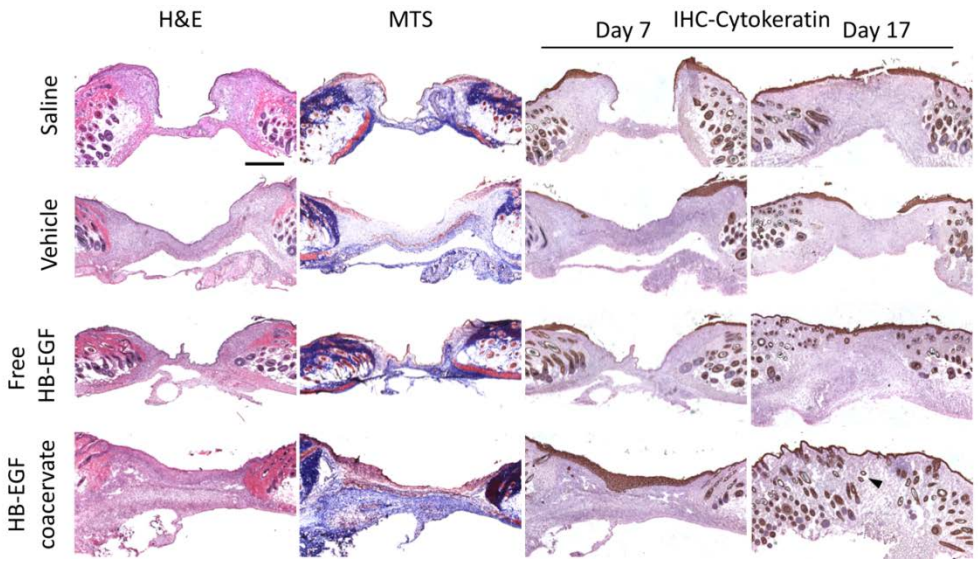

Figure 14. HB-EGF coacervate accelerates epithelialization and granulation. Wound sections stained with hematoxylin and eosin (H&E) for general observation, Masson's trichrome (MTS) for collagen, and immunohistochemically for cytokeratin (IHC-Cytokeratin) as a marker of epithelial cells. Representative light microscopy images of sections from the center of day 7 wounds are presented for all three staining methods, and of day 17 wound sections stained for IHC-Cytokeratin. Arrows indicate newly formed dermal appendages present within the granulation tissue. Bar = 500 μm.

3.3.5 HB-EGF coacervate increases keratinocyte proliferative and migratory potential *in vivo*

To further investigate the effect of HB-EGF on the behavior of keratinocytes after wounding, day 7 wound sections were immunostained for proliferation and migration. The former was reflected by Ki-67, a marker of cell proliferation [215]. The latter was observed by staining of β4 integrins, which heterodimerize with α6 subunits on the surface of epithelial cells and play a key role in cell motility, especially during wound healing [216-218]. Both markers were localized almost exclusively to the epidermis (**Fig. 15a**). In the unwounded skin, normal epidermal

stratification was accurately reflected with β4 integrin -positive cells overlying cells positive for Ki-67; however the majority of cells at the wound margin were double-positive. Saline and vehicle groups showed minimal cell migration beyond the proliferating cells at the wound margin. Free HB-EGF induced migration of non-proliferating (Ki-67-negative) cells, consistent with the inhibited proliferation observed *in vitro.* In contrast, keratinocytes in wounds treated by HB-EGF coacervate exhibited co-localization of both markers well beyond the wound margin, indicating that the migratory cells still retain their proliferative capacity. Only HB-EGF coacervate-treated wounds showed a complete layer of epithelial (β4 integrin-positive) cells across the entire wound length on day 7.

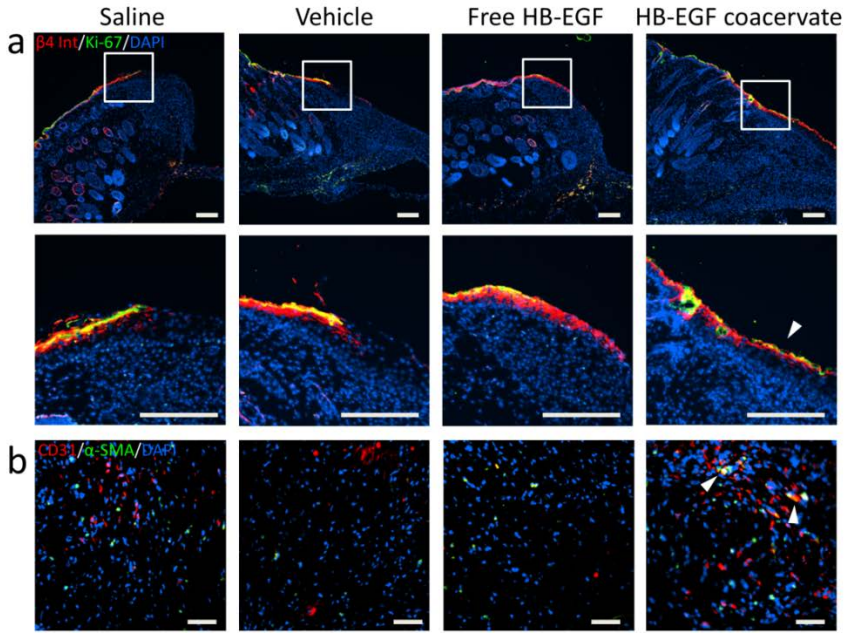

Figure 15. HB-EGF induces epithelial migration and proliferation. (a) Immunofluorescent staining of day 7 wound sections for β4 integrin (red) and Ki-67 (green) with DAPI (blue) nuclear staining. High magnification images of the wound margin reveal epithelial cells with retained proliferation potential (co-localization of markers; red + green = yellow). Arrow indicates significant migration of these dual-positive cells. Bars = 200 μm. (b)

Immunofluorescent staining of day 17 wound sections for CD31 (red) and α-smooth muscle actin (green) with DAPI (blue) nuclear staining. Representative images of granulation tissue near the wound margin show endothelial cell and mural cell infiltration from the adjacent dermis. Arrows indicate co-localization of cells (red + green = yellow) as potential nascent vessels. Bars = 50 μm.

3.3.6 Angiogenesis accompanies faster healing

The vascularization of day 17 wounds was examined with immunofluorescent staining for endothelial cells ($CD31^+$) and mural cells (α-smooth muscle $actin^+$). At the base of the granulation region near the wound margins, endothelial cells were observed in the HB-EGF coacervate-treated wounds (**Fig. 15b**). Additionally, mural cells were observed co-localizing with endothelial cells in the HB-EGF coacervate group, indicating early blood vessel formation not present in other groups.

3.4 DISCUSSION – NORMAL WOUND HEALING

Many delivery systems have been developed to provide controlled spatio-temporal release of EGF, including sponges [219], hydrogels [220], polymer pellets [221], electrospun nanofibers [91], and microspheres [222]. However, clinical translation of these systems has been deterred by setbacks such as poor loading efficiency, large initial burst release, and low bioactivity of the released growth factors [223]. It is likely that these challenges can be overcome by examining the integral role the ECM plays in sequestering, protecting, coordinating, and enhancing growth factor activity. Thus, a particularly effective approach to design biomimetic growth factor

delivery systems is to incorporate ECM components such as hyaluronic acid [224], collagen [225], and vitronectin [226]. These systems utilize controlled release while also mimicking the natural extracellular environment of regenerating tissue [227].

Of similar structure to ECM-derived heparan sulfate proteoglycans, heparin is also used in many delivery systems [28]. In addition to protecting growth factors from proteolytic degradation, heparin potentiates the activity of some factors by facilitating their interaction with cell receptors [228, 229]. Delivering growth factors pre-bound to heparin also prevents their rapid sequestration by the endogenous ECM. This may be especially important in a cutaneous wound setting where growth factors are required at the wound margin to stimulate re-epithelialization and are less useful if immobilized elsewhere in the wound [230]. In support of this notion is the finding that adding heparanase, which cleaves heparan sulfate thereby liberating bound growth factors, enhanced wound healing and angiogenesis [231].

Our delivery approach is one of a handful of systems that utilize intact, native heparin, thereby fully retaining its natural functionality. Others have incorporated intact heparin by conjugation to fibrin matrices via bi-domain peptides [232], to peptide amphiphiles [233], or within dendrimer-crosslinked collagen gels [234]. Our delivery system employs a polycation that is a simplistic mimetic of the heparin-binding domain of the fibroblast growth factor receptor [235]. This bio-inspired ternary complex is stable, held together by polyvalent ionic interactions. Thus heparin imparts significant bioactivity to our delivery system, which PEAD keeps localized to the application site in a simple, unobtrusive way. This work represents, to the best of our knowledge, the first use of a bio-active controlled release system to deliver HB-EGF in a pre-clinical animal model.

HB-EGF release from the coacervate, governed by degradation of PEAD and dissociation of the delivery complex, was slow and sustained over at least 10 days *in vitro* with a steady release rate of 15 ng per day. We expect that release is accelerated *in vivo*, driven by additional enzymatic activity in the wound bed. Degradation of the coacervate *in vivo* is catalyzed by esterases and heparinases, however we do not observe any toxic effects of PEAD or its degradation products, locally or systemically [212]. Indeed, the vehicle did not inhibit healing in the present study, showing no difference from the control. The viscous liquid-like properties of a coacervate, not too different from wound fluid, also make it highly attractive for use in a wound healing therapeutic. It is prepared in water and then simply applied topically in this work. The coacervate can also be injected [211] or could be incorporated into bandages.

The effect of HB-EGF on epithelial cell proliferation and migration was examined individually using primary human keratinocytes. HB-EGF significantly increased keratinocyte migratory capacity but not proliferation, in accordance with previous reports [203]. HB-EGF coacervate consistently produced results similar to that of the free growth factor group; however, our release study shows that only 12% and 15% HB-EGF was released by the end of the 1 day migration study and 4 day proliferation study, respectively. This indicates an enhanced bioactivity of HB-EGF released from the coacervate. This is consistent with potentiated activity of fibroblast growth factors released from this delivery system [21]. Though not statistically significant, a slight advantage of free growth factor over coacervate was evident in the scratch migration assay, particularly during the first 12 hours. Interestingly, the difference in means between these two groups gradually decreased over the course of the experiment, reflecting the increasing concentration of HB-EGF in the medium in the coacervate group. At high concentrations, free HB-EGF inhibited cell proliferation, as previously reported [202]. However,

using the coacervate to maintain a low, stable concentration of free HB-EGF avoided this inhibition.

Splinted excisional wound models in rodents force healing to occur by re-epithelialization as in humans, rather than by contraction as in most loose-skinned mammals [236]. Thus they provide an ideal first validation tool for the potential of HB-EGF coacervate to accelerate wound closure *in vivo*. We found that controlled delivery is essential to effective HB-EGF therapy, as free growth factor healed wounds at the same rate as controls at a dosage of 1 μg. HB-EGF coacervate significantly accelerated wound closure over 17 days by comprehensive healing which included expedited re-epithelialization, improved granulation tissue formation, and angiogenesis.

Endogenous HB-EGF expression is normally low but is upregulated in cutaneous wounds [202]. It is produced by multiple cells and in the setting of dermal injury acts primarily as a potent stimulator of re-epithelialization [203]. The presence of exogenous HB-EGF delivered by the coacervate accelerated re-epithelialization, as evident by a complete keratinized layer with regained barrier function 7 days after administration. We also observed keratinocytes well beyond the wound margin which stained positive for β4 integrin co-localized with Ki-67 protein, expressed exclusively in nuclei of cells in active cell cycle. In agreement with our *in vitro* results, these migrating keratinocytes continued to proliferate as long as the soluble HB-EGF concentration was maintained below threshold levels by the coacervate. Conversely, free HB-EGF stimulated cell migration beyond that of the controls, however proliferation was restricted to near the wound margin and ultimately led to no difference in wound closure rate.

In the first week of acute wound healing, dermal fibroblasts enter the wound bed, proliferate, and gradually replace the provisional fibrin- and fibronectin-rich matrix with a

collagenous one, also containing proteoglycans. This collagen matrix, primarily type I and III, serves as inductive scaffolding for infiltrating stromal cells and provides strength and structure to the new tissue as remodeling occurs [237, 238]. HB-EGF may act as a fibroblast mitogen and indeed, we observed that granulation tissue in HB-EGF coacervate-treated wounds had high collagen content 7 days after injury. This likely resulted from both direct effects on dermal fibroblasts and indirect effects such as activation of paracrine signaling by epithelial cells [239]. The presence of dermal appendages within the granulation region at day 17 further indicates that HB-EGF coacervate-treated wounds were at a later stage of healing compared to other groups.

Angiogenesis also plays a critical role in the wound healing process. Endothelial sprouts derived from adjacent tissue invade the provisional wound matrix and support the formation of granulation tissue [238]. HB-EGF may have direct mitogenic and motogenic effects on endothelial cells [206] and vascular smooth muscle cells [205], or may influence the angiogenic process by initiating paracrine signaling by keratinocytes and fibroblasts in the wound bed. HB-EGF may also be involved through the stimulation of matrix metalloproteinases (MMPs), which are critical in the initial stages of angiogenesis [240]. Our results indicate that controlled release of HB-EGF to the wound seemed to induce endothelial cell infiltration and signs of nascent blood vessels, not observed in other groups. The exact mechanisms by which HB-EGF affects angiogenic response require further investigation.

3.5 INTRODUCTION – DIABETIC WOUND HEALING

The global prevalence of diabetes mellitus was 382 million in 2013 and is projected to rise to 592 million by 2035 [241]. Fifteen percent of diabetics will develop a skin ulcer in their lifetime

resulting from neuropathies, peripheral ischemia, and infection [242]. Healing of diabetic ulcers does not progress normally but rather is plagued by an abnormal inflammatory response, low growth factor availability, and impaired cell function and angiogenesis, among others deficiencies [22]. Unsuccessful treatment of diabetic ulcers drives exorbitant healthcare costs, leads to substantial pain and morbidity, and precedes 85% of all non-traumatic foot amputations [243]. Clearly, therapies to initiate and accelerate the healing of diabetic wounds are important and timely.

Growth factors (GF) orchestrate the process of tissue repair in the body and thus hold great potential for regenerative therapies if applied strategically. However, their clinical use is currently limited by the fact that if applied alone, they are rapidly degraded and removed from the site of application [244]. Chronic wounds have particularly high protease activity and are deficient in extracellular matrix heparan sulfate proteoglycans which play a critical role in GF signaling [9, 245]. As a result, most experimental GF therapies have required frequent applications and high dosages to have positive albeit marginal effects on healing outcomes [4, 244]. We hypothesized that a delivery system releasing the GF pre-stabilized by heparin sulfate could circumvent the deficiencies of chronic wounds and promote their healing.

Unlike many GF evaluated for wound healing, HB-EGF is a pleiotropic factor influencing many stages of the wound healing process such as re-epithelialization, granulation tissue deposition and remodeling, wound contraction, and angiogenesis [161, 203, 206, 246]. HB-EGF is also a matrikine factor which requires the presence of heparin for binding and activation of its cell receptors [247, 248]. Thus we developed a heparin-based coacervate delivery system to provide sustained, localized release of HB-EGF in a chronic wound environment. We designed a simple polycation, poly(ethylene argininylaspartate diglyceride)

(PEAD), that self-assembles with heparin to form a complex coacervate, a liquid-liquid separation held together by electrostatic interactions between oppositely charged molecules. HB-EGF is bound to heparin and thus encapsulated by the liquid coacervate droplets and separated from the aqueous environment. The coacervate may then be applied directly to the wound and covered with an occlusive dressing where it will slowly and steadily release HB-EGF [141]. This delivery system is ideal for HB-EGF as it offers both protection from proteolytic degradation, and potentiation of GF bioactivity by mimicking the signaling environment in normal wounds where healing proceeds unhindered. The aim of this study is to evaluate the potential of HB-EGF coacervate as a therapy for diabetic wound healing using a genetically type 2 diabetic mouse model. We expect the impact of this heparin-based coacervate to extend beyond treatment for diabetic wounds. We believe it is a platform technology for delivery of any heparin-binding factor and combinations thereof for many applications.

3.6 MATERIALS AND METHODS – DIABETIC WOUND HEALING

3.6.1 HB-EGF coacervate preparation

PEAD was synthesized as we have described previously [249]. PEAD and heparin USP (Scientific Protein Labs, Waunakee, WI) were each dissolved in 0.9 % saline at 10 mg/ml and filtered at 0.22 μm to sterilize. Heparin was initially combined with recombinant human HB-EGF (R&D Systems, Minneapolis, MN) and PEAD was then added. Immediately following addition of the polycation the HB-EGF coacervate self-assembled and was visible as a turbid solution.

3.6.2 Diabetic mouse wound healing model

Approval was received by the University of Pittsburgh's Institutional Animal Care and Use Committee (IACUC) prior to beginning all animal work. Male 10-week old NONcNZO10/LtJ mice (Jackson Labs) were fed a minimum 10 % fat diet to maintain their diabetic phenotype. Blood glucose was assessed prior to wounding and at the time of sacrifice using an AlphaTRAK veterinary glucometer (Abbott). A blood glucose level of 200 mg/dL was considered diabetic and animals with lower levels were excluded from the study. Mice were anesthetized with isoflurane and dorsal hair was removed with depilatory cream (Nair). Two identical 5 mm full-thickness wounds including the panniculous carnosus were created using a round skin biopsy punch. Saline, 1 µg Free HB-EGF, or 1 µg HB-EGF coacervate was applied to the wound by sterile pipet as a 10 µl solution. Both wounds on each mouse received the same treatment to avoid cross-contamination. A Polyskin II hydrocolloid dressing (Tyco Healthcare) was applied followed by Coban self-adhesive wrap (3M) around the midsection. Animals were sacrificed on days 3, 7, 14, and 28 and wounds and surrounding tissue were collected for histological analysis.

3.6.3 Histological analysis

Skin tissue was immersed in Tissue-Tek O.C.T. Compound (Sakura), frozen, and 5 µm sequential sections were cut using a MICROM HM525 cryomicrotome (Thermo Fisher Scientific). Only sections from the center of the wound were used for analysis. Slides were fixed in 2% paraformaldehyde and blocked in 5% normal goat serum (Sigma) for 1 h at 37 ˚C. Primary antibodies used included rabbit anti-wide spectrum cytokeratin (1:200, Abcam), rabbit anti-Ki-67 (1:400, Abcam), rabbit anti-vWF (1:400, Abcam) and anti-α-SMA (1:500, Sigma). Primary

antibodies were incubated for either 1 h at 37 ˚C or overnight at 4 ˚C. Goat anti-rabbit IgG Alexa Fluor 488 and Alexa Fluor 594-conjugated secondary antibodies (1:200, Invitrogen) were incubated for 45 m at 37 ˚C. All slides were counterstained with DAPI (Sigma). Slides were also stained with hematoxylin and eosin (Ricca) or with Picosirius Red Stain Kit (Polysciences Inc.) following the manufacturer's protocols. All images were acquired using an Eclipse Ti inverted microscope (Nikon) and all image analyses were performed using NIS Elements Version 3.2 software (Nikon).

3.6.4 Wound healing assessments

Re-epithelialization was measured in day 3 and day 7 wound sections stained for pan-cytokeratin. The total wound length (WL), left neo-epithelial length (LL), and right neo-epithelial length (RL) were measured using the innermost hair follicles on each side to delineate the wound margins. Percent re-epithelialization was calculated as: Re-epithelialization (%) = [(LL+RL)/WL] *100 %. Proliferating keratinocytes were identified in day 3 wound sections stained for pan-cytokeratin and Ki-67 as cells co-expressing these markers in the basal layer of the neo-epidermis. The number of these cells beyond the wound margin was counted and normalized to the total number of DAPI nuclei counted in the basal epidermis. Collagen content was measured in day 14 and day 28 wound sections stained with Picosirius Red. Wounds were observed under polarized light which illuminates collagenous structures bright red. The wound zone perimeter was traced as the region of interest and area fraction positive for collagen was quantified using image thresholding. Wound contraction was evaluated in day 14 and day 28 sections stained with hematoxylin and eosin. The gap between wound margins, indicated by the innermost hair follicles on each side of the wound, was measured and reported as the contraction

gap. Blood vessels were observed in day 28 wound sections stained for vWF and α-SMA. The number of endothelial tubes was counted as vWF-positive cross-sectional or longitudinal tubes in the neo-dermal region. Mature vessels were counted as those endothelial tubes which also had adjacent α-SMA-positive cells. Both measurements were normalized to the total wound area (mm^2) for each wound.

3.6.5 Keratinocyte scratch migration assay

Diabetic and normal human epidermal keratinocytes (Lonza) were cultured in Keratinocyte Growth Medium-Gold (Lonza) and used at between passages 3-4. Cells were seeded at $2x10^6$ per well in a 24-well plate and cultured to confluency. A single scratch was made through the center of each well using a 1 ml pipette tip and wells were then rinsed once with DPBS to remove cell debris and 0.5 ml media was added. HB-EGF dosages of 10, 100, or 250 ng/ml were added to the media in free-form or incorporated within the coacervate, formed at a 500:100:1 mass ratio of PEAD:heparin:HB-EGF. One group of DHEK and the NHEK received no HB-EGF as controls. Scratch width was measured in the center of 3 wells per group at 0, 6, 12, and 18 hours and reported as percent scratch closure.

3.6.6 Statistical analysis

Statistical analysis was performed using Minitab 16.0 software (Minitab Inc., State College, PA). Data was tested for normality and equal variance before analysis. Statistical differences were calculated using analysis of variance (ANOVA) followed by Tukey post-hoc testing. Differences were considered significant at $p < 0.05$.

3.7 RESULTS – DIABETIC WOUND HEALING

3.7.1 HB-EGF coacervate accelerates re-epithelialization of diabetic wounds

To evaluate the effects of HB-EGF in diabetic wounds, we used the NONcNZO10/LtJ strain of genetically type 2 diabetic mice available from Jackson Labs. Although porcine skin is most similar to that of humans, there is no established porcine model that captures the pathology of type 2 diabetes. Of the rodent models currently available, the NONcNZO10/LtJ best resembles the presentation of type 2 diabetes in humans [250-252]. We created 5 mm full-thickness excisional dorsal wounds, then applied a single dose of HB-EGF coacervate (containing 1 μg HB-EGF), the same amount of HB-EGF in free-form, or saline only, and we tracked their healing over 4 weeks. We first assessed the rate of re-epithelialization, characterized by epithelial cell migration into the wound to form a new protective epidermis. We identified epidermal cells in the wounds by immunofluorescence staining for cytokeratin and reported their lengths of migration as a percent of the total wound length (**Fig. 16a**). Three days after wounding, we observed that HB-EGF coacervate had significantly increased re-epithelialization compared to the other groups (**Fig. 16b**). Furthermore, the same 1 μg dose of HB-EGF applied in free-form without the protection of the coacervate showed no significant difference from the saline group. This trend continued to day 7, at which point re-epithelialization in the HB-EGF coacervate group was more than 85 % complete whereas in saline and free HB-EGF groups it was less than 55 %. These data indicate that HB-EGF coacervate can induce diabetic mouse epidermal cell migration and we next evaluated its effect on their proliferative capacity.

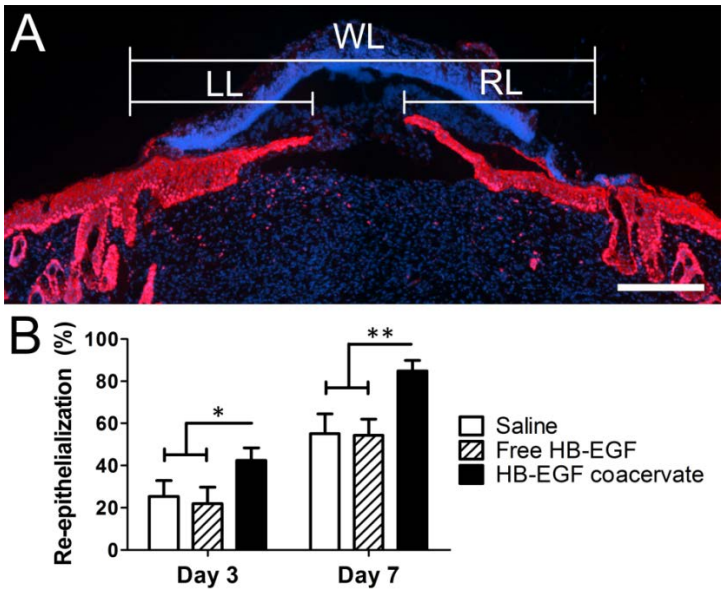

Figure 16. Wound re-epithelialization on day 3 and day 7. (*A*) Wound sections were stained for pan-cytokeratin (red) and counterstained with DAPI (blue). Re-epithelialization was measured as the percentage of the total wound length (WL) covered by both the right (RL) and left neo-epithelial lengths (LL). Bar = 100 μm. (*B*) Percent re-epithelialization measured on day 3 and day 7. Data represent means ± SD of 6-8 wounds per group per timepoint, *$p < 0.05$, **$p < 0.01$.

3.7.2 HB-EGF coacervate stimulates diabetic keratinocyte proliferation

In the classical paradigm of wound repair, keratinocyte proliferation occurs in order to contribute to the re-epithelialization process, however it is limited to the cells located at the wound margin [253]. We wondered if stimulation by HB-EGF throughout the wound bed might encourage epidermal cells to maintain their proliferative capacity even as they migrated into the wound. We identified proliferating keratinocytes in the basal layer of the neo-epidermis by immunofluorescence staining for Ki-67, which is exclusively expressed in the nucleus of cells in

active cell cycle [254]. As expected, in the saline and free HB-EGF treated wounds, Ki-67^{+} keratinocytes were mostly located at the wound margin on day 3 (**Fig. 17a,b**), and only 24% and 28% of keratinocytes beyond the wound margin were proliferative, respectively (**Fig. 17d**). On the other hand, 61% of keratinocytes beyond the wound margin were positive for Ki-67 in HB-EGF coacervate treated wounds and these cells were distributed throughout the basal neo-epidermis, even out to the tip of the leading edge (**Fig. 17c**). These results demonstrate that HB-EGF can increase keratinocyte proliferation during diabetic wound repair, provided sufficient concentrations of active GF exist in the wound bed. They also indicate that cell proliferation likely contributed to the faster re-epithelialization observed in HB-EGF coacervate wounds, although the relative contributions of migration and proliferation to this end require further investigation.

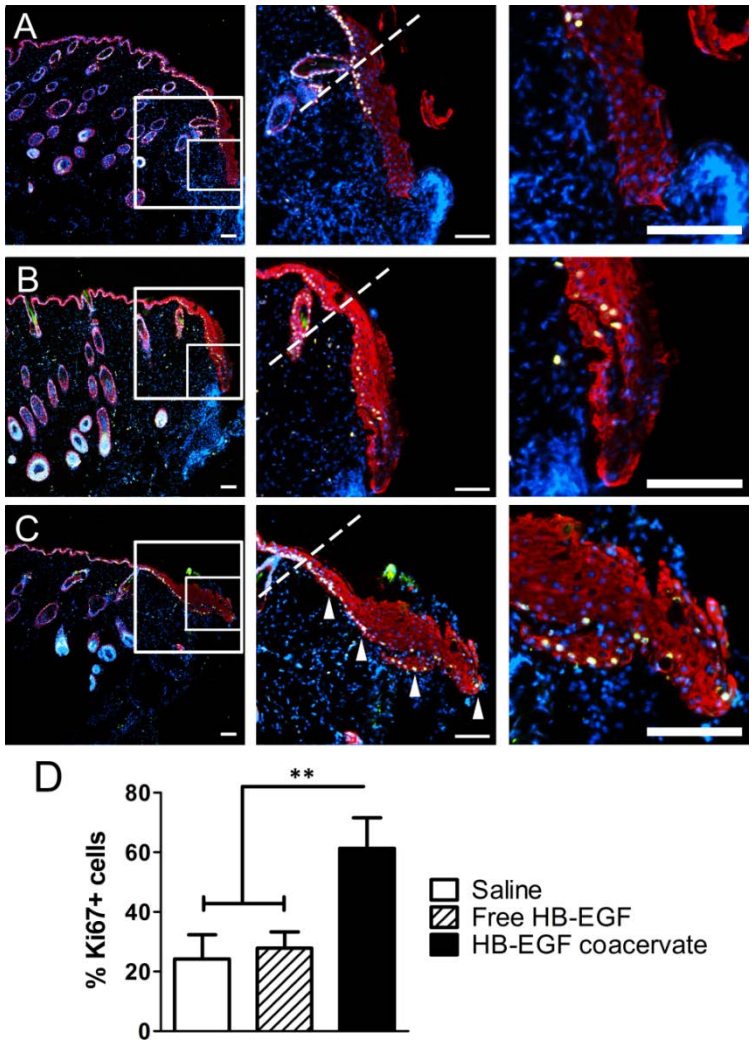

Figure 17. Basal keratinocyte proliferation on day 3. Wounds treated with (*A*), Saline (*B*) Free HB-EGF, or (*C*) HB-EGF coacervate, were stained for pan-cytokeratin (red), Ki-67 cell proliferation marker (green), and DAPI (blue), thus the nuclei of proliferating keratinocytes appear yellow. Indicated regions of the left column are magnified in the center and right columns. Dotted lines indicate the wound margin. Arrows indicate Ki-67^{+} keratinocytes in the basal neo-epidermis. Bars = 100 μm. (*D*) Ki-67^{+} cells beyond the wound margin were counted and reported as a percent of the total number of DAPI nuclei in the basal epidermis. Data represent means ± SD of 6-8 wounds per group, ***p* <0.01.

3.7.3 HB-EGF coacervate increases collagen deposition in diabetic wounds

To further test the benefit of HB-EGF coacervate in diabetic wound healing, we examined the wound granulation and remodeling processes after 2 and 4 weeks. We evaluated the quantity and arrangement of collagen fibers in Picosirius Red stained wound sections by polarized light microscopy. The stain accentuates the birefringent properties of collagen and allows observation as bright red fibers against a black background, permitting quantification of the collagen-positive area (**Fig. 18a**). Within the granulation region on day 14, there was a slightly greater collagen-positive area in HB-EGF coacervate wounds compared to others, yet this result was not statistically significant (**Fig. 18b**). However, by day 28 collagen content in wounds treated with HB-EGF coacervate was more than twice that of the other groups and closest to that of the normal NONcNZO10 mouse dermis (35.6 ± 8.7 %) with most fibers in parallel orientation, although the fibers are shorter and thinner. These data indicate that over 4 weeks, HB-EGF plays a role in the activities of dermal fibroblasts in the wound bed including provisional matrix remodeling and collagen deposition.

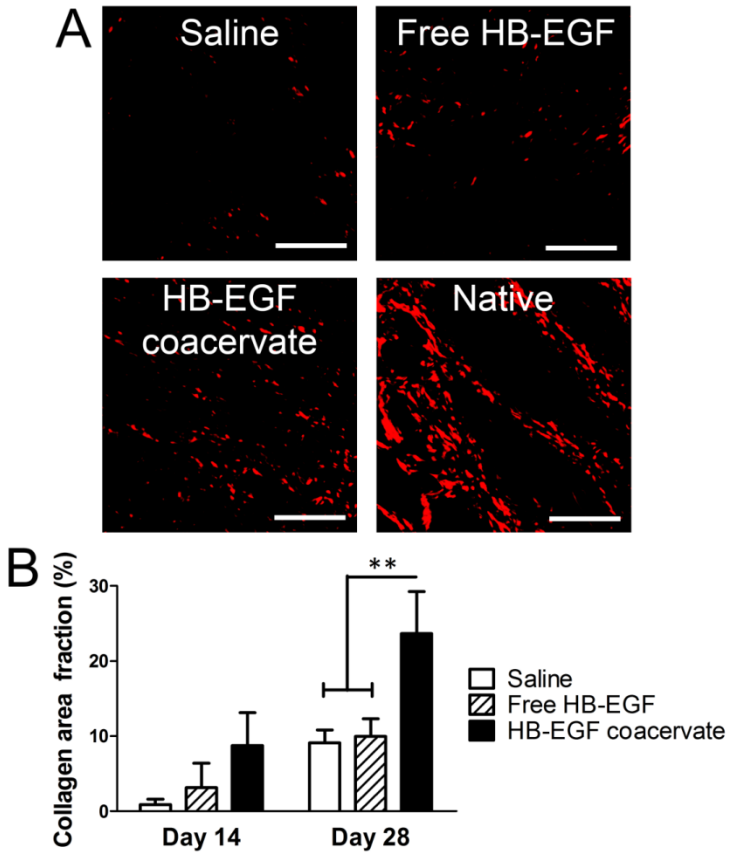

Figure 18. Collagen content of wounds on day 14 and day 28. (*A*) Representative images of day 28 wounds and normal skin stained with Picosirius Red and evaluated under polarized light to observe collagen. Bars = 100 μm. (*B*) The percent of the wound region positive for collagen was quantified. Data represent means ± SD of 6-8 wounds per group per timepoint, $^{**}p < 0.01$.

3.7.4 HB-EGF coacervate enhances diabetic wound contraction

The functional readout of a healthy, collagenous wound matrix is wound contraction. During this process myofibroblasts anchor to the collagen fibers and begin to pull the wound margins together. We evaluated wound contraction at week 2 and week 4 by measuring the gap between the wound margins, identified by the innermost hair follicle on each side of the wound (**Fig. 19a-**

c). On day 14, wounds treated with HB-EGF coacervate had a significantly smaller contraction gap compared to saline treated wounds (**Fig. 19d**). Although free HB-EGF appeared to have a small beneficial effect on contraction at 2 weeks, it was not significantly different from either group. On day 28, contraction in HB-EGF coacervate treated wounds was nearly complete and the contraction gap was significantly smaller than in both the saline and free HB-EGF groups. Clearly, the robust collagen matrix in HB-EGF coacervate wounds preceded an improved contraction response and faster wound closure.

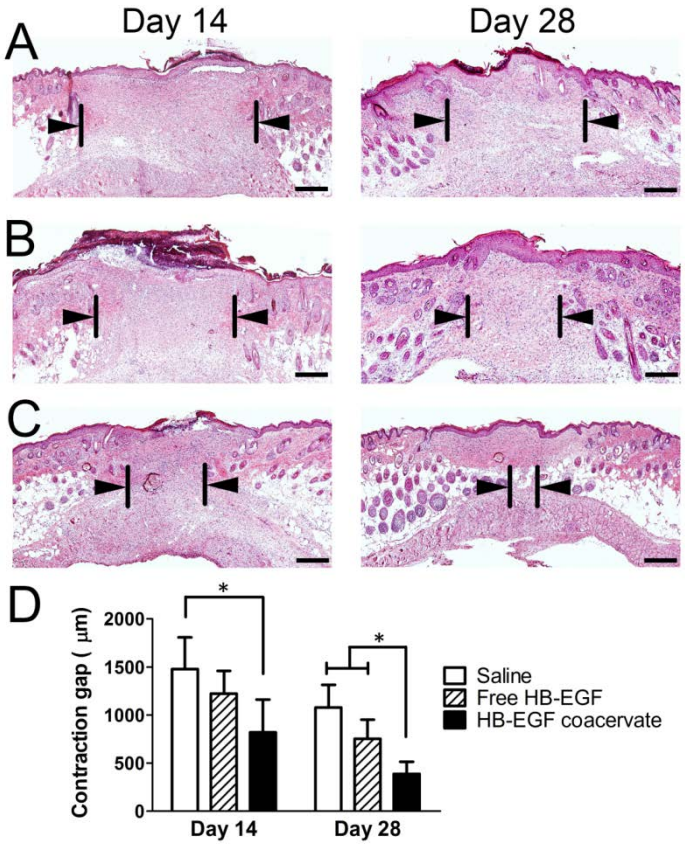

Figure 19. Wound contraction on day 14 and day 28. Wounds treated with (*A*) Saline, (*B*) Free HB-EGF, or (*C*) HB-EGF coacervate were stained with hematoxylin and eosin. Arrows indicate boundaries of the

contraction gap. Bars = 500 μm. (*D*) Wound contraction was quantified by measuring the gap between the wound margins. Data represent means ± SD of 6-8 wounds per group per timepoint, $*p < 0.05$.

3.7.5 HB-EGF coacervate encourages diabetic wound re-vascularization

Another sign of neo-dermal maturity is the formation of blood vessels to support the new tissue. We used immunofluorescence staining to evaluate the vessel numbers present in the granulation region on day 28, staining for von Willebrand Factor (vWF) as an endothelial cell marker and alpha smooth muscle actin (α-SMA) to identify mural cells (pericytes or smooth muscle cells) (**Fig. 20a**). We found significantly more endothelial tubes within the neo-dermis of HB-EGF coacervate treated wounds compared to others (**Fig. 20b**), and also more mature vessels, classified as those endothelial tubes which had mural cell stabilization (**Fig. 20c**). These data demonstrate that sustained delivery of HB-EGF can promote angiogenesis in a diabetic wound environment. We conclude that HB-EGF coacervate treatment leads to an advanced state of healing compared to saline and free HB-EGF treatment by 4 weeks after wounding.

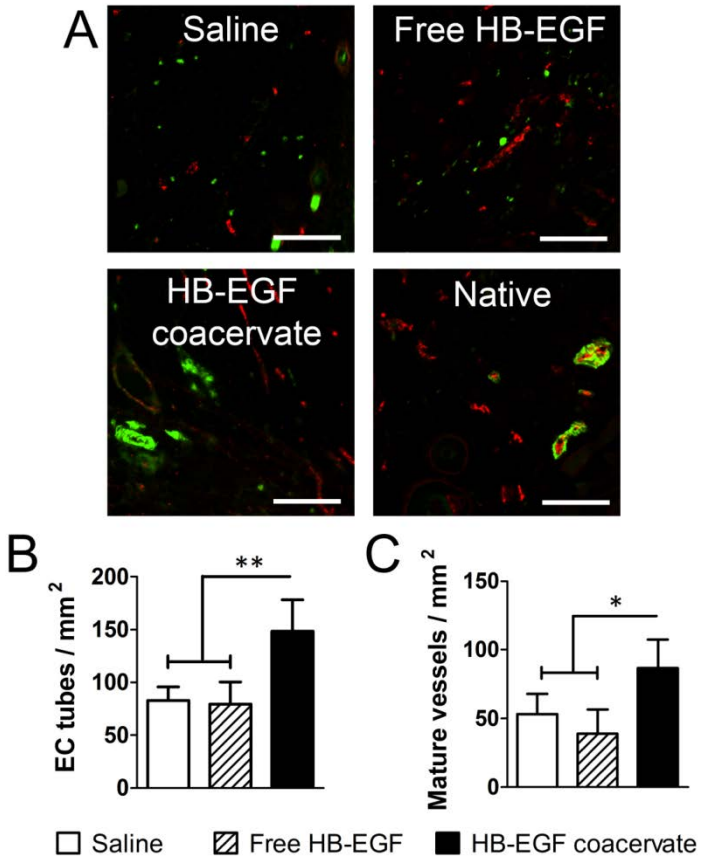

Figure 20. Wound re-vascularization on day 28. (*A*) Wounds and normal skin were stained for vWF (red) to indicate endothelial cells and α-SMA (green) for mural cells. Bars = 100 μm. (*B*) Endothelial cell (EC) tubes were identified as vWF^{+} vessel structures and quantified. (*C*) Mature vessels were identified as endothelial tubes stabilized by mural cells and quantified. Data represent means ± SD of 6-8 wounds per group, **p* <0.05, ***p* <0.01.

3.7.6 HB-EGF coacervate stimulates migration of diabetic human cells *in vitro*

As a test of clinical relevance, we assessed the effect of HB-EGF coacervate on diabetic human epidermal keratinocytes (DHEK) in a scratch wound migration assay. We scratched confluent monolayers of the cells to mimic epithelial injury and then measured the percent scratch closure by cell migration. With no HB-EGF added, DHEK displayed impaired migration by 18 h post-

wounding compared to normal human epidermal keratinocytes (NHEK) (**Fig. 21a**). However, 10 ng/ml of HB-EGF, both free and in the coacervate, significantly increased DHEK migration by 6 h, and the scratches were completely healed by 12 h (**Fig. 21b**). Overexpression of HB-EGF has been previously shown to exert an inhibitory effect on epithelial cells [162]. Consistent with those findings, we observed no significant benefit of free HB-EGF at concentrations of 100 ng/ml at 6 h and 250 ng/ml at 12 and 18 h (**Fig. 21c,d**). On the other hand, those same concentrations of HB-EGF delivered by the coacervate did significantly stimulate cell migration compared to the DHEK control group and the corresponding free HB-EGF group. These data demonstrate that HB-EGF coacervate can stimulate diabetic human cells and can circumvent the limitations of free GF administration.

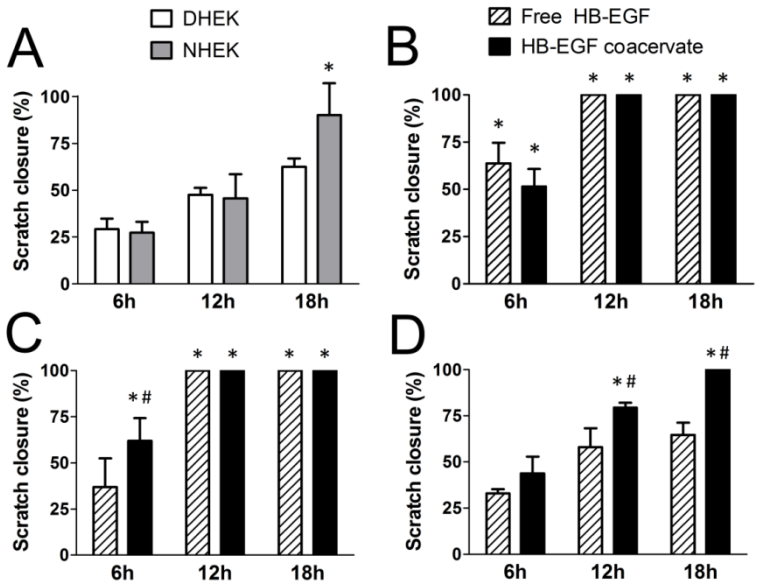

Figure 21. In vitro scratch wound migration assay with human keratinocytes. (*A*) NHEK or DHEK cultured with no HB-EGF as controls. (*B*) DHEK cultured with 10 ng/ml HB-EGF free or in the coacervate (*C*) DHEK cultured with 100 ng/ml HB-EGF free or in the coacervate (*D*) DHEK cultured with 250 ng/ml HB-EGF free or in the coacervate. Data represent means ± SD of 3 samples per group per timepoint, $*p < 0.05$ compared to

DHEK control group at similar timepoint, #$p < 0.05$ compared to free HB-EGF group at similar timepoint and dosage.

3.8 DISCUSSION – DIABETIC WOUND HEALING

Conventional treatment of diabetic ulcers includes debridement, off-loading pressure, and maintenance of a moist wound environment with frequent dressing changes [242]. If wounds do not show signs of healing with standard treatment, advanced biological therapies are employed such as Regranex, the only recombinant GF therapy currently approved by the FDA for skin wound healing [255]. Regranex contains recombinant human platelet-derived growth factor suspended in a carboxymethyl cellulose gel which offers minimal protection of the GF, leaving it prone to rapid degradation in the protease-rich wound environment [245]. Frequent applications and high doses are therefore necessary to produce a positive, albeit marginal effect on healing outcomes [256]. However, high doses also pose a risk of inducing tumor formation [69] and can also be cost-prohibitive in low- and middle-income countries where diabetes is also prevalent [241]. Unfortunately, these shortcomings have significantly limited its clinical use [257, 258]. Dosage reduction is therefore a key aim of our approach. In this study, we used a GF dosage per wound area that is approximately 1000-fold lower than Regranex. Furthermore, the coacervate is phase-separated from wound fluid which keeps the GF localized to site of application by preventing systemic uptake. Altogether, we do not anticipate undesirable side effects of this therapy in humans.

The half-life of HB-EGF after intravenous and gastric administration is 26 m and 11 h, respectively [259] and is likely to be even shorter in a wound environment which has high

proteolytic activity [245]. Consequently, numerous delivery systems have been developed for protection and sustained release of epidermal growth factor (EGF) family proteins and tested in animal models of diabetic wounds [4]. One focus has been employment of sulfated proteoglycans such as heparan sulfate, which play a key role in the human body of providing stabilization, localization, and potentiated bioactivity of signaling molecules [9, 260]. These benefits have motivated the incorporation of heparin or heparin-mimetic components into many different types of delivery systems for proteins [261]. However, few systems use heparin in its native form, unconjugated to any scaffold or gel. Covalent conjugation may affect its properties such as its charge density and macromolecular structure which could reduce its binding affinity to certain proteins which rely on specific oligosaccharide sequences [262-264]. Several benefits of heparin in its native form have been elucidated by complexing it with peptide amphiphiles for protein delivery [15, 265]. Intact heparin is particularly appealing for delivery of HB-EGF as it is required for binding and phosphorylation of EGF cell receptors [247, 248]. This motivated our development of a simple delivery system utilizing intact heparin to load HB-EGF and facilitate its biological activities.

PEAD is a synthetic polycation designed to mimic the strongly cationic domain of the fibroblast growth factor receptor which interacts with heparin through polyvalent charge attraction [11, 12]. By similar mechanism, PEAD:heparin:GF complexes self-assemble and form micron-sized coacervate droplets which are phase-separated from water and thereby protect the incorporated GF from proteolysis [249]. Preservation of heparin in its native conformation enables its interaction with cell receptors and potentiates GF bioactivity [20, 21, 136, 160, 166, 169]. The coacervate incorporates 1 μg HB-EGF with greater than 92% loading efficiency and then releases approximately 15 ng per day with no initial burst release [141]. PEAD was

designed with a hydrolytically cleavable backbone, resulting in slow biodegradation which releases HB-EGF and heparin. Release may also occur in part by disassembly of the coacervate due to ionic interference. PEAD has been demonstrated to be non-cytotoxic; it does not elicit an appreciable inflammatory response or any adverse effects when injected subcutaneously in rats [249]. We have also demonstrated that the unloaded coacervate has no significant effect on the healing process of excisional wounds in mice [141]. For these reasons we elected not to include the coacervate alone as a control group in this study.

NONcNZO10 mice were selected for this study from numerous diabetic mouse models available. Unlike chemical induction with streptozotocin or the *db*/*db* monogenic strain, NONcNZO10 mice display moderate obesity, whole-body insulin resistance, and an age-associated progression of metabolic abnormalities resembling those of the human diabetic condition [252]. The shortcomings of monogenic models in replicating a polygenic disease like diabetes mellitus are underscored in studies showing that wound closure rates of *db*/*db* mice do not correlate with the severity of their diabetic condition [250, 266]. On the other hand, models with polygenic etiology provide a better representation of the genetic and metabolic profiles of diabetes in humans. In a recent comparison of four common diabetic mouse strains, only NONcNZO10 mice exhibited impairment in every step of the wound healing cascade [250]. It is worth noting that a second polygenic strain, TallyHo/JnJ, displays similar phenotype to NONcNZO10 and will also prove useful for studies of diabetic wound healing in the future [251].

We previously reported that coacervate delivery of HB-EGF accelerates scratch wound closure of NHEK and avoids the inhibitory effect of HB-EGF on keratinocyte proliferation *in vitro* [141]. We also demonstrated *in vivo* that HB-EGF coacervate accelerates re-

epithelialization and stimulates keratinocyte proliferation in full-thickness wounds on C57BL/6 mice [141]. We performed similar evaluations in diabetic wounds as reduced cell proliferation is one key complication leading to non-healing chronic ulcers [22]. We observed more than twice the number of Ki-67^{+} cells in HB-EGF coacervate treated diabetic wounds compared to saline treatment. Moreover, these cells were distributed out to the tips of epithelial leading edges, whereas proliferative cells in saline wounds were mainly limited to the margins as is typical [203]. These results indicate that, additional to enhanced migration, keratinocyte proliferation also contributed to wound re-epithelialization. We conclude that stimulation of diabetic keratinocytes by HB-EGF coacervate is sufficient for them to overcome several phenotypical impairments of their diabetic condition.

HB-EGF plays an important role in the process of remodeling the largely fibrin-based provisional matrix to a robust collagenous matrix [246]. The quantity and quality of collagen deposited is critical to other processes such as wound contraction and re-vascularization. Unfortunately, matrix remodeling is often severely impaired in chronic wounds [24, 267]. Nonetheless, we found the collagen content of HB-EGF coacervate treated wounds to be significantly higher than that of other groups after 4 weeks of healing. Consequently, wound contraction was also accelerated because myofibroblasts were able to securely attach to the collagen matrix and begin to pull the wound margins together. Taken together, these data demonstrate that sustained release of HB-EGF in a diabetic wound environment can stimulate dermal fibroblasts to improve the overall wound maturation process and contribute to timely closure.

Angiogenesis is a critical process in the wound healing cascade which provides oxygen, nutrients, and cells the wound bed and contributes to waste removal [268]. HB-EGF has been

previously demonstrated to promote angiogenesis through some direct and some indirect pathways acting on endothelial cells and vascular smooth muscle cells [205, 206, 269, 270]. Our results indicate that HB-EGF coacervate increases the numbers of both neo-vessels and stable, mature vessels in diabetic wounds after 4 weeks of healing.

We and others have reported that the migratory capacity of NHEK is enhanced by HB-EGF [141, 203]. Here, we demonstrate that HB-EGF has a similar effect on diabetic cells. Low concentration (10 ng/ml) of HB-EGF, both free and in the coacervate, significantly stimulated DHEK migration compared to control groups. However, higher concentrations of free HB-EGF did not have this effect. The benefit of controlled release is apparent when the same concentrations of HB-EGF in the coacervate did successfully stimulate DHEK. These results indicate that the coacervate alters the concentration of HB-EGF available to cell receptors, avoiding the inhibitory effect of high dosages which oversaturates receptors [141, 162]. Furthermore, we proved that diabetic human cells respond well to HB-EGF released from the coacervate, which clears a major translational hurdle towards making this experimental therapy a clinical reality.

3.9 CONCLUSIONS

This study assesses the benefit of a controlled release approach to the utility of HB-EGF therapy for wound healing. We demonstrated that sustained coacervate-based delivery of HB-EGF significantly accelerated wound closure within 17 days, while free growth factor application had no effect on closure rate compared to controls. Keratinocyte migratory capacity was significantly

increased and proliferative capacity was maintained by HB-EGF coacervate. This led to accelerated wound re-epithelialization which was accompanied by healthy granulation tissue formation and angiogenesis. These results suggest that coacervate-based controlled delivery of HB-EGF can induce fast and comprehensive healing of cutaneous wounds.

In summary, we elucidated the multifunctional role of HB-EGF in the chronic wound healing process, provided sufficient levels exist in the wound bed. HB-EGF released from the coacervate stimulated human keratinocyte migration *in vitro*, and in a diabetic wound model enhanced re-epithelialization, wound matrix remodeling, and wound contraction and re-vascularization. HB-EGF coacervate represents a promising regenerative therapy for diabetic wounds. In the future, the efficacy of this HB-EGF coacervate will be evaluated using diabetic pigs, which are the standard pre-clinical model for therapies to treat diabetic wounds.

4.0 CONTROLLED DELIVERY OF SONIC HEDGEHOG TO PROMOTE CARDIAC REPAIR

4.1 INTRODUCTION

Ischemic heart disease is now the leading cause of death in the U.S. and worldwide [271]. Myocardial infarction (MI) is the most prevalent life-threatening manifestation of progressed heart disease and those who survive often develop congestive heart failure [170]. Heart failure afflicts 5.7 million Americans, a prevalence that is expected to rise 25% by 2030 [272]. The treatments patients currently receive after MI aim to slow the progression of heart failure [273], with total heart transplantation being the gold standard; still there is insufficient donor availability and is not without complications [274]. Thus new therapies seeking to preserve and regenerate the patient's own heart following MI are urgently needed.

Numerous candidate technologies have been developed for alleviating or reversing the damage caused by cardiac ischemia [275-277]. These technologies fall into two general categories: bioactive therapies or structural "bulking" therapies. The former aims to provide the necessary resources for tissue regeneration, and several therapeutic approaches including stem cells [278-281], growth factors [282], and gene therapy [283] have been evaluated in U.S. controlled clinical trials. On the other hand, the primary aim of structural therapies is to reinforce the damaged heart wall and thereby alleviate wall stress and prevent wall thinning and

ventricular dilation [276, 277]. Clinical trials have been initiated to evaluate intramyocardial injections of alginate and cell-seeded collagen [284]. However, no regenerative therapy, biological or structural, has shown enough promise to receive FDA approval.

The best therapy may involve “master switch” agents which activate multiple downstream pathways [285]. Sonic hedgehog (Shh) is one such master regulator, acting as a powerful morphogen during development when it typically influences cell fate but can also affect cell growth and survival [286, 287]. Shh signaling remains active in the adult mammalian heart at very low levels though it is upregulated during ischemic heart injury such as myocardial infarction (MI) and congestive heart failure [163, 288]. Currently, damage to the adult heart is considered permanent as cardiomyocytes have limited proliferative capability and fibrosis occurs post-MI instead of healing [273, 289]. However, during development, when cardiac tissue patterning is controlled by powerful morphogens such as Shh [290], the embryonic mammalian heart briefly displays the ability to regenerate itself [291]. Temporarily recapitulating this embryonic signaling environment through exogenous application of cardiac morphogen Shh is therefore a possible approach towards repair of the damaged adult heart.

Shh has previously been applied to the heart as a free protein. Direct injection has been shown to restore blood flow in a critical hindlimb ischemia model [164]. However, this approach is highly inefficient due to short morphogen half-lives in the body [292] and therefore requires multiple injections. High dosage is also necessary to elicit a desired effect which is expensive and may carry similar safety concerns to gene therapy. Investigations using gene therapy [163, 293] and transduced cell therapy [165] have been shown to improve cardiac function following MI. However, both of these approaches carry high risk of inducing tumor formation, especially considering the potency of morphogens [294], and thus trials have not progressed beyond large

animal models. On the contrary, a controlled delivery approach provides stabilization and protection of Shh and can release it slowly to maintain a constant local concentration within the therapeutic range.

We developed a controlled delivery system comprised of heparin and a synthetic polycation that interact polyvalently and phase separate from water to form sub-micron sized spherical droplets. These emulsion-like aggregations are referred to as a "coacervate". Shh is incorporated into the coacervate by high-affinity binding to heparin and is then released in a slow and sustained fashion. We demonstrate that Shh delivered by the coacervate can have multiple beneficial effects on cardiac cells, stimulating trophic factor expression and affording cytoprotection from oxidative stress, and may therefore have the potential to protect the heart from ischemia or promote tissue regeneration following insult. This is, to the best of our knowledge, the first investigation of controlled delivery of Shh for cardiac repair.

Poly(ethylene glycol) (PEG) is a suitable hydrogel material because it has variable stiffness based on concentration and crosslinking, and it is biologically inert [295]. We have previously described the structural benefit of a non-degradable PEG hydrogel, which prevented early LV wall thinning and dilation. However, it was unable to mitigate long-term pathological remodeling, likely due to chronic inflammation [296]. We were therefore motivated to develop a PEG gel crosslinked by peptides which were matrix metalloproteinase (MMP)-specific. The degradable nature of this hydrogel appeared to pacify the issue of chronic inflammation, however functional improvement was only observed if injection was delayed until 1 week after infarction [297]. On the other hand, cytoprotective therapies such as Shh will be most effective if applied as soon as possible after ischemic event. We therefore elected to include interleukin-10 (IL-10), an

anti-inflammatory cytokine that could temporarily reduce gel degradation by diminishing the inflammatory response to MI.

The anti-inflammatory effects of IL-10 are due, in part, to a downregulation of IL-1β, IL-6, and TNF-α signaling [298]. IL-10 thereby restricts macrophage activation and phagocytic capacity [299], and promotes their transition from the M1 to the M2 phenotype which is critical to enable tissue regeneration [300]. IL-10 expression in the infarcted human myocardium has been positively correlated with improved ventricular function [301], and direct injection of IL-10 attenuated ventricular remodeling in mice [302]. Furthermore, heparin binds IL-10 with high affinity (K_d = 54 nM) and modulates its bioactivity [303], providing rationale for its delivery with the heparin-based coacervate alongside Shh.

Here we describe a co-therapy of a controlled release Shh and IL-10 coacervate distributed within an MMP-degradable PEG hydrogel. The combination of regenerative molecules and a structural bulking agent has significant potential for synergistic effects. While the hydrogel may improve coacervate retention within the heart wall after injection, the regenerative environment engendered by Shh and IL-10 may improve gel integration and prolong its structural benefit. We evaluated this combinatorial therapy using an established *in vivo* MI model of permanent coronary ligation in rats [304].

4.2 MATERIALS AND METHODS

4.2.1 Ethics statement

Animals were cared for in compliance with a protocol approved by the Institutional Animal Care and Use Committee of the University of Pittsburgh, following NIH guidelines for the care and use of laboratory animals (NIH publication No. 85–23 rev. 1985).

4.2.2 Shh coacervate preparation

Poly(ethylene argininylaspartate diglyceride) (PEAD) was synthesized as previously described [158]. PEAD and clinical-grade heparin (Scientific Protein Labs, Waunakee, WI) were each dissolved in 0.9 % saline at 10 mg ml^{-1} and 0.22 μm filter-sterilized. Heparin was initially complexed with recombinant mouse Shh (N-terminus peptide; R&D Systems, Minneapolis, MN), then PEAD was added. Self-assembly of PEAD and heparin:Shh immediately precipitated the ternary complex out of solution to form the Shh coacervate.

4.2.3 Shh coacervate imaging

Shh was fluorescently labeled using Alexa Fluor 488 Protein Labeling Kit (Invitrogen, Carlsbad, CA). A fluorescently labeled Shh coacervate was prepared in water with 0.2 ng fluorescently labeled Shh, 100 μg heparin, and 500 μg PEAD. The coacervate was added to a 96-well plate and imaged using an Eclipse Ti inverted microscope (Nikon, Tokyo, Japan).

4.2.4 Shh release profile

200 µl Shh coacervate containing 10 µg heparin, 100 ng Shh, and 50 µg PEAD was prepared in 0.9% sterile saline and was then pelleted by centrifugation at 12,100 g for 5 min. The supernatant was aspirated and stored at -80 ^{0}C and 200 µl fresh saline was replaced to cover the pellet. The sampling procedure was repeated on day 1, 4, 7, 10, 14, and 21 for three separate tubes. Released Shh in the fractions was quantified by DuoSet ELISA kit (R&D Systems) according to the manufacturer's instructions.

4.2.5 Cardiac cell isolation

Primary cardiac cells were isolated from 1-2 day old Sprague-Dawley rat pups (Jackson Labs, Bar Harbor, ME). The pups' hearts were excised aseptically and the Worthington Neonatal Cardiomyocyte Isolation System (Worthington, Lakewood, NJ) was used following the manufacturer's instructions. Two pre-plates of 1.5 h each were used to separate cardiac fibroblasts (fast-adhering cells) from cardiomyocytes (slow-adhering cells). The purified cardiomyocyte population was seeded into 24-well plates coated with 1 µg cm^{-2} fibronectin (Millipore, Billerica, MA) at 1.5 x 10^{5} myocytes per well for experiments. Cardiomyocytes were cultured in DMEM/F12 50/50 supplemented with 5 % fetal bovine serum (FBS), ITS supplement (Sigma, St. Louis, MO), and 100 µM 5-bromo-2′-deoxyuridine (BrdU; Sigma) to inhibit proliferation of any remaining fibroblasts. Cardiac fibroblasts from the first pre-plate were cultured in DMEM supplemented with 10 % FBS through 3 passages before use in experiments.

4.2.6 Immunofluorescent staining

Immediately after isolation, purity of cardiac cell populations was analyzed by immunostaining using a mouse anti-myosin heavy chain (MHC) antibody (1:80, Millipore) followed by goat anti-mouse IgG Alexa Fluor 594-conjugated secondary antibody (1:200, Invitrogen) and counterstained with DAPI. All images were taken using an Eclipse Ti inverted microscope (Nikon).

4.2.7 Cardiac fibroblast growth factor signaling

Isolated neonatal rat cardiac fibroblasts were used at passage 4. 5 x 10^4 cells were seeded per well in a 24-well plate and cultured to 90 % confluency. Cells were then washed once with DPBS and 500 µl "stimulation media" containing 1mg ml^{-1} Shh free or in the coacervate, or normal culture media was added. After 6, 12, 24, 48 h the conditioned media from two wells per group was removed and frozen. Indirect ELISA was run using rabbit polyclonal antibodies against VEGF (1:50, Peprotech, Rocky Hill, NJ), SDF-1α (1:30, Santa Cruz Biotech, Santa Cruz, CA), and IGF-1 (1:30, Santa Cruz Biotech). Results were normalized to total protein content, determined using Pierce 660 nm Protein Assay (Thermo Fisher Scientific, Waltham, MA). For Shh quantification, western blot was employed with samples being denatured and reduced. Lacking a well-accepted protein loading control for conditioned media, total protein assay results were used to determine appropriate loading volumes for each sample, such that 47.5 µg protein was loaded to each well. Following transfer, the PVDF membrane was incubated for 5 m in Ponceau-S staining solution (Sigma), rinsed in DI water and imaged. Immunoblotting was then performed using a rabbit anti-human Shh polyclonal antibody (1:200, Santa Cruz Biotech)

followed by a peroxidase conjugated anti-rabbit IgG antibody (Sigma). Band intensities were measured using NIH Image J Version 1.46r software.

4.2.8 Cardiomyocyte oxidative stress-induced apoptosis

Isolated cardiomyocytes were cultured for 2 d after which cells were spontaneously contracting at approximately 1 beat per second. Cells were pre-treated for 48 h with 500 ng ml^{-1} Shh or recombinant human fibroblast growth factor-2 (FGF2; Peprotech) as either free protein or delivered by the coacervate. The FGF2 coacervate was prepared similarly to the Shh coacervate. Cells were then exposed to 200 μM H_2O_2 in serum-free media to induce oxidative stress. Two control groups received no growth factor pre-treatment and then one received H_2O_2 and one did not. After 2 h, cells were harvested, lysed, and assayed using EnzChek Caspase-3 Kit #2 (Invitrogen). Immediately before harvesting the cardiomyocytes, videos were taken in the center of the wells using an Eclipse Ti inverted microscope (Nikon) using standard light microscopy settings.

4.2.9 Coacervate and PEG hydrogel preparation

To prepare the coacervate, PEAD was synthesized as previously described [212]. PEAD and clinical-grade heparin (Scientific Protein Labs, Waunakee, WI) were each dissolved in DI water and 0.22 μm filter-sterilized. 0.33 mg Heparin was combined with 1.5 μg recombinant human Shh (Peprotech, Rocky Hill, NJ) and 150 ng recombinant human IL-10 (Peprotech), followed by addition of 1.65 mg PEAD. The coacervate was pelleted by centrifugation and the supernatant removed and discarded. To prepare the PEG hydrogel, vinyl sulfone-derivatized 8-arm PEG

(MW=20 kDa) was synthesized as previously described [296] and dissolved in PBS. MMP-1 (GenScript, Piscataway, NJ) was dissolved in PBS, then used to re-suspend the coacervate thoroughly. PEG and MMP-1 solutions were combined to form 10 % w/v PEG hydrogels of 100 µl total volume with the Shh+IL-10 coacervate homogeneously dispersed throughout.

4.2.10 Fluorescence labeling and imaging

The coacervate was prepared as described above, except fluorescein-labeled heparin (Creative PEGWorks, Winston Salem, NC) was used. The PEG hydrogel was labeled with Alexa Fluor 660 nm dye (Life Technologies, Carlsbad, CA) as previously described [297]. Fluorescent gel loaded with coacervate was immersed in optimal cutting temperature (OCT) compound (Sakura Finetek, Torrance, CA) and 12 µm frozen sections were cut by cryomicrotome. Images were captured using an Eclipse Ti inverted fluorescence microscope (Nikon, Tokyo, Japan).

4.2.11 Rat MI model

Animals were cared for in compliance with NIH guidelines and all experiments were approved by the University of Cape Town's Animal Research Ethics Committee. MI and intramyocardial injections were performed as we previously described [297]. Briefly, male Wistar rats (180-200 g) underwent permanent left anterior descending coronary artery ligation using 6-0 Prolene suture (Ethicon, Somerville, NJ). Treatments were applied immediately as 100 µl divided into 3 injections in evenly spaced around the infarct center thru a 31G needle. Treatment groups included saline (n=8), coacervate alone (n=10), PEG hydrogel alone (n=9), or gel and coacervate combined (n=10), and animals were randomized to the treatment groups.

4.2.12 Coacervate retention study

Fluorescence-labeled coacervate was prepared as described above and was injected into infarcts alone (n=4 rats), or in the PEG hydrogel (n=5 rats). After 24 h the animals were sacrificed and their hearts explanted and frozen in OCT. 10 µm thick sections were cut every 500 µm beginning at the apex and continuing through the entire heart. Fluorescence images of the infarct zone were acquired and Image J 1.47v was used quantify the percent area positive for the coacervate as: Percent positive area (%) = Coacervate positive area (mm^2) / Infarct zone area (mm^2) * 100 %. Results for each animal were the average of all sections taken for that animal.

4.2.13 Gel retention study

Fluorescence-labeled gel was prepared as described above with or without the coacervate and injected into the infarct zone (n=3 rats). The animals were sacrificed after 14 days and the hearts were frozen in OCT and sequentially sectioned at 6 µm thickness. Sections were observed by fluorescence microscopy and the area positive for gel (mm^2) was multiplied by the spacing thickness (500 µm) and summed to estimate the gel volume (mm^3).

4.2.14 Echocardiography

Echocardiography was performed prior to surgery and on days 14 and 28 by blinded investigator using a Vivid i Ultrasound imaging system (GE Healthcare, Little Chalfont, United Kingdom). Short-axis M-mode measurements of the LV were performed and fractional shortening (FS %)

was calculated as: (EDD - ESD) / EDD * 100 % (EDD=end-diastolic diameter, ESD=end-systolic diameter).

4.2.15 Histological analysis

Rats were sacrificed on day 28 and their hearts removed, rinsed in PBS, and fixed in 10 % formalin for 24 h. Hearts were processed through graded alcohol and xylene, paraffin-embedded, and 3 μm sections cut and then de-waxed. Heart sections were stained by Masson's trichrome as previously described [297].

4.2.16 Statistical analysis

Statistical analysis was performed using SPSS 16.0 software (SPSS Inc, Chicago, IL). Data was tested for normality and equal variance before analysis. Statistical differences between groups were calculated using one-way analysis of variance (ANOVA) followed by Tukey post-hoc testing. Differences were considered significant at $P<0.05$.

4.3 RESULTS

4.3.1 Shh coacervate characterization and release

Fluorescent imaging of the Shh coacervate revealed round droplets ranging from 0.5-10 μm in size (**Fig. 22**). Shh release from the coacervate into saline was sustained for at least 3 weeks with 80% being released in total (**Fig. 23**). Less than 5% Shh was detected in the supernatant

immediately after forming the coacervate and pelleting, therefore loading efficiency is greater than 95%. There was effectively no initial burst release. Of the 100 ng loaded, approximately 6 ng day^{-1} was released until day 10, then slowing to around 2 ng day^{-1} until day 21.

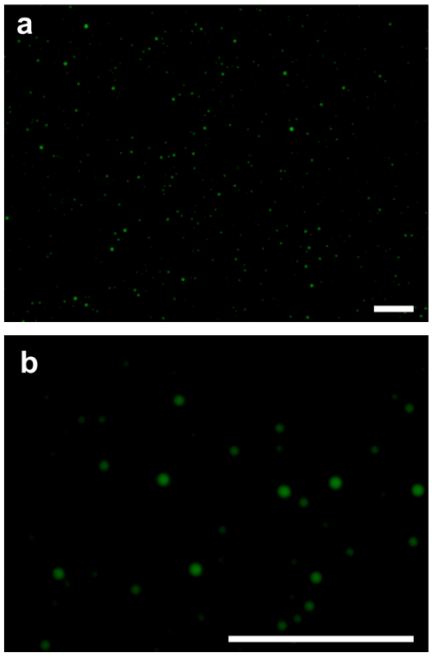

Figure 22. Shh coacervate imaging. Alexa Fluor 488-labeled Shh was incorporated into the coacervate in water and imaged by fluorescence microscopy. (a) 10X magnification. (b) 40X magnification. Scale bars = 100 μm.

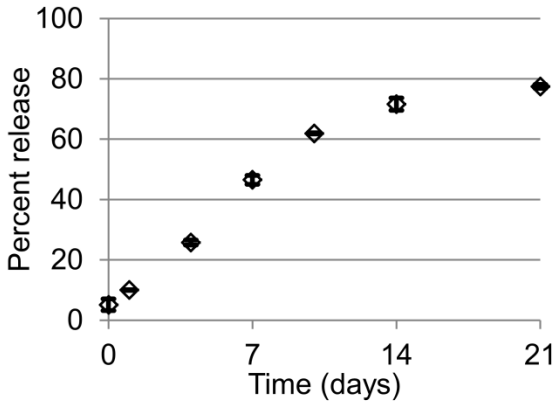

Figure 23. Shh release profile. *In vitro* release of Shh from the coacervate into saline over 21 days, quantified by sandwich ELISA. Percent release is relative to total amount loaded. Bars indicate means ± SD.

4.3.2 Shh coacervate upregulates growth factor secretion by cardiac fibroblasts

Isolated neonatal rat cardiac fibroblasts were stimulated with Shh, free or in the coacervate, and analyzed for expression of various growth factors over 2 days. Shh itself was detected in increasing concentrations, up to 7.8 times the initially added amount by 48h (**Fig. 24a**). VEGF, SDF-1α, and IGF-1 were at 2- to 4-fold higher levels by 6 hours after stimulation with both free Shh and Shh coacervate and remained upregulated for 48 h (**Fig. 24b-d**). The VEGF level at the 6 hour timepoint stimulated by Shh coacervate was significantly greater than that stimulated by free Shh. Conditioned media from cells treated with normal culture media had undetectable concentrations of all growth factors tested at every timepoint (data not shown).

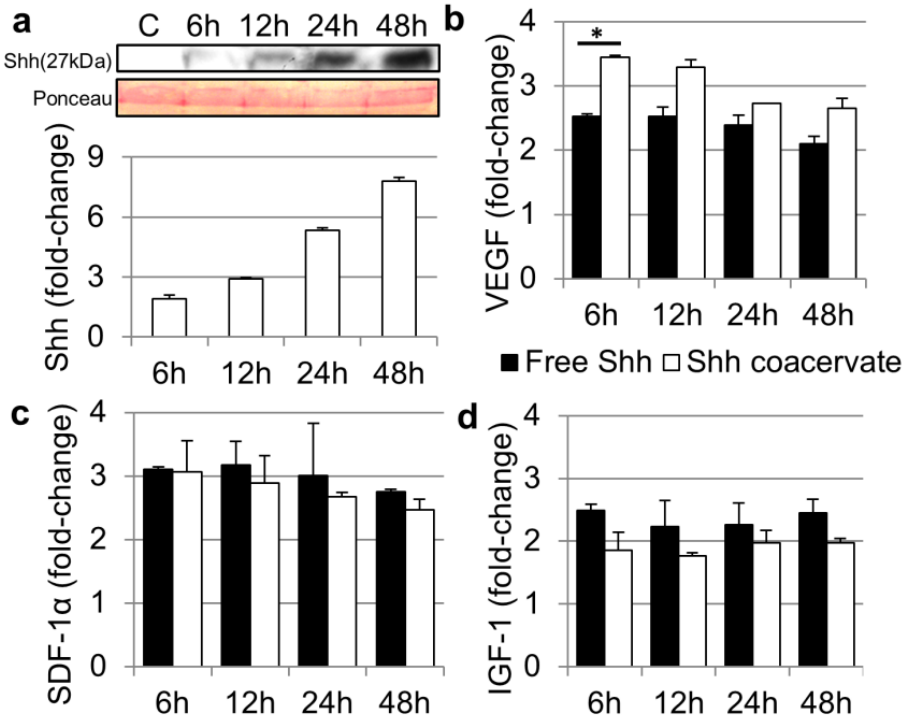

Figure 24. Shh-stimulated cardiac fibroblast signaling. Near-confluent cardiac fibroblasts were incubated with Shh, free or in the coacervate, and growth factor levels in the conditioned media were assessed after 6, 12, 24, and 48h. Data is presented as a fold-change from the stimulation media (C). Bars indicate means ± SD. (a) Quantification of Shh concentration in the cardiac fibroblast-conditioned media by western blot. Ponceau-S staining of protein bands near 27 kDa is shown as the loading control. (b) Quantification of VEGF in the cardiac fibroblast-conditioned media by indirect ELISA, **P*<0.05. (c) Quantification of SDF-1α in the cardiac fibroblast-conditioned media by indirect ELISA. (d) Quantification of IGF-1 in the cardiac fibroblast-conditioned media by indirect ELISA.

4.3.3 Shh coacervate protects cardiomyocytes from apoptosis

Caspase-3 is a well-known indicator of cell apoptosis due to oxidative stress, mimicked here with 200μM H_2O_2 in culture media. This concentration of H_2O_2 is higher than has been

previously reported to induce myocyte apoptosis [305]. Cardiac cell isolation yielded a highly pure population of primary neonatal rat cardiomyocytes (**Fig. 25**).

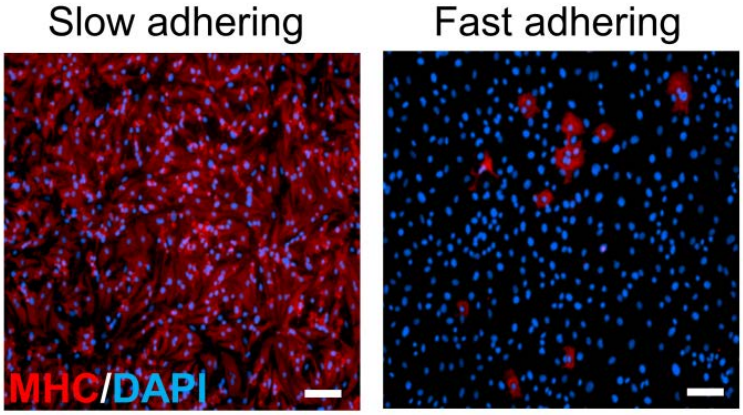

Figure 25. Neonatal rat cardiac cell populations were separated by pre-plate technique. Slow-adhering cardiomyocytes did not adhere to the pre-plate while fast-adhering cardiac fibroblasts did adhere. Both populations were immunofluorescent stained for myosin heavy chain (MHC) muscle cell marker (red) and counterstained with DAPI for cell nuclei (blue). Scale bars = 100 μm.

Myocytes pre-treated with FGF2 coacervate or Shh coacervate showed significantly lower levels of apoptosis compared to the H_2O_2 treated control, but higher levels than the control group not treated with H_2O_2 (**Fig. 26**). Additionally, the difference in means compared to the H_2O_2 treated control was more statistically significant for Shh coacervate than for FGF2 coacervate ($p=0.003$ vs. $p=0.012$). Incubation with free FGF2 or Shh did reduce caspase-3 levels, however these differences were not statistically significant ($p=0.094$ and $p=0.083$) from the H_2O_2 treated control. Videos taken at the experiment endpoint show that cardiomyocytes were beating normally in the non-H_2O_2 treated control, but rapidly and irregularly in the Free Shh group and

Shh coacervate group. Additionally, more cells were beating in the Shh coacervate group than in the Free Shh group in accordance with our caspase-3 results.

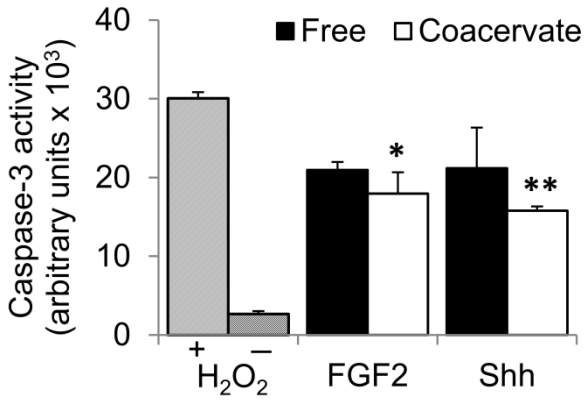

Figure 26. Cytoprotection of cardiomyocytes from oxidative stress-induced apoptosis. Myocytes were pre-treated for 48h with FGF2 or Shh, free or delivered in the coacervate. Cells were then exposed to oxidative stress conditions with H_2O_2 for 2h. Two control groups were not pre-treated with any growth factors and then one received H_2O_2 for 2h (+) and one did not (-). Cell apoptosis levels were measured by caspase-3 activity. *P<0.05, **P<0.01 compared to the +H_2O_2 control group.

4.3.4 Fluorescence imaging of Gel+Coacervate

To ensure the coacervate and PEG gel were compatible we began by fluorescence-labeling each and formed the gel *ex vivo*. Fluorescence microscopy indicated that the coacervate was homogenously distributed throughout the gel with an embedded appearance and consisted of spherical droplets with diameters ranging from approximately 0.5-10 µm, consistent with our previous reports [166] (**Fig. 27**).

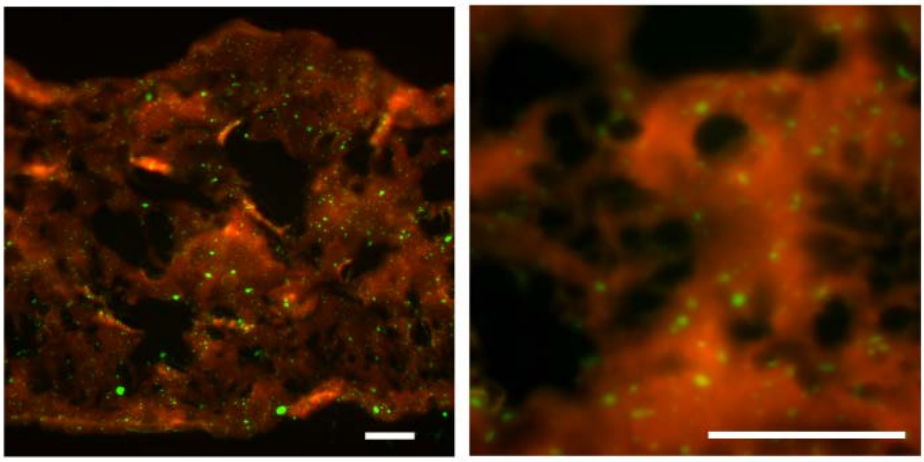

Figure 27. Fluorescence-labeled PEG gel and coacervate. PEG gel was labeled with AlexaFluor 660 dye (red) and the coacervate was labeled with fluorescein (green). Scale bars = 100 μm.

4.3.5 Gel improves coacervate retention after myocardial injection

We next wanted to test the effectiveness of the PEG gel at improving the retention of the coacervate after injecting into the heart wall. We created MI in rats by permanent left anterior descending (LAD) ligation, then injected the fluorescence-labeled coacervate alone or dispersed within the PEG gel. One day after injection we observed a much lower fluorescence signal when applied alone (**Fig. 28a**) compared to in the PEG gel (**Fig. 28b**). The coacervate also had a vastly different appearance in each case; when injected alone it had a punctated morphology and when in the gel it looked striated. The gel appeared to have been forced into interstices between myocytes and the coacervate congealed and followed the contours of the gel, thus resembling the morphology we described previously [297]. We also quantified the area of the infarct region that was positive for fluorescent coacervate signal and found it to be 3-fold higher when the gel was

used (**Fig. 28c**). These data demonstrate that the gel increases coacervate retention and spreading within the myocardium.

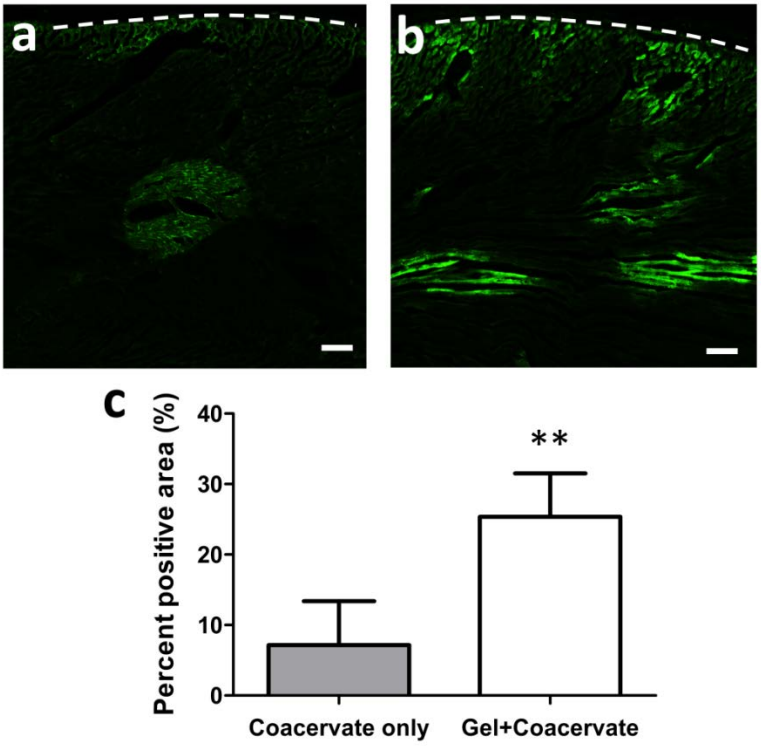

Figure 28. Coacervate retention 1 day post-injection. The coacervate was fluorescence-labeled (green) and infarcted rat hearts were injected with a) Coacervate only or b) Gel+Coacervate. Animals were sacrificed after 24 h and the coacervate was identified by fluorescence microscopy. Dotted lines indicate the outer boundary of the left ventricular wall. Scale bars = 100 µm. c) Percent area of the heart positive for coacervate. Bars indicate means ± SD of 4-5 rats per group. $^{**}p<0.01$.

4.3.6 Coacervate improves gel integration after myocardial injection

We were also interested in the effect of the coacervate on the gel residence time in the myocardium. We created infarcts and injected the fluorescence-labeled PEG gel either with or without the coacervate, then observed the gel by fluorescence microscopy after 2 weeks. We observed numerous regions of gel without the coacervate remaining after 2 weeks that were completely acellular, indicating incomplete acceptance of the material by the body (**Fig. 29a**). In contrast, the gel containing the coacervate was evenly distributed throughout the wall and had much higher cell infiltration (**Fig. 29b**). We estimated the total volume of gel remaining by quantifying the fluorescence area in sequential sections thru the entire infarct. These results revealed a trend towards more gel remaining when injected without than with the coacervate, though this difference was not statistically significant ($p=0.39$) (**Fig. 29c**). Taken together, these data indicate that the coacervate does promote integration of the gel into the myocardial wall. Although this generally leads to bulk rather than surface degradation which should increase the local degradation rate as the trend suggests, the coacervate may not significantly affect the overall rate of gel degradation. Consequently, no gel was observed in hearts from either group after 4 weeks. These results were surprising because we predicted that IL-10 released from the coacervate would suppress the inflammatory response towards the gel, thereby prolonging its residence. However, Shh has been shown to upregulate cardiac fibroblast expression of stromal-cell derived factor-1α, a stem cell homing chemokine [163]. This may result in a larger stem cell presence which enhance the regenerative environment but also secrete MMPs and may contribute to polymer degradation [306].

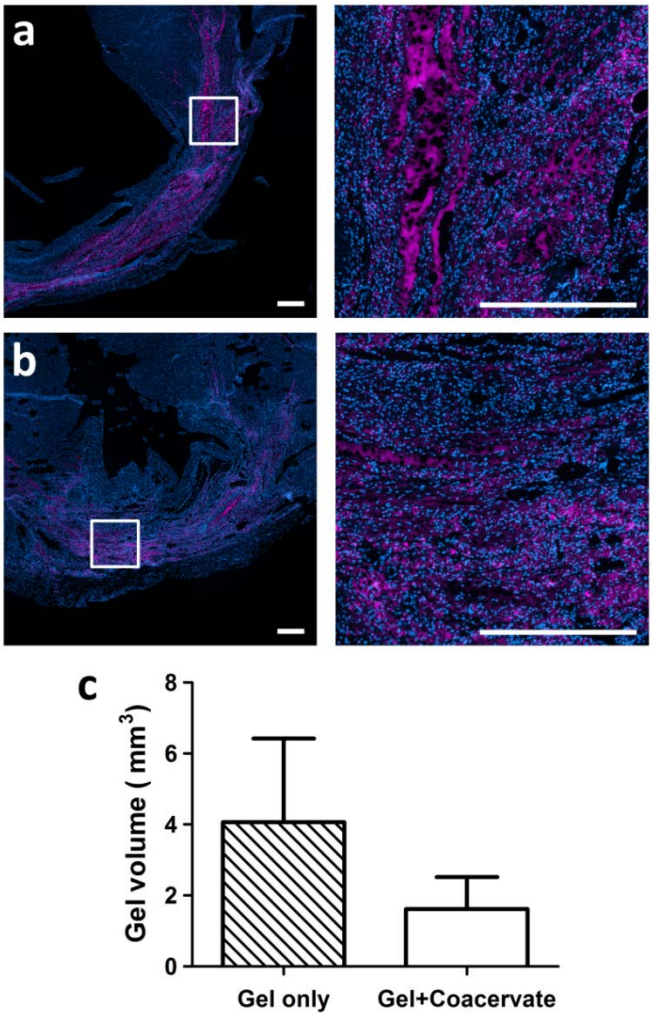

Figure 29. Gel integration 2 weeks post-injection. The gel was fluorescence-labeled (purple) and infarcted rat hearts were injected with a) Gel only or b) Gel+Coacervate. After 14 days the animals were sacrificed and the gel was identified by fluorescence microscopy in sections co-stained with DAPI for cell nuclei (blue). Indicated regions of the left column are magnified in the right column. Scale bars = 500 µm. c) Gel volume quantified in the infarct region. Bars represent means ± SD of 3 rats per group.

4.3.7 Gel+Coacervate preserves heart function after MI

We next assessed the synergistic benefits of the gel and coacervate towards heart function following MI. We performed LAD coronary ligation in rats, then immediately injected the therapy at 3 locations, evenly spaced around the infarct zone. Echocardiography performed after 2 and 4 weeks revealed a higher fractional shortening with the combined gel and coacervate treatment compared to all other groups, and these differences were statistically significant at both timepoints (**Fig. 30**). Either therapy alone showed no significant benefit over the saline control group. This is consistent with our previous report that the PEG gel alone has no significant effect on heart function when injected immediately after infarction [297]. As in our previous study, delayed injections of the combined gel and coacervate performed 1 week after MI also resulted in functional benefit, and furthermore it was not significantly different from immediate injection (**Fig. 31**). These results demonstrate that the gel and coacervate is still effective when applied within this 1 week timeframe which may have greater clinical relevance than immediate injection [307]. The ineffectiveness of the coacervate alone is likely due to the low retention after injection without the support of the gel. Taken together, these results indicate that the synergism between the gel and coacervate is vital to its successful preservation of heart function after MI.

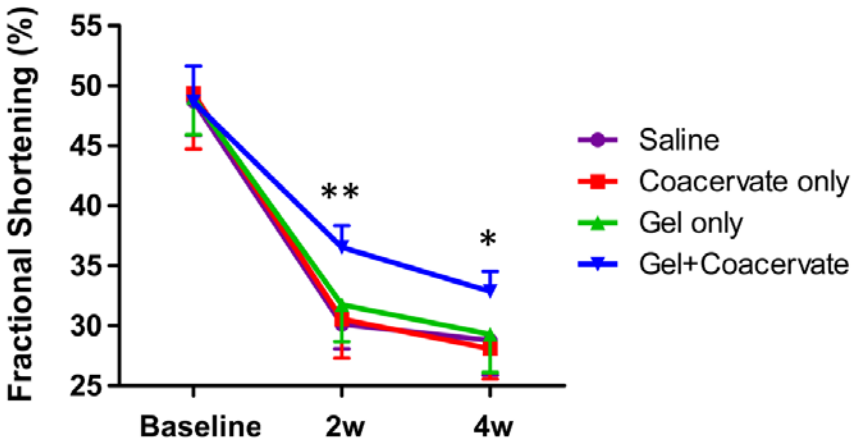

Figure 30. Functional analysis. Rat infarcts were injected with saline, coacervate alone, gel alone, or the combined gel and coacervate. Echocardiography was performed prior to MI (baseline) and 2 and 4 weeks after MI, and data presented as fractional shortening. Bars indicate means ± SD of 8-10 rats per group. *p<0.05, **p<0.01 compared to all other groups.

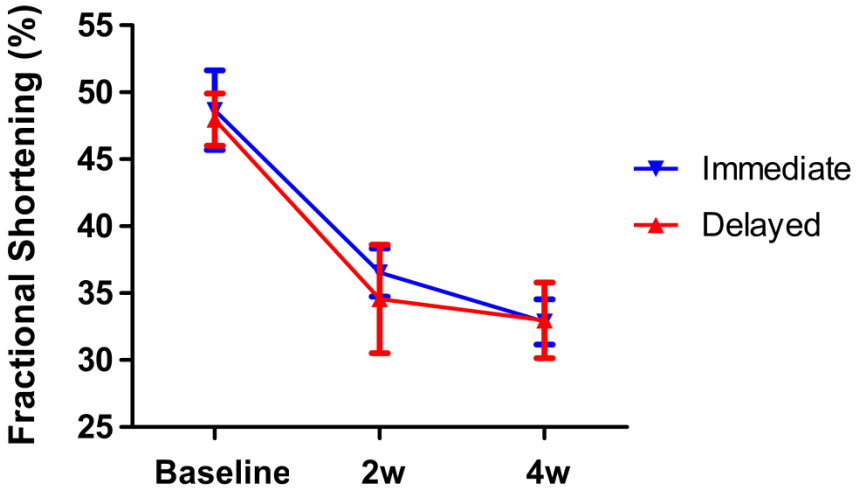

Figure 31. Effect of Gel+Coacervate injection timing on cardiac function. Rat infarcts were injected with Gel+Coacervate immediately or 1 week after infarction (delayed). Echocardiography was performed prior to MI (baseline) and 2 and 4 weeks after MI, and data presented as fractional shortening. Bars indicate means ± SD of n=10 for Immediate group and n=3 for Delayed group.

4.3.8 Gel+Coacervate reduces scar burden

Fibrotic scar formation is often the main factor leading to reduced cardiac function and eventually congestive heart failure. We observed the dense collagen-rich scar tissue of the rat infarcts after 4 weeks using Masson's trichrome staining. Hearts receiving the combined gel and coacervate treatment had a noticeably smaller scar region compared to other groups; however, there appeared to be no obvious difference between groups in the heart wall thickness of the scar region (**Fig. 32a-d**). Quantification of the scar burden, the percent of the heart circumference containing scar, revealed a lower mean value with the combined treatment compared to other groups, although these differences were not statistically significant (**Fig. 32e**). As observed, there were also no statistically significant differences in wall thickness between groups, though the saline group had the lowest mean value (**Fig. 32f**). Fibrosis occurs to replace voids left by cardiomyocyte death, thus the two are directly correlated [308]. Shh can reduce oxidative stress on myocytes directly or indirectly through upregulation of IGF-1 [163]. Therefore animals receiving the coacervate likely experienced lower levels of myocyte apoptosis which reduces fibrotic scarring; differences between these groups can be attributed to greater coacervate retention with the gel than without.

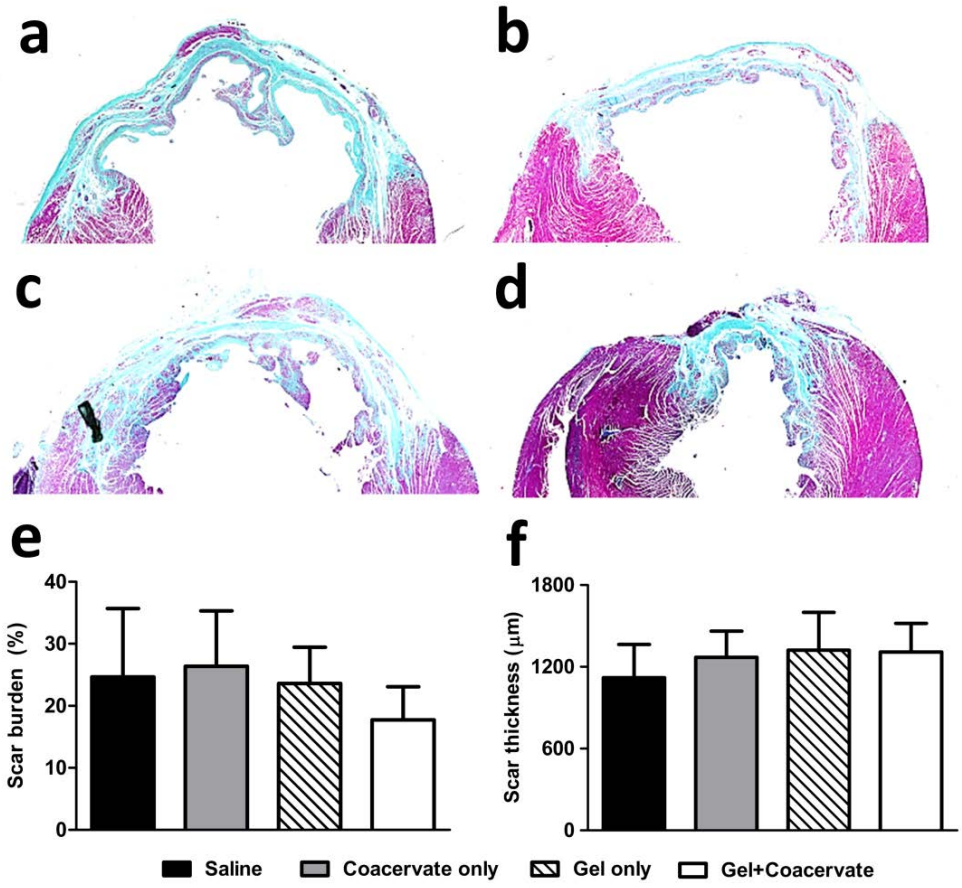

Figure 32. Scar burden and wall thickness. Masson's trichrome staining was performed 4 weeks after MI to observe fibrosis in hearts treated with a) Saline, b) Coacervate only, c) Gel only, d) Gel+Coacervate. Collagenous scar tissue appears blue and healthy muscle appears red. Bars indicate means ± SD of 8-10 rats per group.

4.3.9 Coacervate induces robust angiogenesis

Vascularization plays a key role in promoting a pro-healing environment by delivery the necessary oxygen, nutrients, and progenitor cells and removing waste. Because the primary supply is cut off during ischemia, angiogenesis must occur from neighboring vessels to gradually reperfuse the tissue. Shh has been shown to play a role in angiogenesis by upregulating local

expression of vascular endothelial growth factor and angiopoeitin-1 [164] and by enhancing the contribution of blood-derived endothelial progenitor cells [309]. We investigated the vascularity within the infarct zone to elucidate the effect of our treatments on angiogenesis or the survival of pre-existing vessels. Animals utilized for the gel retention study provided an indication of vascularization at 2 weeks post-MI in groups receiving the gel (**Fig. 33a,b**). We observed significantly more blood vessels in hearts also receiving the coacervate compared to the gel alone (**Fig. 33c**). In the early timeframe after MI, more vessels in groups receiving the co-therapy explains in part the reduced fibrosis and better cardiac function. At 4 weeks post-MI we observed nearly 3-fold the number of vessels in hearts treated with coacervate alone (16.3±2.2) compared to saline (6.1±0.9), and the addition of the gel did not significantly alter the angiogenic effect of the coacervate alone (**Fig. 33d**). Surprisingly, the gel alone also showed a higher number of vessels per volume infarct at 4 weeks, though like the co-therapy, this was not a statistically significant difference from saline. Perhaps a late inflammatory response to the gel resulted in increased growth factor and cytokine expression in the infarct region by macrophages. We also observed a similar trend of treatment effect on blood vessel numbers in the border zone surrounding the infarct, though the numbers were significantly less than within the infarct (**Fig. 34**). These results indicate that the effects of the coacervate can propagate beyond the application area either by growth factor translocation via the extracellular matrix, or indirectly through paracrine signaling.

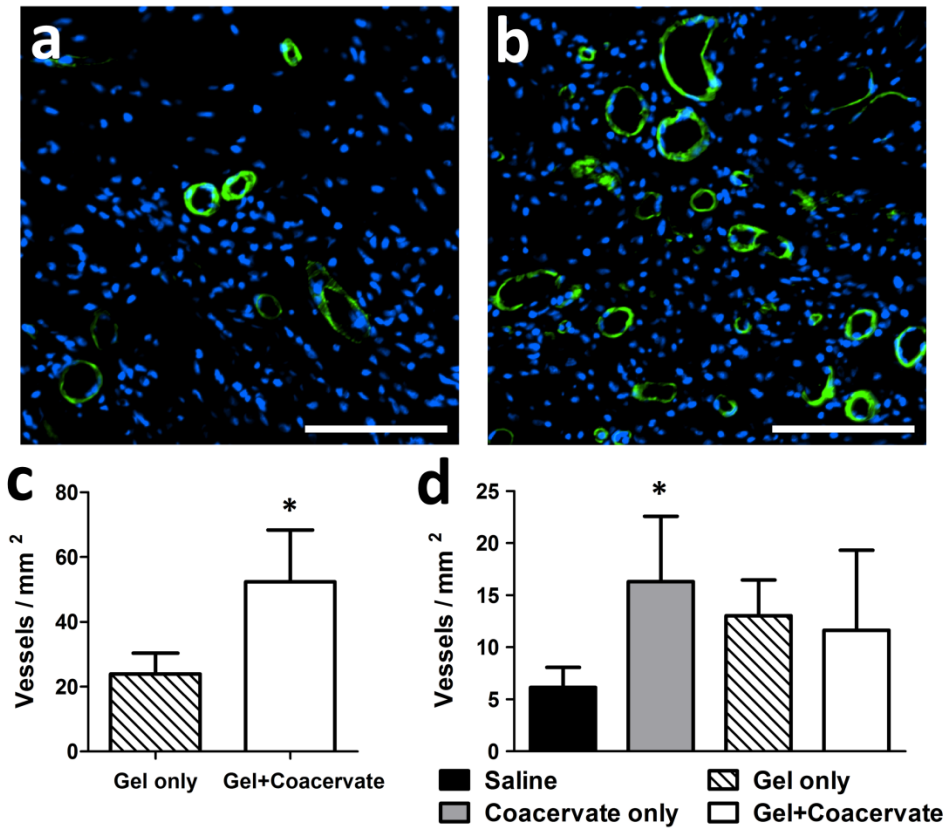

Figure 33. Blood vessel quantification. Mature blood vessels were identified by α-smooth muscle actin immunohistochemical staining for smooth muscle cells. Representative images from within the infarct region 2 weeks post-MI, treated with: a) Gel only, or b) Gel+Coacervate. Scale bars = 100 μm. c) 2 week blood vessel quantification. Bars indicate means ± SD of 3 rats per group. *$p<0.05$. d) 4 week blood vessel quantification. Bars indicate means ± SD of 8-10 rats per group. *$p<0.05$.

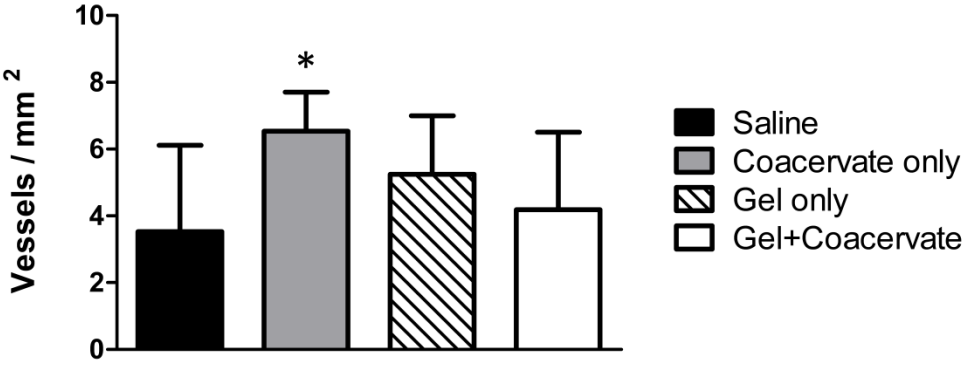

Figure 34. Border zone blood vessel quantification. Mature blood vessels were identified by α-smooth muscle actin immunohistochemical staining for smooth muscle cells. Blood vessels were quantified at the 4 week timepoint in the border zone surrounding the infarct. Bars indicate means ± SD of 8-10 rats per group. *$p<0.05$.

4.4 DISCUSSION

Ischemic damage to the heart may be mitigated by Shh through three key mechanisms: i) Angiogenesis- the sprouting of new blood vessels from pre-existing ones, ii) Cytoprotection of cardiomyocytes under oxidative stress, and iii) Recruitment of cardiac progenitor cells.

Shh-induced neovascularization is a result of upregulated paracrine signaling by fibroblasts of several angiogenic factors including vascular endothelial growth factor (VEGF) and angiopoetin-1 [164, 309, 310]. It has also been shown to increase the contribution of bone marrow-derived endothelial progenitor cells (EPCs) to the neovascularization process [309, 311, 312]. Additionally, recent reports have revealed that Shh acts through the Rho-associated protein kinase (ROCK) pathway, rather than its traditional Gli-dependent pathway, to stimulate expression of matrix metalloproteinase-9 (MMP-9) and osteopontin (OPN) in endothelial cells [313, 314]. These multiple complex roles of Shh underscore its importance in ischemic

revascularization. In the present work we show that the Shh coacervate can stimulate cardiac fibroblasts to significantly upregulate expression of VEGF. Furthermore, Shh coacervate acutely (6 hour timepoint) stimulated significantly more VEGF production than free Shh. This may be attributed to enhanced morphogen bioactivity when delivered by the coacervate, as discussed later. *In vivo*, this upregulated angiogenic growth factor expression may induce angiogenesis to re-vascularize the ischemic myocardium.

The cytoprotective effects Shh displays for cardiomyocytes have also been attributed to multiple mechanisms. One contributor is insulin-like growth factor (IGF-1) which has been shown to be upregulated in Shh-stimulated cardiac fibroblasts [163] and bone marrow-derived cells [315]. IGF-1 interferes with the transcription of angiotensin II, thereby preventing the formation of reactive oxygen species during oxidative stress [316, 317]. A more direct anti-apoptotic role of Shh has also been demonstrated *in vitro* for cardiomyocytes, which express the Shh receptor Patched-1 [163]. Our results seem to confirm this direct role, as recombinant Shh protein applied alone to stressed cardiomyocytes reduced cell apoptosis. Yet we must still consider that the cardiomyocyte population was not entirely pure and may have contained a small number of fibroblasts. Upregulated secretion of IGF-1 by these fibroblasts may have therefore played a role as well. FGF2 was included as a positive control in apoptosis experiments as it is a well-known survival factor for numerous cell types [318-320] including cardiomyocytes [321], and we have experience delivering it with the coacervate [21, 160, 322]. We observed the coacervate to enhance the bioactivity of both FGF2 and Shh compared to either factor in free form. We also found that Shh coacervate protected stressed cardiomyocytes better than FGF2 coacervate. This is significant because FGF2 expression by fibroblasts has actually been shown

to be downregulated in response to Shh stimulation [164]. The anti-apoptotic effects of Shh must therefore be ascribed to non-FGF2-related pathways.

Stromal cell-derived factor-1 (SDF-1), also known as CXCL12, is a trafficking chemokine for stem and progenitor cells [323]. It has been shown to act in local recruitment of cardiac progenitor cells [324-326], as well as EPCs [327] and smooth muscle progenitor cells [328]. It is well accepted that SDF-1 plays a pivotal role in stem and progenitor cell homing to sites of injury [329]. We prove here that Shh coacervate can upregulate production of SDF-1α at least as well as equal dose of free Shh, therefore the bioactivity of released Shh is well maintained. *In vivo*, high local levels of SDF-1α may encourage recruitment of blood derived EPCs to aid in neovascularization, and of cardiac progenitor cells to engender myocardial tissue repair.

Clearly, Shh acts as a "master switch" agent in many tissues including the heart, activating multiple downstream pathways in response to injury. Shh has been shown to activate the ERK1/2 [330], PKC [165], ROCK [313], and PI3K/Akt [311] signaling pathways, among others. Shh morphogen may therefore provide benefits similar to co-delivery of multiple different growth factors. However, a multi-factor approach would require extensive optimization of growth factor dosage and release rate, while Shh stimulates a natural healing environment, similar to the embryonic state when cardiac regeneration is possible. Finally, we also observed upregulated Shh expression by cardiac fibroblasts in response to stimulation with Shh, a positive autoregulation that has been previously reported [163].

Regarding the role the coacervate plays in enhancing the effects of Shh, we point to heparin as a major player. Proteoglycans associated with the extracellular matrix or cell surface play a vital role in the transduction of cell signaling pathways [331]. Heparin binds many growth

factors, cytokines, and morphgens, stabilizes and protects them, and in some cases modulates their activity [260, 332]. It has been shown to interact with a growth factor molecule and its corresponding cell receptor simultaneously, forming a stable ternary complex which facilitates signal activation [12]. Heparan sulfate proteoglycans have also been shown to play a vital role in developmental patterning and specifically in regulating Hedgehog distribution and pathway activation [333, 334]. Heparin binds Shh with high affinity (K_d = 99nM) [335] and may inherently enhance its bioactivity by mimicking the *in situ* signaling environment. Indeed, the biological activity of Shh has been shown to be directly related to its affinity for heparin [335]. We suggest that utilizing heparin in our delivery system may thereby potentiate the activity of Shh. This is supported by our previous reports using the coacervate to deliver FGF2 [160, 322], neuronal growth factor [21], and heparin-binding EGF-like growth factor [141]. However, the efficacy of the coacervate at maintaining or enhancing the bioactivity of Shh in an *in vivo* environment requires further evaluation.

The activity of bound factors is further preserved within the coacervate, which is in a separate phase from water. This isolation provides further protection from proteases. The heparin:Shh complex is soluble in water and if injected *in vivo* would therefore be quickly diluted and removed from the injection site. To maintain the complex locally, an insoluble coacervate is formed using a synthetic polycation, PEAD. This ariginine-based polycation was designed to imitate the highly cationic heparin-binding domain [12]. Heparin-bound factors are incorporated into the coacervate and protected from proteolysis and denaturation. Release from the coacervate is based on slow hydrolysis of the polycation [158], as well as dissolution of the complex in an ionic environment. We expect the release of Shh from the coacervate to be accelerated *in vivo* in in the presence of enzymes. We have previously shown this polycation to

be highly biocompatible and to complex with heparin to control the release of many different growth factors [158]. The results presented here suggest that a simple liquid coacervate has high potential as a system of controlled delivery for heparin-binding morphogens, in addition to growth factors.

4.5 CONCLUSIONS

The results of this study indicate that PEAD-heparin coacervate can load Shh with high efficiency and sustain its release for at least 21 days. Shh released from the coacervate displays bioactivity equal to or higher than that of free Shh. We demonstrate the ability of Shh coacervate to protect cardiomyocytes from oxidative stress and to upregulate secretion of multiple growth factors by cardiac fibroblasts. These results warrant further investigation of Shh coacervate for treating cardiac ischemia.

5.0 CONTROLLED DELIVERY OF BMP-2 TO IMPROVE STEM CELL THERAPY FOR BONE REGENERATION

5.1 INTRODUCTION

The existence of osteoprogenitor cells in the skeletal muscle has long been postulated [336-340]. A number of candidates have been proposed, such as satellite cells [341] and primary myoblasts [341, 342]. Our group has also isolated and characterized a slowly-adherent cell population (MDSCs) from skeletal muscle via a modified pre-plate technique [343-346]; however, their exact relationship to satellite cells and blood vessel derived progenitor cells remains unclear [347]. When provided with osteogenic stimuli such as BMPs, they can produce osseous-like tissue *in vitro* [341, 343], and when retrovirally transduced to express BMP2 or BMP4 have been shown to differentiate into osteocytes and chondrocytes and enhance bone and articular cartilage repair *in vivo* [344, 348-352]. More importantly, BMP-transduced MDSCs show superior bone healing capabilities compared to other similarly transduced muscle-derived cells [353, 354]. These reports suggest that progenitor cells derived from skeletal muscle, especially MDSCs, could be a promising alternative cell source to bone marrow derived mesenchymal stem cells (BMSCs) for bone tissue engineering.

Despite the promise that MDSCs hold for bone regeneration, without the presence of BMPs they do not differentiate towards an osteogenic lineage, rather they form myotubes and

myofibers when injected alone into a muscle pocket [340, 355, 356]. Applying the proper stimuli to create an osteoinductive environment *in vivo* is therefore important for harnessing the osteogenic potential of MDSCs. BMP2 and BMP4 have been shown to produce the most successful results using gene transduction [344, 350-352]; however, from a translational point of view, a non-viral approach is preferred, and thus far has received limited exploration.

It is known that prolonged exposure to BMPs at an appropriate concentration is necessary to induce MDSC differentiation and subsequent osteo-chondrogenesis *in vivo*; however, BMPs have very short half-lives in the body [357, 358], and maintaining an adequate local BMP concentration is challenging. A controlled delivery method that can protect and sustain the release of BMPs would be particularly attractive for muscle cell-based bone engineering. To this end, we employed a recently developed growth factor delivery platform comprised of native heparin and a synthetic polycation, poly(ethylene argininylaspartate diglyceride) (PEAD), to deliver BMP. In this delivery platform, heparin tightly binds BMP2 via its high-affinity heparin binding site and then PEAD interacts with heparin by polyvalent charge attraction (Fig. 1). The polycation-heparin complex loaded with BMP2 self-assembles into a coacervate, held together by Coulombic forces. A coacervate is an emulsion-like aggregation of organic molecules separated from the aqueous phase. The PEAD-heparin coacervate contains spherical droplets ranging from 10-500 nm in diameter [359]. We have previously shown that this controlled release platform can effectively deliver fibroblast growth factor-2 (FGF2) for therapeutic angiogenesis [211]. The coacervate delivery vehicle displayed nearly 100% loading efficiency, minimal burst release, and potentiated the bioactivity of released FGF2 [211]. In this study, we employ the use of this PEAD-heparin coacervate delivery system to obtain a constant release of BMP2 in a temporally- and spatially-controlled manner in order to promote osteogenesis by

MDSCs. We hypothesized that the coacervate delivery system could effectively stabilize, localize, and sustain the release of BMP2, to sufficiently stimulate MDSCs to undergo osteoblastic lineage differentiation *in vitro* and to form bone at an ectopic site *in vivo* (**Fig. 35**).

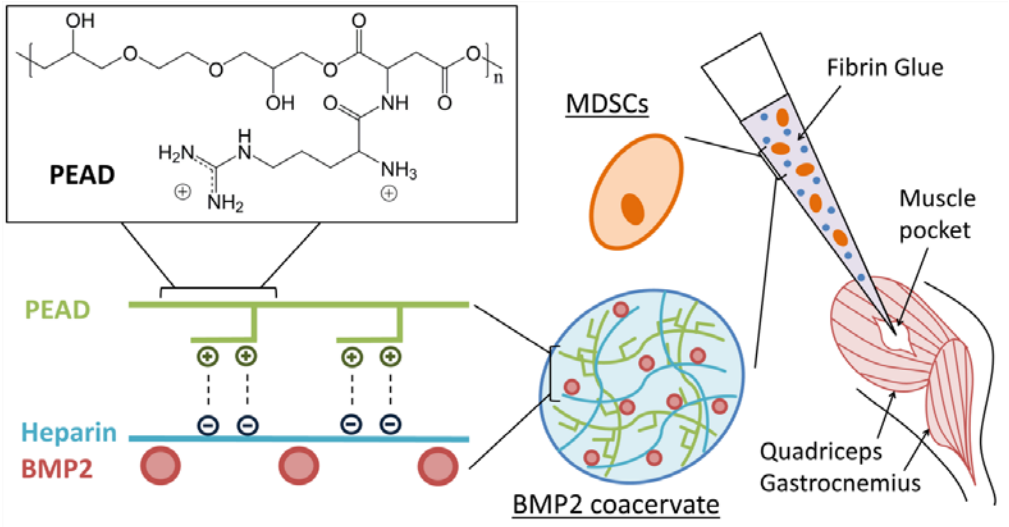

Figure 35. Schematic diagram of ectopic bone formation model in vivo. Heparin and BMP2 are combined initially to allow growth factor binding. Then PEAD, a polycation bearing 2 positive charges per repeating unit, is added which interacts with heparin (a polyanion) by polyvalent charge attraction. This induces self-assembly of nanometer-sized coacervate droplets, separate from the aqueous phase and incorporating the BMP2 molecules. The coacervate is then mixed with MDSCs, suspended in a fibrin gel and pipetted into a quadricep muscle pocket created in the hind limbs of mice. The implantation site is evaluated after 2 and 4 weeks for ectopic bone formation by MDSCs stimulated by the BMP2 coacervate.

5.2 MATERIALS AND METHODS

5.2.1 Preparation of the BMP2 coacervate

Poly(ethylene argininylaspartate diglyceride) (PEAD) was synthesized as previously described [212, 213]. Clinical-grade Heparin Sodium, USP from porcine intestine (Scientific Protein Labs, Waunakee, WI) and PEAD were each dissolved in saline at 0.125mg/ml and filter-sterilized at 0.22μm. Heparin and recombinant human BMP2 (Medtronic, Fridley, MN) were combined initially and pipetted to mix and allow for growth factor binding. PEAD was added at a 5:1 PEAD:heparin mass ratio, previously shown to produce an overall neutrally-charged solution[213]. The BMP2 coacervate formed immediately upon addition of PEAD, visible as a turbid solution. The BMP2 coacervate was then added by pipet to cell culture media for *in vitro* testing, or suspended in fibrinogen solution for *in vivo* implantation.

5.2.2 BMP2 loading and release assays

The BMP2-coacervate was formed with 100μg heparin, 100ng BMP2, and 500μg PEAD in Dulbecco's phosphate buffered saline (DPBS) and centrifuged at 12,100 x g for 5 min to pellet the coacervate. For determination of loading efficiency, western blot was performed by mixing the supernatant and pellet with sample buffer followed by denaturation at 95°C for 5min. The proteins were separated by SDS-PAGE and then transferred to a PVDF membrane. Rabbit anti-human BMP2 primary antibody (PeproTech, Rocky Hill, NJ) and HRP-conjugated anti-rabbit IgG secondary antibody (Sigma-Aldrich, St. Louis, MO) were used, followed by the addition of a chemiluminescent substrate (Thermo Fisher Scientific, Waltham, MA). Band intensities were

quantified using ImageLab software (Bio-Rad, Hercules, CA) and compared to a standard band of 100ng free BMP2 in DPBS for calculation of loading efficiency. To determine the release profile, media supernatant was aspirated at various time points and replaced with fresh DPBS and incubated at 37°C. BMP2 levels in the supernatant were quantified by BMP2 ELISA kit (PeproTech).

5.2.3 Isolation, culture, and transduction of mouse MDSCs

MDSCs were isolated from the hind limb skeletal muscle of 3 week old C57/BL10J mice (Jackson Labs, Bar Harbor, ME) via a modified pre-plate technique that has been described previously [343-345]. MDSCs were cultured on collagen I-coated flasks in MDSC basal media, defined as Dulbecco's Modified Eagle's Medium (DMEM) supplemented with 10% fetal bovine serum (FBS), 10% horse serum, 1% penicillin/streptomycin (all from Invitrogen, Carlsbad, CA), and 0.5% chick embryo extract (CEE; Accurate, Westbury, NY). Cells were trypsinized and replated at a density of 250 cells/cm^2 until a sufficient number of cells were available for the assays. For *in vivo* cell tracking, MDSCs were retrovirally transduced with a green fluorescent protein (GFP) vector as described previously[360]. The transduced cells were sorted for GFP signal by fluorescence-activated cell sorting (FACSAria; BD Biosciences, San Jose, CA) and cultured for 2 passages prior to use in the experiments.

5.2.4 *In vitro* MDSC proliferation assay

Cell growth over time was assessed by DNA quantification assay as described previously[361]. Briefly, 2×10^3 MDSCs were seeded in a 48-well plate in MDSC basal medium and incubated

overnight. The next day, the medium was replaced with MDSC basal medium supplemented with 0 (control), 0.125, 0.25, or 0.5mg/ml coacervate (PEAD:heparin). The coacervate was prepared by dissolving PEAD and heparin in DPBS and then combining them at a 5:1 PEAD:heparin mass ratio. Appropriate volumes of pre-formed coacervate were then added to the media at the desired concentrations. On days 1, 3, and 5, cell lysates were prepared by the addition of 0.1% Triton X-100 (Sigma-Aldrich) followed by 3 freeze-thaw cycles. Double-stranded DNA (dsDNA) content of the cell lysate was measured using a Quant-iT dsDNA high-sensitivity assay kit (Invitrogen).

5.2.5 *In vitro* assays of osteogenic potential of C2C12 cells and MDSCs

The bioactivity of delivered BMP2 was determined by its ability to stimulate alkaline phosphatase (ALP) production by a mouse myoblast cell line, C2C12 (CRL-1772; ATCC, Manassas, VA), in monolayer culture. The osteogenic effects of delivered BMP2 were also evaluated *in vitro* by ALP expression of the MDSCs in both monolayer and 3-D culture within a fibrin gel. Briefly, for monolayer culture the cells were seeded in a 24-well plate in MDSC basal media and a cell culture insert (BD Biosciences) with 0.4μm pores was placed in each well. 100ng free BMP2 or BMP2 coacervate was added to the media in the insert. For the multi-dose group, 100ng free BMP2 was added on days 0, 2, and 4, for a total of 300ng BMP2. Cells were cultured for 5 days, followed by ALP activity quantification, ALP staining, and real-time reverse-transcription (RT) PCR analysis for the osteogenic markers Runx2 and Collagen type I. BMP4-transduced MDSCs, which have been shown to undergo osteogenesis both *in vitro* and *in vivo*, served as a positive control[344, 348-352]. For 3-D culture, 100ng free BMP2 or BMP2 coacervate was suspended in serum-free MDSC basal medium containing 10mg/ml dissolved

bovine fibrinogen (Sigma-Aldrich) and used to resuspend 2×10^5 MDSCs. 9.5 NIH U/ml thrombin (Sigma-Aldrich) in 2.5mM $CaCl_2$ (aq.) was then added, mixed briefly by pipet, moved to a 96-well plate and solidified at 37°C to form a 100μl gel. Finally, 100μl of MDSC basal medium was overlaid on each gel. After 5 days of culture, fibrin gels were disassociated using a rotor-stator type homogenizer (IKA, Wilmington, NC) and ALP activity of MDSCs was quantified. Briefly, cells were lysed with 0.1% Triton X-100 and subjected to three freeze-thaw cycles. Cell debris was removed by centrifugation, and 10μl supernatant was transferred to a 96-well plate. 100μl Alkaline Phosphatase (pNPP) Liquid Substrate (Sigma-Aldrich) was added and incubated at room temperature for 15min in the dark. The reaction was stopped with 50μl of 3N sodium hydroxide and the absorbance at 405nm was measured by spectrophotometer (Infinite M200; Tecan, Männedorf, Switzerland). ALP activity was normalized by total DNA content, and quantified as described above. The ALP expression patterns of the cultured cells were observed by ALP staining (86C-1KT, Sigma-Aldrich) following the manufacturer's instructions. For RT-PCR, cellular RNA of MDSCs was extracted using an RNeasy Mini Kit (Qiagen). Aliquots of 1μg total RNA were hybridized with random primers and converted into cDNA using a SuperScript First-Stand Synthesis System (Invitrogen). Real time PCR was performed on an iCycler iQ5 PCR machine (BioRad) using SYBR Green Master mix (Thermo Scientific). The gene-specific primer sets (Runx.2: Forward-GACTGTGGTTACCGTCATGGC, Reverse-ACTTGGTTTTTCATAACAGCGGA; COL1A1: Forward- GCTCCTCTTAGGGGCCACT, Reverse- ATTGGGGACCCTTAGGCCAT; β-actin: Forward- AGCGGGAAATCGTGCGTG, Reverse- CAGGGTACATGGTGGTGCC) were used at a final concentration of 0.3μM. All real time PCR assays were performed in triplicate. Gene expression was calculated using the relative

standard curve method. Expression of the specific markers were normalized to β-actin and then scaled according to the control sample, for which the value was set to 1.

5.2.6 *In vivo* bone formation at a heterotopic site

University of Pittsburgh Institutional Animal Care and Use Committee (IACUC) approval was obtained prior any animal studies being performed. Power analysis was based on a pilot study performed under identical conditions but with different treatment groups which all contained MDSCs and BMP2 in a fibrin gel. The pooled standard deviation of bone volume after 4 weeks of healing was 1.032mm^3 for this pilot study (unpublished data). A power analysis calculation indicated that in order to detect 1.5 standard deviations of the variable means (α-error=0.05, β-error=0.2), 6 ectopic sites per group were required (Minitab). Thus, fifteen 6-8 week old C57/BL10J mice were randomly allocated into 5 groups: Control (no cells, no coacervate), MDSCs only, BMP-2 coacervate only, Free BMP-2+MDSCs, and BMP-2 coacervate+MDSCs. Mice were anesthetized with isoflurane and a 1cm incision was made on the lateral aspect of both thighs (6 thighs per group). The quadricep muscles were identified and a small incision was made and held open with forceps. Immediately before implantation, 2μg of free BMP2 or BMP2 coacervate (2μg BMP2, 40μg heparin, and 200μg PEAD) and 5×10^5 MDSCs were suspended in 40μl of 10mg/ml fibrinogen solution, and combined with 9.5 NIH U/ml thrombin. The solution was pipetted into the open muscle pocket where it conformed to the pocket space and was allowed to solidify briefly, forming the fibrin gel. The incision was then closed with 4-0 Prolene suture. The animals were examined radiographically 2 and 4 weeks after implantation and histologically at week 4. No immune-suppressive treatment was given as the MDSCs were isolated from C57/BL10J mice from the same inbred colony.

5.2.7 *In vivo* bone formation of human MDSCs

University of Pittsburgh Institutional Animal Care and Use Committee (IACUC) approval was obtained prior any animal studies being performed. $5x10^5$ hMDSCs were suspended in fibrin glue with 2µg of BMP2 (free BMP2+hMDSCs) or via the coacervate delivery system containing 2µg of BMP2 (BMP2 coacervate+hMDSCs) and transplanted into a skeletal muscle pocket or into a 5mm critical-sized cranial defect created in CD1 (nude) mice (Jackson Labs).

5.2.8 Radiographical and histological analysis

At each time point, animals were anesthetized by inhalation of isoflurane. Both thighs were scanned with a Micro-CT scanner (VivaCT 40; Scanco, Brüttisellen, Switzerland) and the mineralized bone tissue within the muscle pocket was quantified. The Micro-CT scanning and quantification of the mineralized bone volume were performed by a specialist in the laboratory who was blinded to the group design. Following sacrifice, quadricep muscles were removed, fixed in 4% paraformaldehyde, embedded in sodium carboxy methyl cellulose (CMC) (NEG50; Richard-Allan Scientific, Kalamazoo, MI), frozen in liquid nitrogen and 5µm non-decalcified cryo-sections were obtained using a cryostat (HM505E; Microm, Walldorf, Germany). Sections were stained with 2% Alizarin red for calcium deposition and 2% silver nitrate for phosphate detection (von Kossa staining), and immunostained for GFP to detect the transplanted MDSCs. For GFP immunostaining, non-decalcified sections were rinsed in PBS, blocked in 10% horse serum and incubated overnight at 4°C with rabbit anti-GFP antibody (ab290; Abcam, Cambridge, MA) in 5% horse serum. After washing, sections were incubated for 1h at room temperature with biotin-labeled horse anti-rabbit IgG antibody. Biotin-immune complexes were

detected using the ABC and diaminobenzidine (DAB) peroxidase substrate kit (Vector, Burlingame, CA). All images were acquired using an upright bright-field microscope (Eclipse E800; Nikon, Tokyo, Japan). The number of GFP positive cells within and at the edge of the osteoid were also counted and normalized to bone surface (mm^2) using NIH ImageJ Version 1.46r software.

5.2.9 Statistical analysis

Statistical tests were performed using SPSS 16.0 (SPSS Inc, Chicago, IL). Data was tested for normality and equal variance before analysis. Statistical differences were calculated using analysis of variance (ANOVA or ANOVA on ranks if equal variance testing failed). Differences were considered significant at $p<0.05$.

5.3 RESULTS

To determine loading efficiency, the amount of BMP2 in the supernatant and coacervate pellet after centrifugation was determined by western blotting. 98.2% of the BMP2 was detected in the pellet, indicating that the coacervate loaded the BMP2 with high efficiency, and the remaining unloaded BMP2 was detected in the supernatant (**Fig. 36a**). The heparin:BMP2 molar ratio used for the ectopic bone formation experiments *in vivo* was approximately 20:1. Assuming a 1:1 binding interaction between BMP2 and heparin, the coacervate has a theoretical loading potential of 20-times the amount of BMP2 used for *in vivo* experiments. The release profile of BMP2 from the coacervate into Dulbecco's phosphate buffered saline (DPBS) was determined by pelleting

the BMP2 coacervate by centrifugation and measuring the concentration of free BMP2 in the supernatant at various time points using ELISA. Less than 1% of the BMP2 was detected in the supernatant immediately after forming the coacervate, confirming the high loading efficiency determined by western blot. A minimal burst release of only 1.3% after one day was observed (**Fig. 36b**). Thereafter, release was linear until day 10 when the release rate slowed and then sustained through the end of the experiment. After 28 days, approximately 25% of the BMP2 had been released from the coacervate. The data indicated that the coacervate can efficiently control the release of incorporated BMP2.

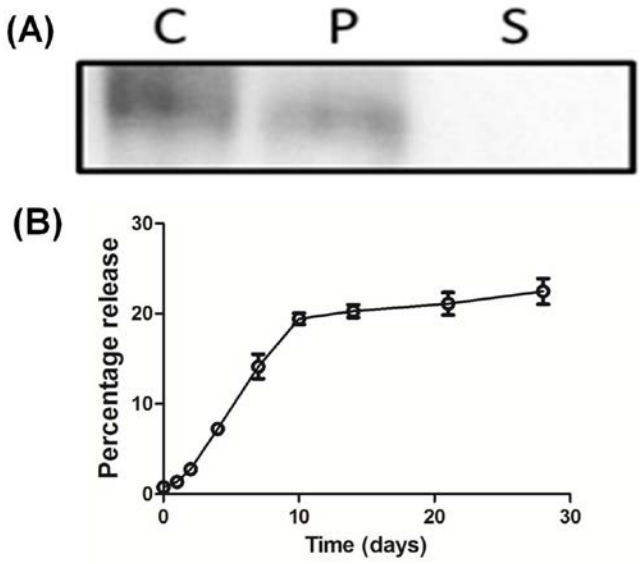

Figure 36. Loading efficacy and release profile of BMP2 from the coacervate. (A) BMP2 coacervate was centrifuged and the amount of BMP2 in the pellet (P) and supernatant (S) were determined by western blot. An equal quantity free BMP2 served as the control (C) and loading efficiency was calculated as percent band intensity of the control. Western blot revealed that 98.2% of BMP2 was in the pellet, indicating a high loading efficiency. (B) BMP2 was released from the coacervate into DPBS at 37°C. Percent release over 28 days was quantified by ELISA. Data represent the mean ± SD (n=3).

5.3.1 Effect of the coacervate on MDSC proliferation

The influence of the coacervate (PEAD:heparin) on the proliferation of MDSCs was tested by adding different concentrations of coacervate to the culture media and assessing cell proliferation after 3 and 5 days by DNA quantification (**Fig. 37**). No significant differences were seen among the groups at days 1 and 3; however, at day 5, the coacervate inhibited the growth of the MDSCs in a dose-dependent manner at concentrations above 0.125mg/ml. The coacervate at 0.125mg/ml showed no difference from the control and therefore had no inhibitory effects on MDSC growth. This concentration was consequently used for all the following experiments, including the *in vivo* tests.

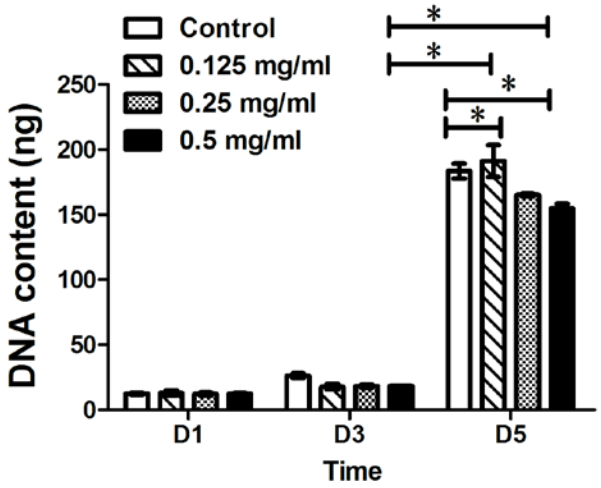

Figure 37. MDSC proliferation with the coacervate. MDSC proliferation was assessed by quantifying DNA content after 1, 3, and 5 days of culture with 0.125, 0.25, or 0.5 mg/ml coacervate in the culture media. The

control group contained only normal basal media without PEAD:heparin coacervate. Data represent the mean ± SD; *P<0.05 (n=4).

5.3.2 Bioactivity of BMP2 released from the coacervate

One important feature of a growth factor delivery vehicle is its ability to maintain growth factor bioactivity. We assessed this capability of the coacervate by stimulating ALP expression of the myogenic cell line, C2C12, with coacervate-released BMP2. Evaluating the expression of this pre-osteoblast marker in C2C12 cells is a common method of determining the activity of BMPs [362-364]. 100ng of BMP2 coacervate was compared to an equal amount of free BMP2 and control groups included DPBS and the delivery vehicle (coacervate) alone (**Fig. 38**). After 5 days of culture, BMP2 released from the coacervate induced significant expression of ALP by the C2C12 cells compared to the control. Furthermore, the ALP expression level induced by the BMP2 coacervate was significantly greater than induction with the same amount of free BMP2. As expected, the delivery vehicle alone had no effect on ALP expression by the C2C12 cells compared to the DPBS control and ALP staining showed similar results. The data suggests that the coacervate delivery system can preserve or even enhance the bioactivity of delivered BMP2 compared to free BMP2.

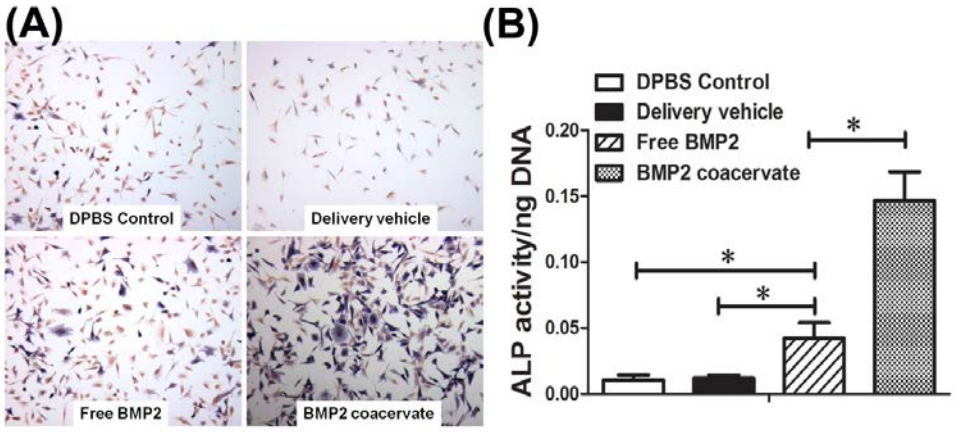

Figure 38. Bioactivity of delivered BMP2. C2C12 cells were cultured in media supplemented with DPBS as a control, delivery vehicle (coacervate only), free BMP2, or BMP2 coacervate. BMP2 dosage in the free BMP2 and BMP2 coacervate groups was equal. (A) Representative images of ALP staining of cultured cells at day 5(10X). (B) ALP activity was evaluated at day 5 and normalized by DNA content. Data represent mean ± SD; **P*<0.05 (n=4).

5.3.3 Effects of BMP2 coacervate on the osteogenesis of MDSCs *in vitro*

Upon stimulation with BMP2, MDSCs undergo osteogenic differentiation which can be evaluated by their expression of ALP [343, 346]. The efficacy of sustained delivery of BMP2 for inducing osteogenesis of MDSC was tested in both monolayer and in a 3-D fibrin gel, representing a potential scaffold for cell delivery to a bone defect. After 5 days in monolayer culture, the ALP activity of the MDSCs was effectively stimulated with 100ng of BMP2 coacervate while an equal single dose of free BMP2 showed no difference from the negative control and the coacervate only groups. (**Fig. 39a**). A multi-dose free BMP2 group was also included to mimic sustained release conditions with an equal dose of free BMP2 being added every two days. This amounted to a 3-fold higher total dosage of BMP2 (300ng) compared to the

BMP2 coacervate group (100ng). Multi-dose free BMP2 group did stimulate ALP activity, indicating that MDSCs require more than just a single initial exposure to free BMP2 to be effective; however, the ALP expression of this multi-dose BMP2 group showed no statistical difference from the BMP2 coacervate group, nor was there a difference between the BMP2 coacervate group and the BMP4-transduced MDSCs group (positive control), which was also supported by positive ALP staining (**Fig. 39c**). RT-PCR analysis showed the mRNA expression level of Runx.2 were slightly higher in MDSCs that stimulated by free BMP2 and BMP2 coacervate when compare to the control. However, no significant differences were found among groups. The mRNA expression level of Collagen type 1 significantly increased in MDSCs that were stimulated by BMP2 coacervate when compared to the MDSCs in control and single dose free BMP2 groups. No difference was observed between the multi-dose free BMP2 and BMP2 coacervate groups (**Fig. 39d**). This further confirms the notion that the coacervate delivery system can potentiate BMP2 activity with a lower dose producing a similar effect to 3-fold amounts of free BMP2.

To better mimic the *in vivo* environment, the effects that BMP2 coacervate had on the osteogenesis of the MDSCs were also examined in a 3-D fibrin gel culture system (**Fig. 39b**). Contrary to the results from the monolayer cultures, after 5 days of culture in fibrin gel, free BMP2 induced ALP expression above that of the control groups, possibly attributable to growth factor protection from degradation afforded by fibrin gel itself. Even so, BMP2 coacervate stimulated significantly more (approximately 2-fold) ALP activity compared to equal amount of free BMP2 (Fig. 5B). It should also be noted that the amount of BMP2 available to the cells in the BMP2 coacervate group was lower due to the nature of controlled release. The release assay indicated that less than 10% of the BMP2 was released by the coacervate after 5 days *in vitro*.

These data indicate that sustained release of BMP2 by the coacervate was more efficient than free BMP2 at stimulating osteogenesis of MDSCs in a 3-D fibrin gel environment.

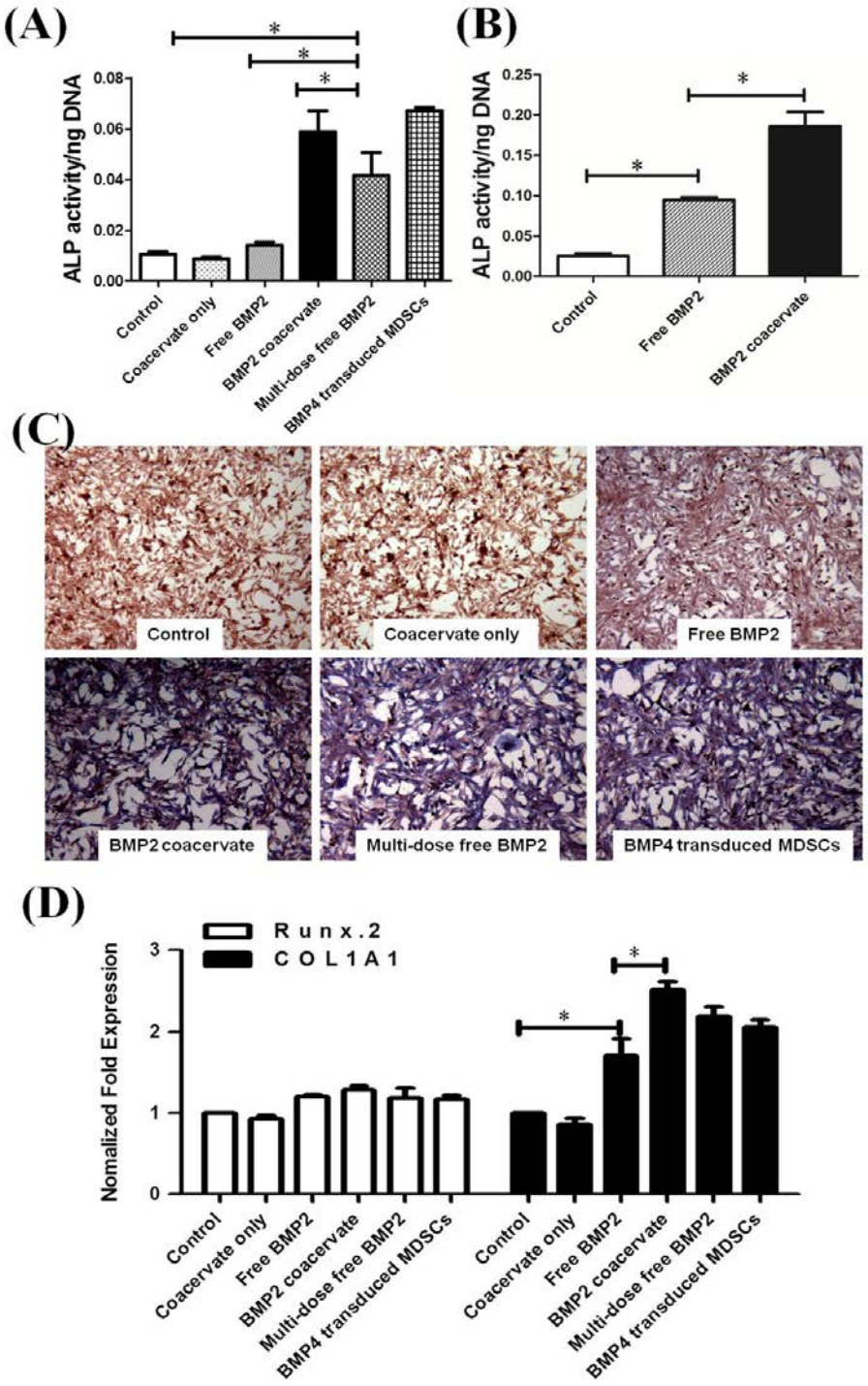

Figure 39. Osteogenic potential of MDSCs in monolayer and 3-D culture in vitro. (A) ALP expression of MDSCs after 5 days of monolayer culture, exposed to a single dose of 100ng free BMP2 or BMP2 coacervate, or to 100ng BMP2 at three different time points to mimic controlled release (Multi-dose free BMP2). Control groups were exposed to DPBS only (Control) or the coacervate only without BMP2. (B) ALP expression by

the MDSCs after 5 days of culture in a 3-D fibrin gel, exposed to 100ng free BMP2 or BMP2 coacervate or DPBS only as a control. Data represent mean ± SD; *P<0.05 (n=4). (C) Representative images of ALP staining of monolayer cultured MDSCs at day 5 (10X). (D) RT-PCR analysis of the expression of Runx.2 and COL1A1 in MDSCs after 5 day culture. Expression of the specific markers were normalized to β-actin and then scaled according to the control sample. This value was set to 1. Data represent mean ± SD; *P<0.05 (n=3)

5.3.4 Effects of BMP2 coacervate on the osteogenesis of mouse MDSCs *in vivo*

We next examined the ability of BMP2 coacervate to stimulate the osteogenic potential of MDSCs in a mouse ectopic bone formation model. Free BMP2 or BMP2 coacervate, with or without MDSCs, was suspended in fibrin glue, to keep the cells and coacervate localized, and then implanted into a muscle pocket created in the hind limbs of mice. All mice survived the experiment and no complications such as infection or peripheral nerve damage were observed. Quantification of calcified tissue (bone volume) by 3D Micro-CT analysis revealed extensive bone formation by the MDSCs stimulated with BMP2 coacervate 2 weeks after implantation and the amount of bone increased at 4 weeks (**Fig. 40a,b**). MDSCs with free BMP2 showed minimal bone formation at week 2 and also increased in volume by week 4 (**Fig. 40a,b**). BMP2 coacervate alone showed some bone formation at week 2 but no increase by week 4. MDSCs alone showed no significant bone formation at either time point, similar to the control group of fibrin gel alone (**Fig. 40a,b**). Significantly greater bone volume was formed by the MDSCs stimulated by BMP2 coacervate compared to all other groups at both time points; bone volume was 9-fold greater at week 2 and 4.5-fold greater at week 4 compared to the free BMP2+MDSC group (**Fig. 38b**).

Histological analysis included both Alizarin red staining and von Kossa staining to verify the calcium phosphate deposition and immunohistochemical (IHC) staining for GFP to determine the location of GFP-labeled MDSCs. Alizarin red and von Kossa staining revealed calcified osteoid matrix at the implantation site in the BMP2 coacervate only, free BMP2+MDSCs, and BMP2 coacervate+MDSCs groups, which is consistent with the Micro-CT data (**Fig. 40c**). This newly formed osteoid was abutting and expanding within the normal muscle tissue and the interface between the muscle and newly formed bone was clearly detectable. The myofibers adjacent to the ectopic bone formation appeared morphologically normal with a slight compression in the transition zone (**Fig. 40c**). Calcified osteoid matrix was found mostly at the edge of the transplantation area in the BMP2 coacervate only group but was found throughout the transplantation area in the free BMP2-MDSCs group and in the BMP2 coacervate+MDSCs group which also displayed a more mature trabecular bone structure (**Fig. 40c**). To determine whether the newly formed bone was derived from the transplanted MDSCs or from local host cells, MDSCs were labeled with GFP and then stained immunohistochemically. In the BMP2 coacervate only group, no GFP was detected in the newly formed bone osteoid which must therefore be derived from the host cells (**Fig. 40c**). In the free BMP2+MDSCs and BMP2 coacervate+MDSCs groups, cells expressing GFP were identified throughout and at the edge the osteoid with significantly more GFP positive cells observed in the BMP2 coacervate+MDSCs group (**Fig. 40c**). The transplanted MDSCs were closely associated with the newly formed osteoid, consistent with the hypothesis that the MDSCs were not only present within the osteoid but also active in the bone formation. Quantification of GFP-positive cells within, and the at the edge of the osteoid showed significantly higher numbers in the BMP2 coacervate+MDSCs group than in the free BMP2+MDSCs group (**Fig. 40d**).

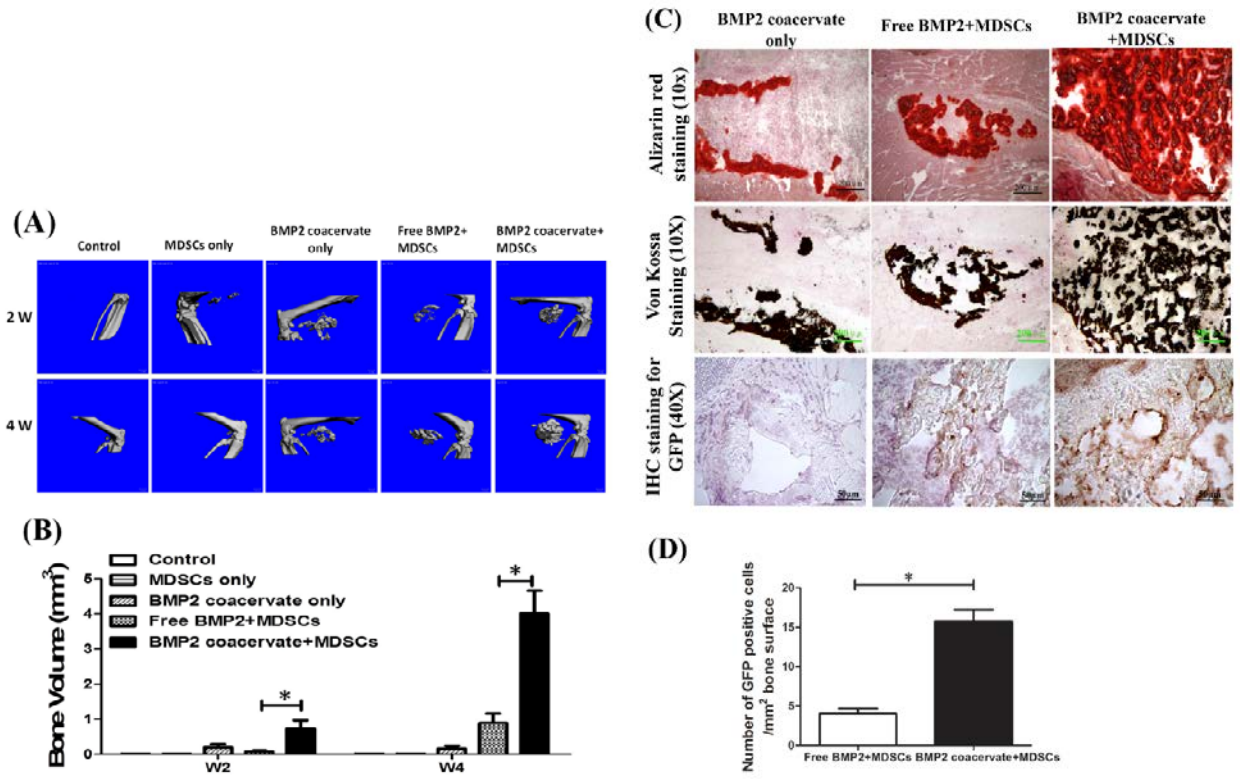

Figure 40. In vivo effects of BMP2 coacervate on the osteogenesis of MDSCs. (A) Representative Micro-CT images of ectopic bone formation after 2 and 4 weeks. Groups were transplanted with a fibrin gel containing 2µg free BMP2 or BMP2 coacervate alongside MDSCs, the BMP2 coacervate alone, MDSCs alone, or fibrin gel alone (Control). (B) Ectopic bone volume (BV) quantification of Micro-CT images after 2 and 4 weeks. Data represent the mean ± SD; **P*<0.05 (n=6). (C) Representative images of newly formed bone with Alizarin red staining (red, scale bars=200µm), von Kossa staining (black, scale bars=200µm) of calcified osteoid matrix, and immunohistochemical (IHC) staining for transplanted MDSCs (GFP-positive, brown, scale bars=50µm). (D) Quantification of the number of GFP-positive cell within and at the edge of the osteoid per mm^2 of bone surface; **P*<0.01 (n=6).

5.3.5 Effects of BMP2 coacervate on human MDSCs in vitro and in vivo

hMDSCs were stimulated *in vitro* with a single free BMP2 dose (100ng) or BMP2 coacervate containing 100ng of BMP2 for 3 days. The ALP expression was significantly higher in the BMP2 coacervate group compared to the free BMP2 group (**Fig. 41a**). We observed significantly more ectopic bone after 2 and 4 weeks in the BMP2 coacervate+hMDSC group when compared to the other groups (**Fig. 41b**). Furthermore, when we transplanted hMDSCs with free BMP2 or with BMP2 coacervate into 5mm critical-size calvarial defects created in CD1 mice, microCT evaluation after 2 weeks revealed significantly larger bone volume in the BMP2 coacervate group compared to the free BMP2 group (**Fig. 41c,d**). The same population of hMDSCs (1.5x106 cells) transduced with lenti-BMP2 was used as a positive control group (BMP2-transduced hMDSCs). Interestingly, there was no significant difference between the BMP2 coacervate+hMDSC and BMP2 transduced hMDSC groups. By 4 weeks we observed only partial healing of the defect in the free BMP2+hMDSC group. In contrast, the bone defect in the BMP2 coacervate group was almost completely covered with regenerated bone, which was similar to the BMP2-transduced hMDSC group (no significant difference was observed between these two groups). These results taken together suggest that the BMP2 coacervate could represent a BMP2 delivery system of choice when combine with hMDSCs to enhance bone repair in order to accelerate the clinical translation of our work, without the requirement of gene therapy.

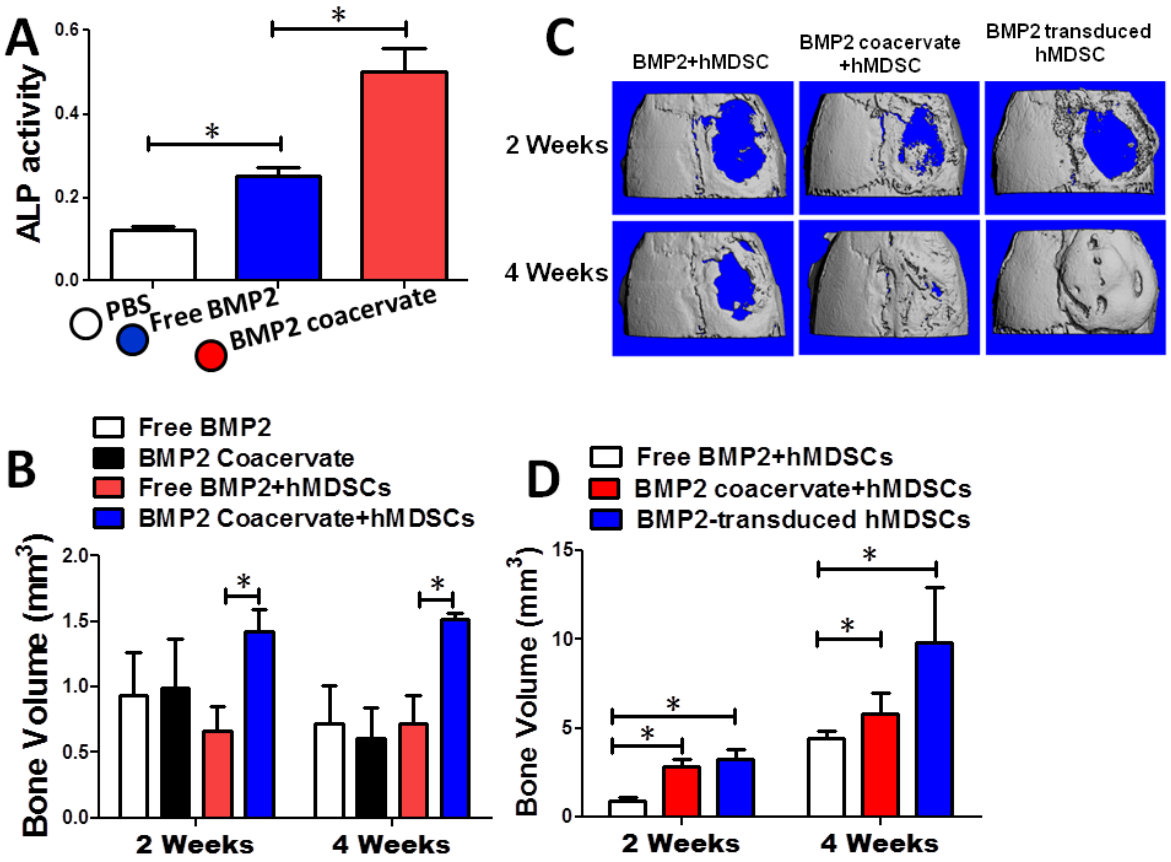

Figure 41. Osteogenic potential of human MDSCs. A) In vitro ALP expression assay. *P<0.05. B) Quantification of *in vivo* ectopic bone formation model. *P<0.05. C) Representative µCT images of *in vivo* cranial defect model. D) Quantification of *in vivo* cranial defect bone formation model. *P<0.05.

5.4 DISCUSSION

Skeletal muscle is a good source of various cellular progenitors with potential musculoskeletal therapeutic applications [338, 339, 343]. Muscle-derived stem cells (MDSCs) are a population of cells that can be isolated by a modified pre-plate technique from mouse skeletal muscle and display a superior regeneration capacity in various musculoskeletal tissues, including skeletal

and cardiac muscles, bone, and articular cartilage when compared to myoblasts [344, 350-352]. MDSCs demonstrate the capacity for self-renewal, long term proliferation, multi-potent differentiation, and have a superior ability for survival due to their increased resistance to oxidative and inflammatory stresses [365]. MDSCs are therefore an alternative cell source, other than bone marrow or fat tissue derived mesenchymal stem cells, for bone tissue engineering.

Since local stimulation of MDSCs by BMPs following transplantation is essential for osteogenic differentiation, maintaining an adequate concentration of stable, active BMPs at the transplantation site is necessary. Unfortunately, for most clinical applications requiring cell transplantation such as bone non-union, delayed non-union, and large bone defects, local BMP shortage is a primary cause for insufficient healing. Without supplementation of exogenous BMPs, most transplanted progenitor cells, such as mesenchymal stem cells (MSCs), fail to undergo osteogenic differentiation and eventually form fibrous tissue instead of functional bone [366, 367]. More importantly for the current study, non-transduced MDSCs do not undergo osteogenic and chondrogenic differentiation when transplanted into bone and articular cartilage defects *in vivo*, rather they undergo default myogenic differentiation [355, 356]. Simply incorporating recombinant BMP protein within a commonly used soluble scaffold such as fibrin glue, fails to sufficiently stimulate MDSCs to undergo osteogenesis [356]. Additionally, the half-lives of BMPs in the body are very short, on the order of minutes to hours [357, 358]. As a result, large doses of BMP are often required to obtain the desired osteogenic effect [368]. Many studies use doses on the order of 1000 times greater than can be found in the entire human body, drawing concerns with regards to cost and safety [369, 370]. With such short half-lives and rapid dilution in the body, even these large doses may not provide adequate local concentrations at critical times to optimally induce bone formation by the transplanted cells. As a result, controlled

delivery systems that supply active BMPs alongside the transplanted progenitor cells to promote osteogenesis are highly important for the future of cell-based bone regeneration strategies.

Developing suitable carriers for BMPs that can preserve their bioactivity and sustain their release over time presents a great challenge. To date, a number of systems have been designed and evaluated for the delivery of BMPs, including gelatin/β-tricalcium phosphate [371], collagen gel [372], poly-L-lactic acid scaffolds [373], a porous hydroxyapatite composite [374], hyaluronic acid [375], and fibrin gel [375]. Bovine type I collagen is currently used in the clinical setting as a carrier and has been approved by the Food and Drug Administration for spine fusion in humans [376, 377]. These delivery systems have been shown to enhance bone repair and accelerate fracture healing to some degree; however, they often suffer issues inherent to poor control over release rate such as low loading efficiency and a large initial burst release of the protein [371-373]. Furthermore, the use of harsh organic solvents in the synthesis of many polymeric delivery systems may denature loaded growth factor proteins and reduce their bioactivity [378]. Clearly, a controlled release system that avoids these common setbacks could greatly advance the field of growth factor delivery for bone regeneration.

In the current study, a PEAD:heparin growth factor delivery system was designed and utilized to provide continual release of BMP2 alongside the transplanted MDSCs. Heparan sulfate glycosaminoglycans are a natural component of the extracellular matrix with a high affinity for many growth factors and cytokines. Heparin has a similar structure and is commonly incorporated into delivery systems for heparin-binding growth factors. Heparin binds BMP2 with high affinity [379] and has been previously shown to retain its bioactivity well [357, 380, 381]. In the presence of heparin, degradation of BMP2 is reduced and its half-life in culture media is prolonged 20-fold [357]. To best preserve heparin in its intact form and maintain its full

functionality we used a polycation which complexes with heparin by charge interactions. PEAD is a synthetic polycation with a high charge density, easy synthesis, and good biocompatibility [212]. Heparin and bound growth factors precipitate out of the aqueous solution upon interaction with PEAD to form a self-assembled coacervate. Once incorporated in the coacervate, growth factors are protected from degradation and slowly released over time based on disassembly of the complex in an ionic environment and hydrolytic degradation of PEAD [212]. Our data using both C2C12 cells and MDSCs demonstrated the retained bioactivity of BMP2 released from the coacervate. Furthermore, BMP2 coacervate stimulated higher cellular ALP activity than equal dose of free BMP2, and showed similar results to a 3-fold higher total dose of free BMP2 added at multiple times during the experiment. These results indicate that the coacervate may directly potentiate the activity of BMP2 beyond what is inherent to sustained release. Indeed, heparin has been shown to modulate the interactions between heparin-binding growth factors and their receptors [382, 383], and likely plays a similar role in promoting the bioactivity of BMP2 [381]. Moreover, heparin has also been shown to protect BMP2 from the inhibition by noggin, which is induced to express as part of the negative feedback loop in response to BMP2 expression [357].

Pharmacokinetic models of BMP release from collagen sponges and other common delivery vehicles show rapid initial effluxes, during which the carrier can lose 30% or more of its loaded BMP [384, 385]. This initial burst release spikes the BMP concentration in the surrounding tissue to supraphysiological levels which can result in severe complications such as ectopic bone formation in the spinal canal, haematomas in soft tissue, and bone resorption around implants [386-389]. Clearly such systems are inefficient and potentially harmful. Conversely, the PEAD-heparin delivery system loaded BMP2 with high efficiency (98.2% loading), showed a negligible initial burst release (1.3% after one day), and thereafter produced

slow and sustained release for at least 4 weeks. Our *in vivo* results showed extensive bone formation by the transplanted MDSCs and minimal participation of surrounding host tissue cells, which indicates the local preservation of BMP2 activity and the efficacy of sustained release of BMP2 on the osteogenesis of the donor MDSCs. The released BMP2 did not appear to have any significant effect on the surrounding tissue, indicating that the coacervate localizes the BMP2 to the site of implantation. Our *in vitro* data showed only 25% of the BMP2 was released after 28 days, yet release is expected to be accelerated *in vivo* where degradation of the polyester backbone of PEAD is catalyzed in the presence of hydrolases [390]. Hydrolases may also be secreted by the MDSCs which could contribute to the targeting of BMP2 release on the transplanted cells.

In the present study, the coacervate served as a multi-functional vehicle for growth factor delivery. The coacervate naturally loads any heparin-binding growth factor, enabling co-delivery of other factors alongside BMP2 in the future. Of particular importance may be angiogenic growth factors to incite the formation of a supportive vascular network to enhance MDSC survival and osteogenesis. Additionally, the strongly polyvalent nature and many free functional groups of the PEAD-heparin coacervate enable easy coating onto a wide range of materials. Held by relatively weak Coulombic forces and hydrogen bonding, the release functionality of the delivery system is unlikely to be affected. This could be useful for stimulating host cell seeding of osteo-inductive scaffolds *in situ*, or to improve the osteogenesis of cells seeded into scaffolds *ex vivo*.

5.5 CONCLUSIONS

This study demonstrated that a dual cell and growth factor delivery approach may serve as a viable therapy for muscle cell based bone regeneration. The controlled delivery of BMP2 from [PEAD:heparin] coacervate can sufficiently stimulate hMDSCs to differentiate into an osteogenic lineage, both *in vitro* and *in vivo*. Lastly, hMDSC combined with BMP2 coacervate showed comparable reparative potential to genetically modified hMDSCs. Therefore, the implantation of non-genetically modified hMDSCs to the injury site with an effective BMP delivery system is a practical option for patients in terms of both safety and long term results.

6.0 FINAL CONCLUSIONS AND FUTURE DIRECTIONS

Here I describe the development of three regenerative therapies for three distinct biomedical applications: skin wound healing, cardiac repair, and bone regeneration. Each approach consists of the three key components of all regenerative therapies: cells, scaffolds, and signals. Based on the application, for each component I chose to apply it exogenously or to rely on provision by the body. For wound healing I applied HB-EGF and relied on endogenous scaffolding and cells to do the rest (**Fig. 42a**). For cardiac repair I included a PEG scaffold along with Shh but relied on the body's own cells to complete the regenerative therapy (**Fig. 42b**). Finally, for bone regeneration I applied BMP2, a fibrin gel, and MDSCs because the body could not sufficiently supply any of these components (**Fig. 42c**). And in all three cases we appreciate the importance of the extracellular matrix in the form of a biomimetic coacervate which I demonstrated was imperative to the success of each therapy (**Fig. 42d**).

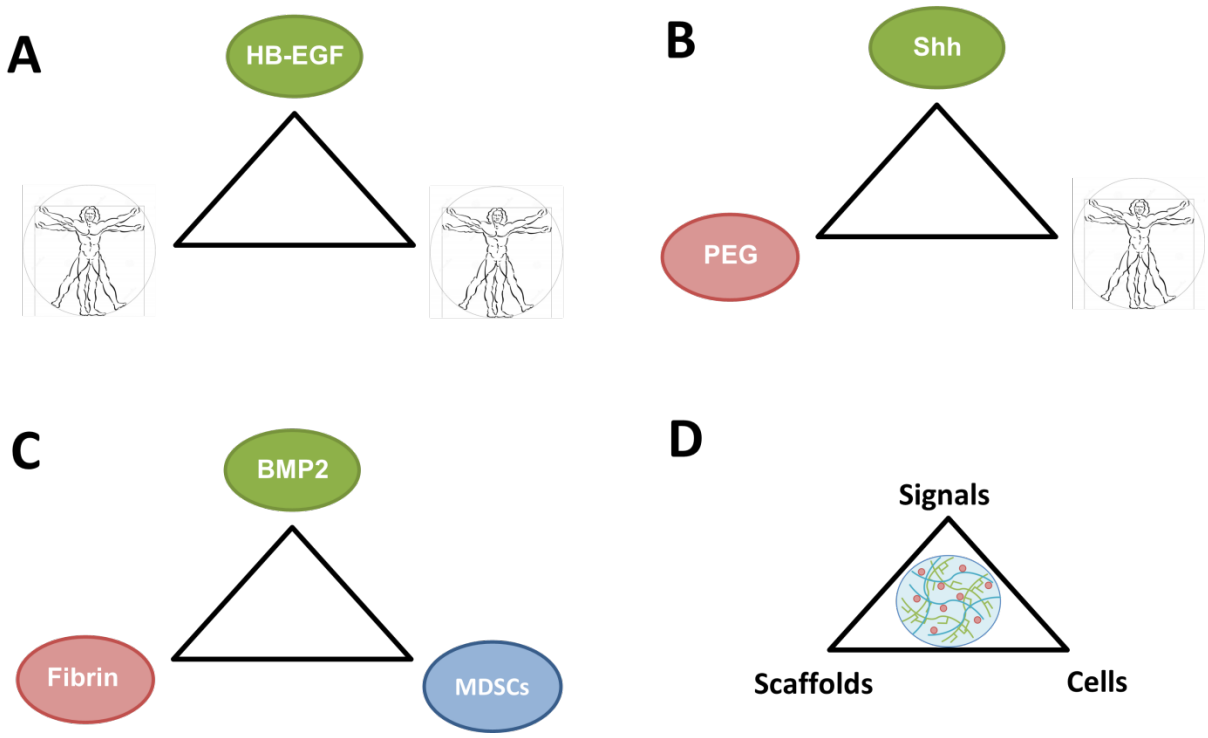

Figure 42. Regenerative therapies for three biomedical applications. A) Wound healing required HB-EGF and the body provided the scaffold and cells. B) Cardiac repair required Shh and PEG hydrogel and the body provided the cells. C) Bone regeneration required BMP2, a fibrin gel, and MDSCs. D) The three therapies are linked by use of a biomimetic coacervate which imitates the role of the ECM in facilitating growth factor signaling in the body.

The ultimate goal of the experimental therapies described here are better clinical treatments for diabetic ulcers, heart failure, and bone defects. Each therapy will require validation in large animal studies and controlled clinical trials; growth factor dosage and application method will require optimization at each step. However, this dissertation lays the foundation, and furthermore should fuel the development of new and innovative regenerative therapies for other diseases in the 21st century.

BIBLIOGRAPHY

[1] Stompro BE, Hansbrough JF, Boyce ST. Attachment of peptide growth factors to implantable collagen. J Surg Res. 1989;46:413-21.

[2] Zisch AH, Lutolf MP, Hubbell JA. Biopolymeric delivery matrices for angiogenic growth factors. Cardiovasc Pathol. 2003;12:295-310.

[3] Hong JP, Jung HD, Kim YW. Recombinant human epidermal growth factor (EGF) to enhance healing for diabetic foot ulcers. Ann Plast Surg. 2006;56:394-8; discussion 9-400.

[4] Demidova-Rice TN, Hamblin MR, Herman IM. Acute and impaired wound healing: pathophysiology and current methods for drug delivery, part 2: role of growth factors in normal and pathological wound healing: therapeutic potential and methods of delivery. Adv Skin Wound Care. 2012;25:349-70.

[5] Yao C, Markowicz M, Pallua N, Noah EM, Steffens G. The effect of cross-linking of collagen matrices on their angiogenic capability. Biomaterials. 2008;29:66-74.

[6] Geer DJ, Swartz DD, Andreadis ST. Biomimetic delivery of keratinocyte growth factor upon cellular demand for accelerated wound healing in vitro and in vivo. Am J Pathol. 2005;167:1575-86.

[7] Ishikawa T, Terai H, Kitajima T. Production of a biologically active epidermal growth factor fusion protein with high collagen affinity. J Biochem. 2001;129:627-33.

[8] Degim Z. Use of microparticulate systems to accelerate skin wound healing. J Drug Target. 2008;16:437-48.

[9] Capila I, Linhardt R. Heparin-protein interactions. Angew Chem. 2002;41:391-412.

[10] Mulloy B, Forster MJ. Conformation and dynamics of heparin and heparan sulfate. Glycobiology. 2000;10:1147-56.

[11] Pellegrini L. Role of heparan sulfate in fibroblast growth factor signalling: a structural view. Curr Opin Struct Biol. 2001;11:629-34.

[12] Pellegrini L, Burke DF, von Delft F, Mulloy B, Blundell TL. Crystal structure of fibroblast growth factor receptor ectodomain bound to ligand and heparin. Nature. 2000;407:1029-34.

[13] Chung H, Kim H, Yoon J, Park T. Heparin immobilized porous PLGA microspheres for angiogenic growth factor delivery. Pharm Res. 2006;23:1835-41.

[14] Li B, Davidson JM, Guelcher SA. The effect of the local delivery of platelet-derived growth factor from reactive two-component polyurethane scaffolds on the healing in rat skin excisional wounds. Biomaterials. 2009;30:3486-94.

[15] Kanya R, Heather AB, Michael JH, Xiaoqiang H, James FH, Jon WL, et al. Heparin Binding Nanostructures to Promote Growth of Blood Vessels. Nano Letters. 2006;6:2086–90.

[16] Wood M, Borschel G, Sakiyama-Elbert S. Controlled release of glial-derived neurotrophic factor from fibrin matrices containing an affinity-based delivery system. J Biomed Mater Res A. 2009;89:909-18.

[17] Brandon LS, Alyssa P. Physical Polymer Matrices Based on Affinity Interactions between Peptides and Polysaccharides. Biomacromolecules. 2003;4.

[18] Seal B, Panitch A. Physical matrices stabilized by enzymatically sensitive covalent crosslinks. Acta Biomater. 2006;2:241-51.

[19] Nie T, Baldwin A, Yamaguchi N, Kiick K. Production of heparin-functionalized hydrogels for the development of responsive and controlled growth factor delivery systems. J Control Release. 2007;122:287-96.

[20] Chu H, Gao J, Chen CW, Huard J, Wang Y. Injectable fibroblast growth factor-2 coacervate for persistent angiogenesis. Proc Natl Acad Sci U S A. 2011;108:13444-9.

[21] Chu H, Johnson NR, Mason NS, Wang Y. A [polycation:heparin] complex releases growth factors with enhanced bioactivity. J Control Release. 2011;150:157-63.

[22] Brem H, Tomic-Canic M. Cellular and molecular basis of wound healing in diabetes. J Clin Invest. 2007;117:1219-22.

[23] Barrientos S, Stojadinovic O, Golinko MS, Brem H, Tomic-Canic M. Growth factors and cytokines in wound healing. Wound Repair Regen. 2008;16:585-601.

[24] Singer AJ, Clark RA. Cutaneous wound healing. New Engl J Med. 1999;341:738-46.

[25] Behm B, Babilas P, Landthaler M, Schreml S. Cytokines, chemokines and growth factors in wound healing. J Eur Acad Dermatol Venereol. 2011.

[26] Werner S, Grose R. Regulation of wound healing by growth factors and cytokines. Physiol Rev. 2003;83:835-70.

[27] Boateng JS, Matthews KH, Stevens HN, Eccleston GM. Wound healing dressings and drug delivery systems: a review. J Pharm Sci. 2008;97:2892-923.

[28] Koria P. Delivery of growth factors for tissue regeneration and wound healing. BioDrugs. 2012;26:163-75.

[29] Katti DS, Robinson KW, Ko FK, Laurencin CT. Bioresorbable nanofiber-based systems for wound healing and drug delivery: optimization of fabrication parameters. J Biomed Mater Res B. 2004;70:286-96.

[30] Branski LK, Pereira CT, Herndon DN, Jeschke MG. Gene therapy in wound healing: present status and future directions. Gene Ther. 2007;14:1-10.

[31] Hirsch T, Spielmann M, Yao F, Eriksson E. Gene therapy in cutaneous wound healing. Front Biosci. 2007;12:2507-18.

[32] Greer N, Foman N, Wilt T, Dorrian J, Fitzgerald P, MacDonald R, et al. Advanced Wound Care Therapies for Non-Healing Diabetic, Venous, and Arterial Ulcers: A Systematic Review. 2012.

[33] Clark RA, Ghosh K, Tonnesen MG. Tissue engineering for cutaneous wounds. J Invest Dermatol. 2007;127:1018-29.

[34] Kamel RA, Ong JF, Eriksson E, Junker JP, Caterson EJ. Tissue engineering of skin. J Am Coll Surg. 2013;217:533-55.

[35] Drury JL, Mooney DJ. Hydrogels for tissue engineering: scaffold design variables and applications. Biomaterials. 2003;24:4337-51.

[36] Ueno H, Mori T, Fujinaga T. Topical formulations and wound healing applications of chitosan. Adv Drug Deliv Rev. 2001;52:105-15.

[37] Mi FL, Wu YB, Shyu SS, Chao AC, Lai JY, Su CC. Asymmetric chitosan membranes prepared by dry/wet phase separation: a new type of wound dressing for controlled antibacterial release. J Membrane Sci. 2003;212:237-54.

[38] Mi FL, Wu YB, Shyu SS, Schoung JY, Huang YB, Tsai YH, et al. Control of wound infections using a bilayer chitosan wound dressing with sustainable antibiotic delivery. J Biomed Mater Res. 2002;59:438-49.

[39] Meng X, Tian F, Yang J, He CN, Xing N, Li F. Chitosan and alginate polyelectrolyte complex membranes and their properties for wound dressing application. J Mater Sci Mater Med. 2010;21:1751-9.

[40] Noel SP, Courtney H, Bumgardner JD, Haggard WO. Chitosan films: a potential local drug delivery system for antibiotics. Clin Orthop Relat Res. 2008;466:1377-82.

[41] Smith JK, Bumgardner JD, Courtney HS, Smeltzer MS, Haggard WO. Antibiotic-loaded chitosan film for infection prevention: A preliminary in vitro characterization. J Biomed Mater Res B. 2010;94:203-11.

[42] Jackson SR, Richelsoph KC, Courtney HS, Wenke JC, Branstetter JG, Bumgardner JD, et al. Preliminary in vitro evaluation of an adjunctive therapy for extremity wound infection reduction: rapidly resorbing local antibiotic delivery. J Orthop Res. 2009;27:903-8.

[43] Smith JK, Moshref AR, Jennings JA, Courtney HS, Haggard WO. Chitosan sponges for local synergistic infection therapy: a pilot study. Clin Orthop Relat Res. 2013;471:3158-64.

[44] Stinner DJ, Noel SP, Haggard WO, Watson JT, Wenke JC. Local antibiotic delivery using tailorable chitosan sponges: the future of infection control? J Orthop Trauma. 2010;24:592-7.

[45] Mizuno K, Yamamura K, Yano K, Osada T, Saeki S, Takimoto N, et al. Effect of chitosan film containing basic fibroblast growth factor on wound healing in genetically diabetic mice. J Biomed Mater Res A. 2003;64:177-81.

[46] Ishihara M, Fujita M, Obara K, Hattori H, Nakamura S, Nambu M, et al. Controlled releases of FGF-2 and paclitaxel from chitosan hydrogels and their subsequent effects on wound repair, angiogenesis, and tumor growth. Curr Drug Deliv. 2006;3:351-8.

[47] Tran NQ, Joung YK, Lih E, Park KD. In situ forming and rutin-releasing chitosan hydrogels as injectable dressings for dermal wound healing. Biomacromolecules. 2011;12:2872-80.

[48] Obara K, Ishihara M, Ishizuka T, Fujita M, Ozeki Y, Maehara T, et al. Photocrosslinkable chitosan hydrogel containing fibroblast growth factor-2 stimulates wound healing in healing-impaired db/db mice. Biomaterials. 2003;24:3437-44.

[49] Breen A, O'Brien T, Pandit A. Fibrin as a delivery system for therapeutic drugs and biomolecules. Tissue Eng Part B Rev. 2009;15:201-14.

[50] Trentin D, Hall H, Wechsler S, Hubbell JA. Peptide-matrix-mediated gene transfer of an oxygen-insensitive hypoxia-inducible factor-1alpha variant for local induction of angiogenesis. Proc Natl Acad Sci U S A. 2006;103:2506-11.

[51] Breen AM, Dockery P, O'Brien T, Pandit AS. The use of therapeutic gene eNOS delivered via a fibrin scaffold enhances wound healing in a compromised wound model. Biomaterials. 2008;29:3143-51.

[52] Breen A, Dockery P, O'Brien T, Pandit A. Fibrin scaffold promotes adenoviral gene transfer and controlled vector delivery. J Biomed Mater Res A. 2009;89:876-84.

[53] Kulkarni M, O'Loughlin A, Vazquez R, Mashayekhi K, Rooney P, Greiser U, et al. Use of a fibrin-based system for enhancing angiogenesis and modulating inflammation in the treatment of hyperglycemic wounds. Biomaterials. 2014;35:2001-10.

[54] Pandit AS, Wilson DJ, Feldman DS. Fibrin scaffold as an effective vehicle for the delivery of acidic fibroblast growth factor (FGF-1). J Biomater Appl. 2000;14:229-42.

[55] Pandit AS, Feldman DS, Caulfield J, Thompson A. Stimulation of angiogenesis by FGF-1 delivered through a modified fibrin scaffold. Growth Factors. 1998;15:113-23.

[56] Lutolf MP, Hubbell JA. Synthetic biomaterials as instructive extracellular microenvironments for morphogenesis in tissue engineering. Nat Biotechnol. 2005;23:47-55.

[57] Yang HS, Shin J, Bhang SH, Shin JY, Park J, Im GI, et al. Enhanced skin wound healing by a sustained release of growth factors contained in platelet-rich plasma. Exp Mol Med. 2011;43:622-9.

[58] Liu Y, Cai S, Shu XZ, Shelby J, Prestwich GD. Release of basic fibroblast growth factor from a crosslinked glycosaminoglycan hydrogel promotes wound healing. Wound Repair Regen. 2007;15:245-51.

[59] Hong SR, Lee SJ, Shim JW, Choi YS, Lee YM, Song KW, et al. Study on gelatin-containing artificial skin IV: A comparative study on the effect of antibiotic and EGF on cell proliferation during epidermal healing. Biomaterials. 2001;22:2777-83.

[60] Rabbany SY, Pastore J, Yamamoto M, Miller T, Rafii S, Aras R, et al. Continuous delivery of stromal cell-derived factor-1 from alginate scaffolds accelerates wound healing. Cell Transplant. 2010;19:399-408.

[61] Henderson PW, Singh SP, Krijgh DD, Yamamoto M, Rafii DC, Sung JJ, et al. Stromal-derived factor-1 delivered via hydrogel drug-delivery vehicle accelerates wound healing in vivo. Wound Repair Regen. 2011;19:420-5.

[62] Balakrishnan B, Mohanty M, Umashankar PR, Jayakrishnan A. Evaluation of an in situ forming hydrogel wound dressing based on oxidized alginate and gelatin. Biomaterials. 2005;26:6335-42.

[63] Balakrishnan B, Mohanty M, Fernandez AC, Mohanan PV, Jayakrishnan A. Evaluation of the effect of incorporation of dibutyryl cyclic adenosine monophosphate in an in situ-forming hydrogel wound dressing based on oxidized alginate and gelatin. Biomaterials. 2006;27:1355-61.

[64] Sokolsky-Papkov M, Agashi K, Olaye A, Shakesheff K, Domb AJ. Polymer carriers for drug delivery in tissue engineering. Adv Drug Deliv Rev. 2007;59:187-206.

[65] Knop K, Hoogenboom R, Fischer D, Schubert US. Poly(ethylene glycol) in drug delivery: pros and cons as well as potential alternatives. Angewandte Chemie. 2010;49:6288-308.

[66] Anumolu SS, Menjoge AR, Deshmukh M, Gerecke D, Stein S, Laskin J, et al. Doxycycline hydrogels with reversible disulfide crosslinks for dermal wound healing of mustard injuries. Biomaterials. 2011;32:1204-17.

[67] Gong C, Wu Q, Wang Y, Zhang D, Luo F, Zhao X, et al. A biodegradable hydrogel system containing curcumin encapsulated in micelles for cutaneous wound healing. Biomaterials. 2013;34:6377-87.

[68] Huang X, Brazel CS. On the importance and mechanisms of burst release in matrix-controlled drug delivery systems. J Control Release. 2001;73:121-36.

[69] FDA. Update of Safety Review: Follow-up to the March 27, 2008, Communication about the Ongoing Safety Review of Regranex (becaplermin). Health and Human Services; 2008.

[70] Glowacki J, Mizuno S. Collagen scaffolds for tissue engineering. Biopolymers. 2008;89:338-44.

[71] Gopinath D, Ahmed MR, Gomathi K, Chitra K, Sehgal PK, Jayakumar R. Dermal wound healing processes with curcumin incorporated collagen films. Biomaterials. 2004;25:1911-7.

[72] Arul V, Kartha R, Jayakumar R. A therapeutic approach for diabetic wound healing using biotinylated GHK incorporated collagen matrices. Life Sci. 2007;80:275-84.

[73] Arul V, Gopinath D, Gomathi K, Jayakumar R. Biotinylated GHK peptide incorporated collagenous matrix: A novel biomaterial for dermal wound healing in rats. J Biomed Mater Res B. 2005;73:383-91.

[74] Arul V, Masilamoni JG, Jesudason EP, Jaji PJ, Inayathullah M, Dicky John DG, et al. Glucose oxidase incorporated collagen matrices for dermal wound repair in diabetic rat models: a biochemical study. J Biomater Appl. 2012;26:917-38.

[75] Gomathi K, Gopinath D, Rafiuddin Ahmed M, Jayakumar R. Quercetin incorporated collagen matrices for dermal wound healing processes in rat. Biomaterials. 2003;24:2767-72.

[76] Matsumoto S, Tanaka R, Okada K, Arita K, Hyakusoku H, Miyamoto M, et al. The Effect of Control-released Basic Fibroblast Growth Factor in Wound Healing: Histological Analyses and Clinical Application. Plast Reconstr Surg. 2013;1:e44 10.1097/GOX.0b013e3182a88787.

[77] Wang W, Lin S, Xiao Y, Huang Y, Tan Y, Cai L, et al. Acceleration of diabetic wound healing with chitosan-crosslinked collagen sponge containing recombinant human acidic fibroblast growth factor in healing-impaired STZ diabetic rats. Life Sci. 2008;82:190-204.

[78] Kanda N, Morimoto N, Takemoto S, Ayvazyan AA, Kawai K, Sakamoto Y, et al. Efficacy of novel collagen/gelatin scaffold with sustained release of basic fibroblast growth factor for dermis-like tissue regeneration. Ann Plast Surg. 2012;69:569-74.

[79] Kanda N, Morimoto N, Ayvazyan AA, Takemoto S, Kawai K, Nakamura Y, et al. Evaluation of a novel collagen-gelatin scaffold for achieving the sustained release of basic fibroblast growth factor in a diabetic mouse model. J Tissue Eng Regen Med. 2014;8:29-40.

[80] Ito R, Morimoto N, Pham LH, Taira T, Kawai K, Suzuki S. Efficacy of the controlled release of concentrated platelet lysate from a collagen/gelatin scaffold for dermis-like tissue regeneration. Tissue Eng Part A. 2013;19:1398-405.

[81] Guo R, Xu S, Ma L, Huang A, Gao C. Enhanced angiogenesis of gene-activated dermal equivalent for treatment of full thickness incisional wounds in a porcine model. Biomaterials. 2010;31:7308-20.

[82] Guo R, Xu S, Ma L, Huang A, Gao C. The healing of full-thickness burns treated by using plasmid DNA encoding VEGF-165 activated collagen-chitosan dermal equivalents. Biomaterials. 2011;32:1019-31.

[83] Yan X, Chen B, Lin Y, Li Y, Xiao Z, Hou X, et al. Acceleration of diabetic wound healing by collagen-binding vascular endothelial growth factor in diabetic rat model. Diabetes Res Clin Pract. 2010;90:66-72.

[84] Tan Q, Chen B, Yan X, Lin Y, Xiao Z, Hou X, et al. Promotion of diabetic wound healing by collagen scaffold with collagen-binding vascular endothelial growth factor in a diabetic rat model. J Tissue Eng Regen Med. 2014;8:195-201.

[85] Sun W, Lin H, Chen B, Zhao W, Zhao Y, Xiao Z, et al. Collagen scaffolds loaded with collagen-binding NGF-beta accelerate ulcer healing. J Biomed Mater Res A. 2010;92:887-95.

[86] Matsumoto Y, Kuroyanagi Y. Development of a wound dressing composed of hyaluronic acid sponge containing arginine and epidermal growth factor. J Biomater Sci Polym Ed. 2010;21:715-26.

[87] Kondo S, Kuroyanagi Y. Development of a wound dressing composed of hyaluronic acid and collagen sponge with epidermal growth factor. J Biomater Sci Polym Ed. 2012;23:629-43.

[88] Sill TJ, von Recum HA. Electrospinning: applications in drug delivery and tissue engineering. Biomaterials. 2008;29:1989-2006.

[89] Yang Y, Xia T, Zhi W, Wei L, Weng J, Zhang C, et al. Promotion of skin regeneration in diabetic rats by electrospun core-sheath fibers loaded with basic fibroblast growth factor. Biomaterials. 2011;32:4243-54.

[90] Yang Y, Xia T, Chen F, Wei W, Liu C, He S, et al. Electrospun fibers with plasmid bFGF polyplex loadings promote skin wound healing in diabetic rats. Mol Pharm. 2012;9:48-58.

[91] Choi JS, Leong KW, Yoo HS. In vivo wound healing of diabetic ulcers using electrospun nanofibers immobilized with human epidermal growth factor (EGF). Biomaterials. 2008;29:587-96.

[92] Choi JS, Choi SH, Yoo HS. Coaxial electrospun nanofibers for treatment of diabetic ulcers with binary release of multiple growth factors. J Mater Chem. 2011;21:5258-67.

[93] Fu SZ, Meng XH, Fan J, Yang LL, Wen QL, Ye SJ, et al. Acceleration of dermal wound healing by using electrospun curcumin-loaded poly(epsilon-caprolactone)-poly(ethylene glycol)-poly(epsilon-caprolactone) fibrous mats. J Biomed Mater Res B. 2014;102:533-42.

[94] Merrell JG, McLaughlin SW, Tie L, Laurencin CT, Chen AF, Nair LS. Curcumin-loaded poly(epsilon-caprolactone) nanofibres: diabetic wound dressing with anti-oxidant and anti-inflammatory properties. Clin Exp Pharmacol Physiol. 2009;36:1149-56.

[95] Bertoncelj V, Pelipenko J, Kristl J, Jeras M, Cukjati M, Kocbek P. Development and bioevaluation of nanofibers with blood-derived growth factors for dermal wound healing. Eur J Pharm Biopharm. 2014.

[96] Hong JP, Kim YW, Lee SK, Kim SH, Min KH. The effect of continuous release of recombinant human epidermal growth factor (rh-EGF) in chitosan film on full thickness excisional porcine wounds. Ann Plast Surg. 2008;61:457-62.

[97] Moura LI, Dias AM, Leal EC, Carvalho L, de Sousa HC, Carvalho E. Chitosan-based dressings loaded with neurotensin--an efficient strategy to improve early diabetic wound healing. Acta Biomater. 2014;10:843-57.

[98] Soppimath KS, Aminabhavi TM, Kulkarni AR, Rudzinski WE. Biodegradable polymeric nanoparticles as drug delivery devices. J Control Release. 2001;70:1-20.

[99] Kumari A, Yadav SK, Yadav SC. Biodegradable polymeric nanoparticles based drug delivery systems. Colloid Surface B. 2010;75:1-18.

[100] Porporato PE, Payen VL, De Saedeleer CJ, Preat V, Thissen JP, Feron O, et al. Lactate stimulates angiogenesis and accelerates the healing of superficial and ischemic wounds in mice. Angiogenesis. 2012;15:581-92.

[101] Chereddy KK, Coco R, Memvanga PB, Ucakar B, des Rieux A, Vandermeulen G, et al. Combined effect of PLGA and curcumin on wound healing activity. J Control Release. 2013;171:208-15.

[102] Chu Y, Yu D, Wang P, Xu J, Li D, Ding M. Nanotechnology promotes the full-thickness diabetic wound healing effect of recombinant human epidermal growth factor in diabetic rats. Wound Repair Regen. 2010;18:499-505.

[103] Park HJ, Lee J, Kim MJ, Kang TJ, Jeong Y, Um SH, et al. Sonic hedgehog intradermal gene therapy using a biodegradable poly(beta-amino esters) nanoparticle to enhance wound healing. Biomaterials. 2012;33:9148-56.

[104] Han G, Nguyen LN, Macherla C, Chi Y, Friedman JM, Nosanchuk JD, et al. Nitric oxide-releasing nanoparticles accelerate wound healing by promoting fibroblast migration and collagen deposition. Am J Pathol. 2012;180:1465-73.

[105] Martinez LR, Han G, Chacko M, Mihu MR, Jacobson M, Gialanella P, et al. Antimicrobial and healing efficacy of sustained release nitric oxide nanoparticles against Staphylococcus aureus skin infection. J Invest Dermatol. 2009;129:2463-9.

[106] Blecher K, Martinez LR, Tuckman-Vernon C, Nacharaju P, Schairer D, Chouake J, et al. Nitric oxide-releasing nanoparticles accelerate wound healing in NOD-SCID mice. Nanomedicine. 2012;8:1364-71.

[107] Gainza G, Pastor M, Aguirre JJ, Villullas S, Pedraz JL, Hernandez RM, et al. A novel strategy for the treatment of chronic wounds based on the topical administration of rhEGF-

loaded lipid nanoparticles: In vitro bioactivity and in vivo effectiveness in healing-impaired db/db mice. J Control Release. 2014;185:51-61.

[108] Chen FM, Zhang M, Wu ZF. Toward delivery of multiple growth factors in tissue engineering. Biomaterials. 2010;31:6279-308.

[109] Xie Z, Paras CB, Weng H, Punnakitikashem P, Su LC, Vu K, et al. Dual growth factor releasing multi-functional nanofibers for wound healing. Acta Biomater. 2013;9:9351-9.

[110] Lai HJ, Kuan CH, Wu HC, Tsai JC, Chen TM, Hsieh DJ, et al. Tailored design of electrospun composite nanofibers with staged release of multiple angiogenic growth factors for chronic wound healing. Acta Biomater. 2014.

[111] Huang S, Deng T, Wu H, Chen F, Jin Y. Wound dressings containing bFGF-impregnated microspheres. J Microencapsul. 2006;23:277-90.

[112] Jiang W, Wang H, Jin F, Yu C, Chu D, Wang L, et al. Improved wound healing in pressure-induced decubitus ulcer with controlled release of basic fibroblast growth factor. J Alloy Compd. 2008;459:508-14.

[113] Adhirajan N, Shanmugasundaram N, Shanmuganathan S, Babu M. Functionally modified gelatin microspheres impregnated collagen scaffold as novel wound dressing to attenuate the proteases and bacterial growth. Eur J Pharm Sci. 2009;36:235-45.

[114] Adhirajan N, Shanmugasundaram N, Shanmuganathan S, Babu M. Collagen-based wound dressing for doxycycline delivery: in-vivo evaluation in an infected excisional wound model in rats. J Pharm Pharmacol. 2009;61:1617-23.

[115] Kawai K, Suzuki S, Tabata Y, Nishimura Y. Accelerated wound healing through the incorporation of basic fibroblast growth factor-impregnated gelatin microspheres into artificial dermis using a pressure-induced decubitus ulcer model in genetically diabetic mice. Br J Plast Surg. 2005;58:1115-23.

[116] Ribeiro MP, Morgado PI, Miguel SP, Coutinho P, Correia IJ. Dextran-based hydrogel containing chitosan microparticles loaded with growth factors to be used in wound healing. Mater Sci Eng C. 2013;33:2958-66.

[117] Losi P, Briganti E, Errico C, Lisella A, Sanguinetti E, Chiellini F, et al. Fibrin-based scaffold incorporating VEGF- and bFGF-loaded nanoparticles stimulates wound healing in diabetic mice. Acta Biomater. 2013;9:7814-21.

[118] Huang Z, Lu M, Zhu G, Gao H, Xie L, Zhang X, et al. Acceleration of diabetic-wound healing with PEGylated rhaFGF in healing-impaired streptozocin diabetic rats. Wound Repair Regen. 2011;19:633-44.

[119] Choi JK, Jang JH, Jang WH, Kim J, Bae IH, Bae J, et al. The effect of epidermal growth factor (EGF) conjugated with low-molecular-weight protamine (LMWP) on wound healing of the skin. Biomaterials. 2012;33:8579-90.

[120] Lee JH, Bae IH, Choi JK, Park JW. Evaluation of a highly skin permeable low-molecular-weight protamine conjugated epidermal growth factor for novel burn wound healing therapy. J Pharm Sci. 2013;102:4109-20.

[121] Uebersax L, Merkle HP, Meinel L. Biopolymer-based growth factor delivery for tissue repair: from natural concepts to engineered systems. Tissue Eng Part B Rev. 2009;15:263-89.

[122] Schultz GS, Wysocki A. Interactions between extracellular matrix and growth factors in wound healing. Wound Repair Regen. 2009;17:153-62.

[123] Martino MM, Tortelli F, Mochizuki M, Traub S, Ben-David D, Kuhn GA, et al. Engineering the growth factor microenvironment with fibronectin domains to promote wound and bone tissue healing. Sci Transl Med. 2011;3:100ra89.

[124] Tortelli F, Pisano M, Briquez PS, Martino MM, Hubbell JA. Fibronectin binding modulates CXCL11 activity and facilitates wound healing. PLoS One. 2013;8:e79610.

[125] Hyde C, Hollier B, Anderson A, Harkin D, Upton Z. Insulin-like growth factors (IGF) and IGF-binding proteins bound to vitronectin enhance keratinocyte protein synthesis and migration. J Invest Dermatol. 2004;122:1198-206.

[126] Hollier B, Harkin DG, Leavesley D, Upton Z. Responses of keratinocytes to substrate-bound vitronectin: growth factor complexes. Exp Cell Res. 2005;305:221-32.

[127] Upton Z, Cuttle L, Noble A, Kempf M, Topping G, Malda J, et al. Vitronectin: growth factor complexes hold potential as a wound therapy approach. J Invest Dermatol. 2008;128:1535-44.

[128] Xie Y, Upton Z, Richards S, Rizzi SC, Leavesley DI. Hyaluronic acid: Evaluation as a potential delivery vehicle for vitronectin:growth factor complexes in wound healing applications. J Control Release. 2011.

[129] Upton Z, Wallace HJ, Shooter GK, van Lonkhuyzen DR, Yeoh-Ellerton S, Rayment EA, et al. Human pilot studies reveal the potential of a vitronectin: growth factor complex as a treatment for chronic wounds. Int Wound J. 2011;8:522-32.

[130] Hardwicke J, Ferguson EL, Moseley R, Stephens P, Thomas DW, Duncan R. Dextrin-rhEGF conjugates as bioresponsive nanomedicines for wound repair. J Control Release. 2008;130:275-83.

[131] Hardwicke J, Moseley R, Stephens P, Harding K, Duncan R, Thomas DW. Bioresponsive dextrin-rhEGF conjugates: in vitro evaluation in models relevant to its proposed use as a treatment for chronic wounds. Mol Pharm. 2010;7:699-707.

[132] Hardwicke JT, Hart J, Bell A, Duncan R, Thomas DW, Moseley R. The effect of dextrin-rhEGF on the healing of full-thickness, excisional wounds in the (db/db) diabetic mouse. J Control Release. 2011;152:411-7.

[133] Li Y, Lee PI. Controlled nitric oxide delivery platform based on S-nitrosothiol conjugated interpolymer complexes for diabetic wound healing. Mol Pharm. 2010;7:254-66.

[134] Overbeek JTG, Voorn MJ. Phase separation in polyelectrolyte solutions. Theory of complex coacervation. J Cell Compar Physl. 1957;49:7-26.

[135] De Kruif CG, Weinbreck F, De Vries R. Complex coacervation of proteins and anionic polysaccharides. Curr Opin Colloid In. 2004;9:340–9.

[136] Lee KW, Johnson NR, Gao J, Wang Y. Human progenitor cell recruitment via SDF-1α coacervate-laden PGS vascular grafts. Biomaterials. 2013;34:9877-85.

[137] Johnson NR, Wang Y. Coacervate delivery systems for proteins and small molecule drugs. Expert Opin Drug Deliv. 2014:1-4.

[138] MacEwan SR, Chilkoti A. Elastin-like polypeptides: biomedical applications of tunable biopolymers. Biopolymers. 2010;94:60-77.

[139] Koria P, Yagi H, Kitagawa Y, Megeed Z, Nahmias Y, Sheridan R, et al. Self-assembling elastin-like peptides growth factor chimeric nanoparticles for the treatment of chronic wounds. Proc Natl Acad Sci U S A. 2011;108:1034-9.

[140] Johnson NR, Ambe T, Wang Y. Lysine-based polycation:heparin coacervate for controlled protein delivery. Acta Biomater. 2014;10:40-6.

[141] Johnson NR, Wang Y. Controlled delivery of heparin-binding EGF-like growth factor yields fast and comprehensive wound healing. J Control Release. 2013;166:124-9.

[142] Pack DW, Hoffman AS, Pun S, Stayton PS. Design and development of polymers for gene delivery. Nat Rev Drug Discov. 2005;4:581-93.

[143] McClements DJ, Li Y. Structured emulsion-based delivery systems: Controlling the digestion and release of lipophilic food components. Adv Colloid Interfac. 2010;159:213-28.

[144] Urry DW. Physical chemistry of biological free energy transduction as demonstrated by elastic protein-based polymers. J Phys Chem B. 1997;101:11007-28.

[145] Urry DW, Luan CH, Parker TM, Gowda DC, Prasad KU, Reid MC, et al. Temperature of Polypeptide Inverse Temperature Transition Depends on Mean Residue Hydrophobicity. J Am Chem Soc. 1991;113:4346-8.

[146] McDaniel JR, Callahan DJ, Chilkoti A. Drug delivery to solid tumors by elastin-like polypeptides. Adv Drug Deliv Rev. 2010;62:1456-67.

[147] Liu WG, McDaniel J, Li XH, Asai D, Quiroz FG, Schaal J, et al. Brachytherapy Using Injectable Seeds That Are Self-Assembled from Genetically Encoded Polypeptides In Situ. Cancer Res. 2012;72:5956-65.

[148] Meyer DE, Kong GA, Dewhirst MW, Zalutsky MR, Chilkoti A. Targeting a genetically engineered elastin-like polypeptide to solid tumors by local hyperthermia. Cancer Res. 2001;61:1548-54.

[149] Dreher MR, Liu W, Michelich CR, Dewhirst MW, Chilkoti A. Thermal cycling enhances the accumulation of a temperature-sensitive biopolymer in solid tumors. Cancer Res. 2007;67:4418-24.

[150] Betre H, Ong SR, Guilak F, Chilkoti A, Fermor B, Setton LA. Chondrocytic differentiation of human adipose-derived adult stem cells in elastin-like polypeptide. Biomaterials. 2006;27:91-9.

[151] Betre H, Setton LA, Meyer DE, Chilkoti A. Characterization of a genetically engineered elastin-like polypeptide for cartilaginous tissue repair. Biomacromolecules. 2002;3:910-6.

[152] Feng C, Wang Z, Jiang C, Kong M, Zhou X, Li Y, et al. Chitosan/o-carboxymethyl chitosan nanoparticles for efficient and safe oral anticancer drug delivery: in vitro and in vivo evaluation. Int J Pharm. 2013;457:158-67.

[153] Feng C, Song R, Sun G, Kong M, Bao Z, Li Y, et al. Immobilization of coacervate microcapsules in multilayer sodium alginate beads for efficient oral anticancer drug delivery. Biomacromolecules. 2014;15:985-96.

[154] Lee BP, Messersmith PB, Israelachvili JN, Waite JH. Mussel-Inspired Adhesives and Coatings. Annu Rev Mater Res. 2011;41:99-132.

[155] Lim S, Choi YS, Kang DG, Song YH, Cha HJ. The adhesive properties of coacervated recombinant hybrid mussel adhesive proteins. Biomaterials. 2010;31:3715-22.

[156] Hwang DS, Waite JH, Tirrell M. Promotion of osteoblast proliferation on complex coacervation-based hyaluronic acid - recombinant mussel adhesive protein coatings on titanium. Biomaterials. 2010;31:1080-4.

[157] Ori A, Wilkinson MC, Fernig DG. A systems biology approach for the investigation of the heparin/heparan sulfate interactome. J Biol Chem. 2011;286:19892-904.

[158] Chu H, Gao J, Wang Y. Design, synthesis, and biocompatibility of an arginine-based polyester. Biotechnol Prog. 2012;28:257-64.

[159] Zern BJ, Chu HH, Osunkoya AO, Gao J, Wang YD. A Biocompatible Arginine-Based Polycation. Adv Func Mater. 2011;21:434-40.

[160] Chu H, Chen CW, Huard J, Wang Y. The effect of a heparin-based coacervate of fibroblast growth factor-2 on scarring in the infarcted myocardium. Biomaterials. 2013;34:1747-56.

[161] Marikovsky M, Vogt P, Eriksson E, Rubin JS, Taylor WG, Joachim S, et al. Wound fluid-derived heparin-binding EGF-like growth factor (HB-EGF) is synergistic with insulin-like growth factor-I for Balb/MK keratinocyte proliferation. J Invest Dermatol. 1996;106:616-21.

[162] Stoll SW, Rittie L, Johnson JL, Elder JT. Heparin-binding EGF-like growth factor promotes epithelial-mesenchymal transition in human keratinocytes. J Invest Dermatol. 2012;132:2148-57.

[163] Kusano KF, Pola R, Murayama T, Curry C, Kawamoto A, Iwakura A, et al. Sonic hedgehog myocardial gene therapy: tissue repair through transient reconstitution of embryonic signaling. Nat Med. 2005;11:1197-204.

[164] Pola R, Ling LE, Silver M, Corbley MJ, Kearney M, Blake Pepinsky R, et al. The morphogen Sonic hedgehog is an indirect angiogenic agent upregulating two families of angiogenic growth factors. Nat Med. 2001;7:706-11.

[165] Ahmed RP, Haider KH, Shujia J, Afzal MR, Ashraf M. Sonic Hedgehog gene delivery to the rodent heart promotes angiogenesis via iNOS/netrin-1/PKC pathway. PLoS One. 2010;5:e8576.

[166] Johnson NR, Wang Y. Controlled delivery of sonic hedgehog morphogen and its potential for cardiac repair. PLoS One. 2013;8:e63075.

[167] Gao X, Usas A, Lu A, Tang Y, Wang B, Chen C, et al. BMP2 is superior to BMP4 for promoting human muscle derived-stem cell mediated bone regeneration in a critical size calvarial defect model. Cell Transplant. 2012.

[168] Valentin-Opran A, Wozney J, Csimma C, Lilly L, Riedel GE. Clinical evaluation of recombinant human bone morphogenetic protein-2. Clin Orthop Relat Res. 2002:110-20.

[169] Li H, Johnson NR, Usas A, Lu A, Poddar M, Wang Y, et al. Sustained release of bone morphogenetic protein 2 via coacervate improves the osteogenic potential of muscle-derived stem cells. Stem Cells Transl Med. 2013;2:667-77.

[170] Go AS, Mozaffarian D, Roger VL, Benjamin EJ, Berry JD, Blaha MJ, et al. Heart disease and stroke statistics--2014 update: a report from the American Heart Association. Circulation. 2014;129:e28-e292.

[171] Burg KJ, Porter S, Kellam JF. Biomaterial developments for bone tissue engineering. Biomaterials. 2000;21:2347-59.

[172] Godbey WT, Wu KK, Mikos AG. Poly(ethylenimine) and its role in gene delivery. J Control Release. 1999;60:149-60.

[173] Agnihotri SA, Mallikarjuna NN, Aminabhavi TM. Recent advances on chitosan-based micro- and nanoparticles in drug delivery. J Control Release. 2004;100:5-28.

[174] Ahn CH, Chae SY, Bae YH, Kim SW. Biodegradable poly(ethylenimine) for plasmid DNA delivery. J Control Release. 2002;80:273-82.

[175] Borchard G. Chitosans for gene delivery. Adv Drug Deliv Rev. 2001;52:145-50.

[176] Illum L, Jabbal-Gill I, Hinchcliffe M, Fisher AN, Davis SS. Chitosan as a novel nasal delivery system for vaccines. Adv Drug Del Rev. 2001;51:81-96.

[177] van der Lubben IM, Verhoef JC, Borchard G, Junginger HE. Chitosan and its derivatives in mucosal drug and vaccine delivery. Eur J Pharm Sci. 2001;14:201-7.

[178] Illum L, Farraj NF, Davis SS. Chitosan as a novel nasal delivery system for peptide drugs. Pharm Res. 1994;11:1186-9.

[179] Garcia-Fuentes M, Alonso MJ. Chitosan-based drug nanocarriers: where do we stand? J Control Release. 2012;161:496-504.

[180] Kean T, Thanou M. Biodegradation, biodistribution and toxicity of chitosan. Adv Drug Del Rev. 2010;62:3-11.

[181] Lv H, Zhang S, Wang B, Cui S, Yan J. Toxicity of cationic lipids and cationic polymers in gene delivery. J Control Release. 2006;114:100-9.

[182] Moghimi SM, Symonds P, Murray JC, Hunter AC, Debska G, Szewczyk A. A two-stage poly(ethylenimine)-mediated cytotoxicity: implications for gene transfer/therapy. Mol Ther. 2005;11:990-5.

[183] De Smedt SC, Demeester J, Hennink WE. Cationic polymer based gene delivery systems. Pharm Res. 2000;17:113-26.

[184] Choi YH, Liu F, Kim JS, Choi YK, Park JS, Kim SW. Polyethylene glycol-grafted poly-L-lysine as polymeric gene carrier. J Control Release. 1998;54:39-48.

[185] Trubetskoy VS, Torchilin VP, Kennel SJ, Huang L. Use of N-terminal modified poly(L-lysine)-antibody conjugate as a carrier for targeted gene delivery in mouse lung endothelial cells. Bioconjugate chemistry. 1992;3:323-7.

[186] Fischer D, Li Y, Ahlemeyer B, Krieglstein J, Kissel T. In vitro cytotoxicity testing of polycations: influence of polymer structure on cell viability and hemolysis. Biomaterials. 2003;24:1121-31.

[187] Hong S, Leroueil P, Janus E, Peters J, Kober M-M, Islam M, et al. Interaction of polycationic polymers with supported lipid bilayers and cells: nanoscale hole formation and enhanced membrane permeability. Bioconjugate chemistry. 2006;17:728-34.

[188] Gao J, Crapo PM, Wang Y. Macroporous elastomeric scaffolds with extensive micropores for soft tissue engineering. Tissue Eng Part A. 2006;12:917-25.

[189] Fischer D, Li Y, Ahlemeyer B, Krieglstein J, Kissel T. In vitro cytotoxicity testing of polycations: influence of polymer structure on cell viability and hemolysis. Biomaterials. 2003;24:1121-31.

[190] Boussif O, Lezoualc'h F, Zanta MA, Mergny MD, Scherman D, Demeneix B, et al. A versatile vector for gene and oligonucleotide transfer into cells in culture and in vivo: polyethylenimine. Proc Natl Acad Sci U S A. 1995;92:7297-301.

[191] Moreau E, Domurado M, Chapon P, Vert M, Domurad D. Biocompatibility of polycations: in vitro agglutination and lysis of red blood cells and in vivo toxicity. J Drug Target. 2002;10:161-73.

[192] Vancha AR, Govindaraju S, Parsa KV, Jasti M, Gonzalez-Garcia M, Ballestero RP. Use of polyethyleneimine polymer in cell culture as attachment factor and lipofection enhancer. BMC Biotechnol. 2004;4:23.

[193] Nguyen HK, Lemieux P, Vinogradov SV, Gebhart CL, Guerin N, Paradis G, et al. Evaluation of polyether-polyethyleneimine graft copolymers as gene transfer agents. Gene Ther. 2000;7:126-38.

[194] Fromm JR, Hileman RE, Caldwell EE, Weiler JM, Linhardt RJ. Pattern and spacing of basic amino acids in heparin binding sites. Arch Biochem Biophys. 1997;343:92-100.

[195] Lee MK, Lander AD. Analysis of affinity and structural selectivity in the binding of proteins to glycosaminoglycans: development of a sensitive electrophoretic approach. Proc Natl Acad Sci U S A. 1991;88:2768-72.

[196] Franz MG, Robson MC, Steed DL, Barbul A, Brem H, Cooper DM, et al. Guidelines to aid healing of acute wounds by decreasing impediments of healing. Wound repair and regeneration : official publication of the Wound Healing Society [and] the European Tissue Repair Society. 2008;16:723-48.

[197] Fonder MA, Lazarus GS, Cowan DA, Aronson-Cook B, Kohli AR, Mamelak AJ. Treating the chronic wound: A practical approach to the care of nonhealing wounds and wound care dressings. J Am Acad Dermatol. 2008;58:185-206.

[198] Barrientos S, Stojadinovic O, Golinko MS, Brem H, Tomic-Canic M. Growth factors and cytokines in wound healing. Wound repair and regeneration : official publication of the Wound Healing Society [and] the European Tissue Repair Society. 2008;16:585-601.

[199] Behm B, Babilas P, Landthaler M, Schreml S. Cytokines, chemokines and growth factors in wound healing. J Eur Acad Dermatol Venereol. 2011;26:812-20.

[200] Goldman R. Growth factors and chronic wound healing: past, present, and future. Adv Skin Wound Care. 2004;17:24-35.

[201] Marikovsky M, Breuing K, Liu PY, Eriksson E, Higashiyama S, Farber P, et al. Appearance of heparin-binding EGF-like growth factor in wound fluid as a response to injury. Proc Natl Acad Sci U S A. 1993;90:3889-93.

[202] Stoll SW, Rittie L, Johnson JL, Elder JT. Heparin-Binding EGF-Like Growth Factor Promotes Epithelial-Mesenchymal Transition in Human Keratinocytes. J Invest Dermatol. 2012:*in press*.

[203] Shirakata Y, Kimura R, Nanba D, Iwamoto R, Tokumaru S, Morimoto C, et al. Heparin-binding EGF-like growth factor accelerates keratinocyte migration and skin wound healing. J Cell Sci. 2005;118:2363-70.

[204] Hashimoto K, Higashiyama S, Asada H, Hashimura E, Kobayashi T, Sudo K, et al. Heparin-binding epidermal growth factor-like growth factor is an autocrine growth factor for human keratinocytes. J Biol Chem. 1994;269:20060-6.

[205] Higashiyama S, Abraham JA, Miller J, Fiddes JC, Klagsbrun M. A heparin-binding growth factor secreted by macrophage-like cells that is related to EGF. Science. 1991;251:936-9.

[206] Mehta VB, Zhou Y, Radulescu A, Besner GE. HB-EGF stimulates eNOS expression and nitric oxide production and promotes eNOS dependent angiogenesis. Growth Factors. 2008;26:301-15.

[207] Abramovitch R, Neeman M, Reich R, Stein I, Keshet E, Abraham J, et al. Intercellular communication between vascular smooth muscle and endothelial cells mediated by heparin-binding epidermal growth factor-like growth factor and vascular endothelial growth factor. FEBS Lett. 1998;425:441-7.

[208] Chen RR, Mooney DJ. Polymeric growth factor delivery strategies for tissue engineering. Pharm Res. 2003;20:1103-12.

[209] Schultz GS, Wysocki A. Interactions between extracellular matrix and growth factors in wound healing. Wound Repair Regen. 2009;17:153-62.

[210] Hynes RO. The extracellular matrix: not just pretty fibrils. Science. 2009;326:1216-9.

[211] Chu H, Gao J, Chen CW, Huard J, Wang Y. Injectable fibroblast growth factor-2 coacervate for persistent angiogenesis. Proceedings of the National Academy of Sciences of the United States of America. 2011;108:13444-9.

[212] Chu H, Gao J, Wang Y. Design, synthesis, and biocompatibility of an arginine-based polyester. Biotechnol Prog. 2012;28:257-64.

[213] Chu H, Johnson NR, Mason NS, Wang Y. A [polycation:heparin] complex releases growth factors with enhanced bioactivity. Journal of controlled release : official journal of the Controlled Release Society. 2011;150:157-63.

[214] Cribbs RK, Harding PA, Luquette MH, Besner GE. Endogenous production of heparin-binding EGF-like growth factor during murine partial-thickness burn wound healing. J Burn Care Rehabil. 2002;23:116-25.

[215] Scholzen T, Gerdes J. The Ki-67 protein: from the known and the unknown. J Cell Physiol. 2000;182:311-22.

[216] Sehgal BU, DeBiase PJ, Matzno S, Chew TL, Claiborne JN, Hopkinson SB, et al. Integrin beta4 regulates migratory behavior of keratinocytes by determining laminin-332 organization. J Biol Chem. 2006;281:35487-98.

[217] Nikolopoulos SN, Blaikie P, Yoshioka T, Guo W, Puri C, Tacchetti C, et al. Targeted deletion of the integrin beta4 signaling domain suppresses laminin-5-dependent nuclear entry of mitogen-activated protein kinases and NF-kappaB, causing defects in epidermal growth and migration. Mol Cell Biol. 2005;25:6090-102.

[218] Russell AJ, Fincher EF, Millman L, Smith R, Vela V, Waterman EA, et al. Alpha 6 beta 4 integrin regulates keratinocyte chemotaxis through differential GTPase activation and antagonism of alpha 3 beta 1 integrin. J Cell Sci. 2003;116:3543-56.

[219] Buckley A, Davidson JM, Kamerath CD, Wolt TB, Woodward SC. Sustained release of epidermal growth factor accelerates wound repair. Proc Natl Acad Sci U S A. 1985;82:7340-4.

[220] Draye JP, Delaey B, Van de Voorde A, Van Den Bulcke A, Bogdanov B, Schacht E. In vitro release characteristics of bioactive molecules from dextran dialdehyde cross-linked gelatin hydrogel films. Biomaterials. 1998;19:99-107.

[221] Cribbs RK, Luquette MH, Besner GE. Acceleration of partial-thickness burn wound healing with topical application of heparin-binding EGF-like growth factor (HB-EGF). J Burn Care Rehabil. 1998;19:95-101.

[222] Ulubayram K, Nur Cakar A, Korkusuz P, Ertan C, Hasirci N. EGF containing gelatin-based wound dressings. Biomaterials. 2001;22:1345-56.

[223] Hardwicke J, Schmaljohann D, Boyce D, Thomas D. Epidermal growth factor therapy and wound healing--past, present and future perspectives. Surgeon. 2008;6:172-7.

[224] Matsumoto Y, Kuroyanagi Y. Development of a wound dressing composed of hyaluronic acid sponge containing arginine and epidermal growth factor. J Biomater Sci Polym Ed. 2010;21:715-26.

[225] Yang CH. Evaluation of the release rate of bioactive recombinant human epidermal growth factor from crosslinking collagen sponges. J Mater Sci-Mater M. 2008;19:1433-40.

[226] Xie Y, Upton Z, Richards S, Rizzi SC, Leavesley DI. Hyaluronic acid: Evaluation as a potential delivery vehicle for vitronectin:growth factor complexes in wound healing applications. J Control Release. 2011;153:225-32.

[227] Lutolf MP, Hubbell JA. Synthetic biomaterials as instructive extracellular microenvironments for morphogenesis in tissue engineering. Nat Biotechnol. 2005;23:47-55.

[228] Mohammadi M, Olsen SK, Goetz R. A protein canyon in the FGF-FGF receptor dimer selects from an a la carte menu of heparan sulfate motifs. Curr Opin Struct Biol. 2005;15:506-16.

[229] Shi Y, Massague J. Mechanisms of TGF-beta signaling from cell membrane to the nucleus. Cell. 2003;113:685-700.

[230] Falanga V, Eaglstein WH. The "trap" hypothesis of venous ulceration. Lancet. 1993;341:1006-8.

[231] Zcharia E, Zilka R, Yaar A, Yacoby-Zeevi O, Zetser A, Metzger S, et al. Heparanase accelerates wound angiogenesis and wound healing in mouse and rat models. Faseb J. 2005;19:211-21.

[232] Sakiyama-Elbert SE, Hubbell JA. Development of fibrin derivatives for controlled release of heparin-binding growth factors. Journal of controlled release : official journal of the Controlled Release Society. 2000;65:389-402.

[233] Rajangam K, Behanna HA, Hui MJ, Han X, Hulvat JF, Lomasney JW, et al. Heparin binding nanostructures to promote growth of blood vessels. Nano letters. 2006;6:2086-90.

[234] Princz MA, Sheardown H. Heparin-modified dendrimer crosslinked collagen matrices for the delivery of heparin-binding epidermal growth factor. J BIOMED MATER RES-A. 2012;100:1929-37.

[235] Zern BJ, Chu H, Wang Y. Control growth factor release using a self-assembled [polycation:heparin] complex. PLoS One. 2010;5:e11017.

[236] Galiano RD, Michaels Jt, Dobryansky M, Levine JP, Gurtner GC. Quantitative and reproducible murine model of excisional wound healing. Wound Repair Regen. 2004;12:485-92.

[237] Singer AJ, Clark RA. Cutaneous wound healing. N Engl J Med. 1999;341:738-46.

[238] Monaco JL, Lawrence WT. Acute wound healing an overview. Clin Plast Surg. 2003;30:1-12.

[239] Werner S, Krieg T, Smola H. Keratinocyte-fibroblast interactions in wound healing. The Journal of investigative dermatology. 2007;127:998-1008.

[240] Ongusaha PP, Kwak JC, Zwible AJ, Macip S, Higashiyama S, Taniguchi N, et al. HB-EGF is a potent inducer of tumor growth and angiogenesis. Cancer Res. 2004;64:5283-90.

[241] Guariguata L, Whiting DR, Hambleton I, Beagley J, Linnenkamp U, Shaw JE. Global estimates of diabetes prevalence for 2013 and projections for 2035 for the IDF Diabetes Atlas. Diabetes Res Clin Pract. 2013.

[242] Frykberg RG, Zgonis T, Armstrong DG, Driver VR, Giurini JM, Kravitz SR, et al. Diabetic foot disorders. A clinical practice guideline (2006 revision). J Foot Ankle Surg. 2006;45:S1-66.

[243] Reiber GE, Lipsky BA, Gibbons GW. The burden of diabetic foot ulcers. Am J Surg. 1998;176:5S-10S.

[244] Tayalia P, Mooney DJ. Controlled growth factor delivery for tissue engineering. Adv Materials. 2009;21:3269-85.

[245] Mast BA, Schultz GS. Interactions of cytokines, growth factors, and proteases in acute and chronic wounds. Wound Repair Regen. 1996;4:411-20.

[246] Kajanne R, Miettinen P, Mehlem A, Leivonen SK, Birrer M, Foschi M, et al. EGF-R regulates MMP function in fibroblasts through MAPK and AP-1 pathways. J Cell Physiol. 2007;212:489-97.

[247] Aviezer D, Yayon A. Heparin-dependent binding and autophosphorylation of epidermal growth factor (EGF) receptor by heparin-binding EGF-like growth factor but not by EGF. Proc Natl Acad Sci U S A. 1994;91:12173-7.

[248] Iwamoto R, Mine N, Kawaguchi T, Minami S, Saeki K, Mekada E. HB-EGF function in cardiac valve development requires interaction with heparan sulfate proteoglycans. Development. 2010;137:2205-14.

[249] Chu H, Gao J, Wang Y. Design, synthesis, and biocompatibility of an arginine-based polyester. Biotechnology Prog. 2012;28:257-64.

[250] Fang RC, Kryger ZB, Buck DW, 2nd, De la Garza M, Galiano RD, Mustoe TA. Limitations of the db/db mouse in translational wound healing research: Is the NONcNZO10 polygenic mouse model superior? Wound Repair Regen. 2010;18:605-13.

[251] Leiter EH, Strobel M, O'Neill A, Schultz D, Schile A, Reifsnyder PC. Comparison of Two New Mouse Models of Polygenic Type 2 Diabetes at the Jackson Laboratory, NONcNZO10Lt/J and TALLYHO/JngJ. J Diabetes Res. 2013;2013:165327.

[252] Cho Y-R, Kim H-J, Park S-Y, Ko H, Hong E-G, Higashimori T, et al. Hyperglycemia, maturity-onset obesity, and insulin resistance in NONcNZO10/LtJ males, a new mouse model of type 2 diabetes. Am J Physiol Endocrinol Metab. 2007;293:36.

[253] Santoro MM, Gaudino G. Cellular and molecular facets of keratinocyte reepithelization during wound healing. Exp Cell Res. 2005;304:274-86.

[254] Scholzen T, Gerdes J. The Ki-67 protein: from the known and the unknown. J Cell Physiol. 2000;182:311-22.

[255] Brem H, Sheehan P, Rosenberg HJ, Schneider JS, Boulton AJ. Evidence-based protocol for diabetic foot ulcers. Plast Reconstr Surg. 2006;117:193S-209S; discussion 10S-11S.

[256] Smiell JM, Wieman TJ, Steed DL, Perry BH, Sampson AR, Schwab BH. Efficacy and safety of becaplermin (recombinant human platelet-derived growth factor-BB) in patients with

nonhealing, lower extremity diabetic ulcers: a combined analysis of four randomized studies. Wound Repair Regen. 1999;7:335-46.

[257] Papanas N, Maltezos E. Benefit-risk assessment of becaplermin in the treatment of diabetic foot ulcers. Drug Saf. 2010;33:455-61.

[258] Papanas N, Maltezos E. Becaplermin gel in the treatment of diabetic neuropathic foot ulcers. Clin Interv Aging. 2008;3:233-40.

[259] Feng J, Mehta VB, El-Assal ON, Wu D, Besner GE. Tissue distribution and plasma clearance of heparin-binding EGF-like growth factor (HB-EGF) in adult and newborn rats. Peptides. 2006;27:1589-96.

[260] Bernfield M, Gotte M, Park PW, Reizes O, Fitzgerald ML, Lincecum J, et al. Functions of cell surface heparan sulfate proteoglycans. Annu Rev Biochem. 1999;68:729-77.

[261] Sakiyama-Elbert SE. Incorporation of heparin into biomaterials. Acta Biomater. 2013;10:1581-7.

[262] Feyzi E, Lustig F, Fager G, Spillmann D, Lindahl U, Salmivirta M. Characterization of heparin and heparan sulfate domains binding to the long splice variant of platelet-derived growth factor A chain. J Biol Chem. 1997;272:5518-24.

[263] Guimond S, Maccarana M, Olwin BB, Lindahl U, Rapraeger AC. Activating and inhibitory heparin sequences for FGF-2 (basic FGF). Distinct requirements for FGF-1, FGF-2, and FGF-4. J Biol Chem. 1993;268:23906-14.

[264] Stringer SE, Gallagher JT. Specific binding of the chemokine platelet factor 4 to heparan sulfate. J Biol Chem. 1997;272:20508-14.

[265] Rajangam K, Arnold MS, Rocco MA, Stupp SI. Peptide amphiphile nanostructure-heparin interactions and their relationship to bioactivity. Biomaterials. 2008;29:3298-305.

[266] Trousdale RK, Jacobs S, Simhaee DA, Wu JK, Lustbader JW. Wound closure and metabolic parameter variability in a db/db mouse model for diabetic ulcers. J Surg Res. 2009;151:100-7.

[267] Falanga V. Wound healing and its impairment in the diabetic foot. Lancet. 2005;366:1736-43.

[268] Tonnesen MG, Feng X, Clark RA. Angiogenesis in wound healing. J Invest Derm Symp Proc. 2000;5:40-6.

[269] Higashiyama S, Abraham JA, Klagsbrun M. Heparin-binding EGF-like growth factor stimulation of smooth muscle cell migration: dependence on interactions with cell surface heparan sulfate. J Cell Biol. 1993;122:933-40.

[270] Mehta VB, Besner GE. HB-EGF promotes angiogenesis in endothelial cells via PI3-kinase and MAPK signaling pathways. Growth Factors. 2007;25:253-63.

[271] Murray CJ, Lopez AD. Measuring the global burden of disease. N Engl J Med. 2013;369:448-57.

[272] Roger VL, Go AS, Lloyd-Jones DM, Benjamin EJ, Berry JD, Borden WB, et al. Heart disease and stroke statistics--2012 update: a report from the American Heart Association. Circulation. 2012;125:e2-e220.

[273] Houser SR, Margulies KB, Murphy AM, Spinale FG, Francis GS, Prabhu SD, et al. Animal models of heart failure: a scientific statement from the American Heart Association. Circ Res. 2012;111:131-50.

[274] Yusen RD, Edwards LB, Kucheryavaya AY, Benden C, Dipchand AI, Dobbels F, et al. The registry of the International Society for Heart and Lung Transplantation: thirty-first adult lung and heart-lung transplant report--2014; focus theme: retransplantation. J Heart Lung Transplant. 2014;33:1009-24.

[275] Radisic M, Christman KL. Materials science and tissue engineering: repairing the heart. Mayo Clinic proceedings. 2013;88:884-98.

[276] Nelson DM, Ma Z, Fujimoto KL, Hashizume R, Wagner WR. Intra-myocardial biomaterial injection therapy in the treatment of heart failure: Materials, outcomes and challenges. Acta Biomater. 2011;7:1-15.

[277] Radhakrishnan J, Krishnan UM, Sethuraman S. Hydrogel based injectable scaffolds for cardiac tissue regeneration. Biotechnology advances. 2014.

[278] Malliaras K, Makkar RR, Smith RR, Cheng K, Wu E, Bonow RO, et al. Intracoronary Cardiosphere-Derived Cells After Myocardial Infarction: Evidence of Therapeutic Regeneration in the Final 1-Year Results of the CADUCEUS Trial (CArdiosphere-Derived aUtologous stem CElls to reverse ventricUlar dySfunction). J Am Coll Cardiol. 2014;63:110-22.

[279] Chugh AR, Beache GM, Loughran JH, Mewton N, Elmore JB, Kajstura J, et al. Administration of cardiac stem cells in patients with ischemic cardiomyopathy: the SCIPIO trial: surgical aspects and interim analysis of myocardial function and viability by magnetic resonance. Circulation. 2012;126:S54-64.

[280] Hamshere S, Choudhury T, Jones DA, Locca D, Mills P, Rothman M, et al. A randomised double-blind control study of early intracoronary autologous bone marrow cell infusion in acute myocardial infarction (REGENERATE-AMI). BMJ Open. 2014;4:e004258.

[281] Suncion VY, Ghersin E, Fishman J, Zambrano JP, Karantalis V, Mandel NS, et al. Does Transendocardial Injection of Mesenchymal Stem Cells Improve Myocardial Function Locally or Globally? An Analysis From the POSEIDON Randomized Trial. Circ Res. 2014.

[282] Simons M, Annex BH, Laham RJ, Kleiman N, Henry T, Dauerman H, et al. Pharmacological treatment of coronary artery disease with recombinant fibroblast growth factor-2: double-blind, randomized, controlled clinical trial. Circulation. 2002;105:788-93.

[283] Losordo DW, Vale PR, Hendel RC, Milliken CE, Fortuin FD, Cummings N, et al. Phase 1/2 placebo-controlled, double-blind, dose-escalating trial of myocardial vascular endothelial growth factor 2 gene transfer by catheter delivery in patients with chronic myocardial ischemia. Circulation. 2002;105:2012-8.

[284] Chachques JC, Trainini JC, Lago N, Cortes-Morichetti M, Schussler O, Carpentier A. Myocardial Assistance by Grafting a New Bioartificial Upgraded Myocardium (MAGNUM trial): clinical feasibility study. Ann Thorac Surg. 2008;85:901-8.

[285] Gupta R, Tongers J, Losordo DW. Human studies of angiogenic gene therapy. Circ Res. 2009;105:724-36.

[286] Charrier JB, Lapointe F, Le Douarin NM, Teillet MA. Anti-apoptotic role of Sonic hedgehog protein at the early stages of nervous system organogenesis. Development. 2001;128:4011-20.

[287] Ingham PW, McMahon AP. Hedgehog signaling in animal development: paradigms and principles. Genes Dev. 2001;15:3059-87.

[288] Pola R, Ling LE, Aprahamian TR, Barban E, Bosch-Marce M, Curry C, et al. Postnatal recapitulation of embryonic hedgehog pathway in response to skeletal muscle ischemia. Circulation. 2003;108:479-85.

[289] Soonpaa MH, Field LJ. Survey of studies examining mammalian cardiomyocyte DNA synthesis. Circ Res. 1998;83:15-26.

[290] Lavine KJ, Ornitz DM. Fibroblast growth factors and Hedgehogs: at the heart of the epicardial signaling center. Trends Genet. 2008;24:33-40.

[291] Porrello ER, Mahmoud AI, Simpson E, Hill JA, Richardson JA, Olson EN, et al. Transient regenerative potential of the neonatal mouse heart. Science. 2011;331:1078-80.

[292] Kicheva A, Bollenbach T, Wartlick O, Julicher F, Gonzalez-Gaitan M. Investigating the principles of morphogen gradient formation: from tissues to cells. asdf. 2012;22:527-32.

[293] Roncalli J, Renault MA, Tongers J, Misener S, Thorne T, Kamide C, et al. Sonic hedgehog-induced functional recovery after myocardial infarction is enhanced by AMD3100-mediated progenitor-cell mobilization. J Am Coll Cardiol. 2011;57:2444-52.

[294] Oro AE, Higgins KM, Hu Z, Bonifas JM, Epstein EH, Jr., Scott MP. Basal cell carcinomas in mice overexpressing sonic hedgehog. Science. 1997;276:817-21.

[295] Tirelli N, Lutolf MP, Napoli A, Hubbell JA. Poly(ethylene glycol) block copolymers. J Biotechnol. 2002;90:3-15.

[296] Dobner S, Bezuidenhout D, Govender P, Zilla P, Davies N. A synthetic non-degradable polyethylene glycol hydrogel retards adverse post-infarct left ventricular remodeling. Journal of cardiac failure. 2009;15:629-36.

[297] Kadner K, Dobner S, Franz T, Bezuidenhout D, Sirry MS, Zilla P, et al. The beneficial effects of deferred delivery on the efficiency of hydrogel therapy post myocardial infarction. Biomaterials. 2012;33:2060-6.

[298] de Waal Malefyt R, Abrams J, Bennett B, Figdor CG, de Vries JE. Interleukin 10(IL-10) inhibits cytokine synthesis by human monocytes: an autoregulatory role of IL-10 produced by monocytes. J Exp Med. 1991;174:1209-20.

[299] Popi AF, Lopes JD, Mariano M. Interleukin-10 secreted by B-1 cells modulates the phagocytic activity of murine macrophages in vitro. Immunology. 2004;113:348-54.

[300] Deng B, Wehling-Henricks M, Villalta SA, Wang Y, Tidball JG. IL-10 triggers changes in macrophage phenotype that promote muscle growth and regeneration. J Immunol. 2012;189:3669-80.

[301] Sato T, Kameyama T, Noto T, Nakadate T, Ueno H, Yamada K, et al. The impact of anti-inflammatory cytokines provoked by CD163 positive macrophages on ventricular functional recovery after myocardial infarction. Journal of thrombosis and thrombolysis. 2013.

[302] Krishnamurthy P, Rajasingh J, Lambers E, Qin G, Losordo DW, Kishore R. IL-10 inhibits inflammation and attenuates left ventricular remodeling after myocardial infarction via activation of STAT3 and suppression of HuR. Circ Res. 2009;104:e9-18.

[303] Salek-Ardakani S, Arrand JR, Shaw D, Mackett M. Heparin and heparan sulfate bind interleukin-10 and modulate its activity. Blood. 2000;96:1879-88.

[304] Pfeffer MA, Pfeffer JM, Fishbein MC, Fletcher PJ, Spadaro J, Kloner RA, et al. Myocardial infarct size and ventricular function in rats. Circ Res. 1979;44:503-12.

[305] Aikawa R, Komuro I, Yamazaki T, Zou Y, Kudoh S, Tanaka M, et al. Oxidative stress activates extracellular signal-regulated kinases through Src and Ras in cultured cardiac myocytes of neonatal rats. J Clin Invest. 1997;100:1813-21.

[306] Ries C, Egea V, Karow M, Kolb H, Jochum M, Neth P. MMP-2, MT1-MMP, and TIMP-2 are essential for the invasive capacity of human mesenchymal stem cells: differential regulation by inflammatory cytokines. Blood. 2007;109:4055-63.

[307] Menasche P. Cardiac cell therapy: lessons from clinical trials. Journal of molecular and cellular cardiology. 2011;50:258-65.

[308] Swynghedauw B. Molecular mechanisms of myocardial remodeling. Physiol Rev. 1999;79:215-62.

[309] Asai J, Takenaka H, Kusano KF, Ii M, Luedemann C, Curry C, et al. Topical sonic hedgehog gene therapy accelerates wound healing in diabetes by enhancing endothelial progenitor cell-mediated microvascular remodeling. Circulation. 2006;113:2413-24.

[310] Kusano KF, Allendoerfer KL, Munger W, Pola R, Bosch-Marce M, Kirchmair R, et al. Sonic hedgehog induces arteriogenesis in diabetic vasa nervorum and restores function in diabetic neuropathy. Arterioscler Thromb Vasc Biol. 2004;24:2102-7.

[311] Fu JR, Liu WL, Zhou JF, Sun HY, Xu HZ, Luo L, et al. Sonic hedgehog protein promotes bone marrow-derived endothelial progenitor cell proliferation, migration and VEGF production via PI 3-kinase/Akt signaling pathways. Acta Pharmacol Sin. 2006;27:685-93.

[312] Palladino M, Gatto I, Neri V, Straino S, Silver M, Tritarelli A, et al. Pleiotropic beneficial effects of sonic hedgehog gene therapy in an experimental model of peripheral limb ischemia. Mol Ther. 2011;19:658-66.

[313] Renault MA, Roncalli J, Tongers J, Thorne T, Klyachko E, Misener S, et al. Sonic hedgehog induces angiogenesis via Rho kinase-dependent signaling in endothelial cells. Journal of molecular and cellular cardiology. 2010;49:490-8.

[314] Chinchilla P, Xiao L, Kazanietz MG, Riobo NA. Hedgehog proteins activate pro-angiogenic responses in endothelial cells through non-canonical signaling pathways. Cell Cycle. 2010;9:570-79.

[315] Nakamura K, Sasajima J, Mizukami Y, Sugiyama Y, Yamazaki M, Fujii R, et al. Hedgehog promotes neovascularization in pancreatic cancers by regulating Ang-1 and IGF-1 expression in bone-marrow derived pro-angiogenic cells. PLoS One. 2010;5:e8824.

[316] Kajstura J, Fiordaliso F, Andreoli AM, Li B, Chimenti S, Medow MS, et al. IGF-1 overexpression inhibits the development of diabetic cardiomyopathy and angiotensin II-mediated oxidative stress. Diabetes. 2001;50:1414-24.

[317] Welch S, Plank D, Witt S, Glascock B, Schaefer E, Chimenti S, et al. Cardiac-specific IGF-1 expression attenuates dilated cardiomyopathy in tropomodulin-overexpressing transgenic mice. Circ Res. 2002;90:641-8.

[318] Soleti R, Lauret E, Andriantsitohaina R, Carmen Martinez M. Internalization and induction of antioxidant messages by microvesicles contribute to the antiapoptotic effects on human endothelial cells. Free Radic Biol Med. 2012;53:2159-70.

[319] Wang Z, Zhang H, Xu X, Shi H, Yu X, Wang X, et al. bFGF inhibits ER stress induced by ischemic oxidative injury via activation of the PI3K/Akt and ERK1/2 pathways. Toxicol Lett. 2012;212:137-46.

[320] Mark RJ, Keller JN, Kruman I, Mattson MP. Basic FGF attenuates amyloid beta-peptide-induced oxidative stress, mitochondrial dysfunction, and impairment of Na+/K+-ATPase activity in hippocampal neurons. Brain Res. 1997;756:205-14.

[321] Jiang ZS, Srisakuldee W, Soulet F, Bouche G, Kardami E. Non-angiogenic FGF-2 protects the ischemic heart from injury, in the presence or absence of reperfusion. Cardiovasc Res. 2004;62:154-66.

[322] Chu H, Gao J, Chen CW, Huard J, Wang Y. Injectable fibroblast growth factor-2 coacervate for persistent angiogenesis. Proc Natl Acad Sci USA. 2011;108:13444-9.

[323] Ceradini DJ, Kulkarni AR, Callaghan MJ, Tepper OM, Bastidas N, Kleinman ME, et al. Progenitor cell trafficking is regulated by hypoxic gradients through HIF-1 induction of SDF-1. Nat Med. 2004;10:858-64.

[324] Kucia M, Dawn B, Hunt G, Guo Y, Wysoczynski M, Majka M, et al. Cells expressing early cardiac markers reside in the bone marrow and are mobilized into the peripheral blood after myocardial infarction. Circ Res. 2004;95:1191-9.

[325] Dong F, Harvey J, Finan A, Weber K, Agarwal U, Penn MS. Myocardial CXCR4 expression is required for mesenchymal stem cell mediated repair following acute myocardial infarction. Circulation. 2012;126:314-24.

[326] Unzek S, Zhang M, Mal N, Mills WR, Laurita KR, Penn MS. SDF-1 recruits cardiac stem cell-like cells that depolarize in vivo. Cell Transplant. 2007;16:879-86.

[327] Yamaguchi J, Kusano KF, Masuo O, Kawamoto A, Silver M, Murasawa S, et al. Stromal cell-derived factor-1 effects on ex vivo expanded endothelial progenitor cell recruitment for ischemic neovascularization. Circulation. 2003;107:1322-8.

[328] Zernecke A, Schober A, Bot I, von Hundelshausen P, Liehn EA, Mopps B, et al. SDF-1alpha/CXCR4 axis is instrumental in neointimal hyperplasia and recruitment of smooth muscle progenitor cells. Circ Res. 2005;96:784-91.

[329] Cencioni C, Capogrossi MC, Napolitano M. The SDF-1/CXCR4 axis in stem cell preconditioning. Cardiovasc Res. 2012;94:400-7.

[330] Chang H, Li Q, Moraes RC, Lewis MT, Hamel PA. Activation of Erk by sonic hedgehog independent of canonical hedgehog signalling. Int J Biochem Cell Biol. 2010;42:1462-71.

[331] Lin X. Functions of heparan sulfate proteoglycans in cell signaling during development. Development. 2004;131:6009-21.

[332] Ornitz DM. FGFs, heparan sulfate and FGFRs: complex interactions essential for development. Bioessays. 2000;22:108-12.

[333] Hacker U, Nybakken K, Perrimon N. Heparan sulphate proteoglycans: the sweet side of development. Nat Rev Mol Cell Biol. 2005;6:530-41.

[334] Gritli-Linde A, Lewis P, McMahon AP, Linde A. The whereabouts of a morphogen: direct evidence for short- and graded long-range activity of hedgehog signaling peptides. Dev Biol. 2001;236:364-86.

[335] Chang SC, Mulloy B, Magee AI, Couchman JR. Two distinct sites in sonic Hedgehog combine for heparan sulfate interactions and cell signaling functions. J Biol Chem. 2011;286:44391-402.

[336] Van de Putte KA, Urist MR. Osteogenesis in the interior of intramuscular implants of decalcified bone matrix. Clin Orthop Relat Res. 1965;43:257-70.

[337] Volek-Smith H, Urist MR. Recombinant human bone morphogenetic protein (rhBMP) induced heterotopic bone development in vivo and in vitro. Proc Soc Exp Biol Med. 1996;211:265-72.

[338] Mastrogiacomo M, Derubeis AR, Cancedda R. Bone and cartilage formation by skeletal muscle derived cells. J Cell Physiol. 2005;204:594-603.

[339] Levy MM, Joyner CJ, Virdi AS, Reed A, Triffitt JT, Simpson AH, et al. Osteoprogenitor cells of mature human skeletal muscle tissue: an in vitro study. Bone. 2001;29:317-22.

[340] Bosch P, Musgrave DS, Lee JY, Cummins J, Shuler T, Ghivizzani TC, et al. Osteoprogenitor cells within skeletal muscle. J Orthop Res. 2000;18:933-44.

[341] Asakura A, Komaki M, Rudnicki M. Muscle satellite cells are multipotential stem cells that exhibit myogenic, osteogenic, and adipogenic differentiation. Differentiation. 2001;68:245-53.

[342] Tajbakhsh S, Rocancourt D, Buckingham M. Muscle progenitor cells failing to respond to positional cues adopt non-myogenic fates in myf-5 null mice. Nature. 1996;384:266-70.

[343] Deasy BM, Jankowski RJ, Huard J. Muscle-derived stem cells: characterization and potential for cell-mediated therapy. Blood Cells Mol Dis. 2001;27:924-33.

[344] Qu-Petersen Z, Deasy B, Jankowski R, Ikezawa M, Cummins J, Pruchnic R, et al. Identification of a novel population of muscle stem cells in mice: potential for muscle regeneration. J Cell Biol. 2002;157:851-64.

[345] Gharaibeh B, Lu A, Tebbets J, Zheng B, Feduska J, Crisan M, et al. Isolation of a slowly adhering cell fraction containing stem cells from murine skeletal muscle by the preplate technique. Nat Protoc. 2008;3:1501-9.

[346] Lee JY, Qu-Petersen Z, Cao B, Kimura S, Jankowski R, Cummins J, et al. Clonal isolation of muscle-derived cells capable of enhancing muscle regeneration and bone healing. J Cell Biol. 2000;150:1085-100.

[347] Zheng B, Cao B, Crisan M, Sun B, Li G, Logar A, et al. Prospective identification of myogenic endothelial cells in human skeletal muscle. Nat Biotechnol. 2007;25:1025-34.

[348] Affolder T, Akimoto H, Akopian A, Albrow MG, Amaral P, Amendolia SR, et al. Production of chi(c1) and chi(c2) in pp collisions at sqrt[S] = 1.8 TeV. Phys Rev Lett. 2001;86:3963-8.

[349] Wright V, Peng H, Usas A, Young B, Gearhart B, Cummins J, et al. BMP4-expressing muscle-derived stem cells differentiate into osteogenic lineage and improve bone healing in immunocompetent mice. Mol Ther. 2002;6:169-78.

[350] Oshima H, Payne TR, Urish KL, Sakai T, Ling Y, Gharaibeh B, et al. Differential myocardial infarct repair with muscle stem cells compared to myoblasts. Mol Ther. 2005;12:1130-41.

[351] Matsumoto T, Cooper GM, Gharaibeh B, Meszaros LB, Li G, Usas A, et al. Cartilage repair in a rat model of osteoarthritis through intraarticular transplantation of muscle-derived stem cells expressing bone morphogenetic protein 4 and soluble Flt-1. Arthritis Rheum. 2009;60:1390-405.

[352] Gates CB, Karthikeyan T, Fu F, Huard J. Regenerative medicine for the musculoskeletal system based on muscle-derived stem cells. J Am Acad Orthop Surg. 2008;16:68-76.

[353] Shen HC, Peng H, Usas A, Gearhart B, Cummins J, Fu FH, et al. Ex vivo gene therapy-induced endochondral bone formation: comparison of muscle-derived stem cells and different subpopulations of primary muscle-derived cells. Bone. 2004;34:982-92.

[354] Musgrave DS, Bosch P, Lee JY, Pelinkovic D, Ghivizzani SC, Whalen J, et al. Ex vivo gene therapy to produce bone using different cell types. Clin Orthop Relat Res. 2000:290-305.

[355] Kuroda R, Usas A, Kubo S, Corsi K, Peng H, Rose T, et al. Cartilage repair using bone morphogenetic protein 4 and muscle-derived stem cells. Arthritis Rheum. 2006;54:433-42.

[356] Usas A, Ho AM, Cooper GM, Olshanski A, Peng H, Huard J. Bone regeneration mediated by BMP4-expressing muscle-derived stem cells is affected by delivery system. Tissue Eng Part A. 2009;15:285-93.

[357] Zhao B, Katagiri T, Toyoda H, Takada T, Yanai T, Fukuda T, et al. Heparin potentiates the in vivo ectopic bone formation induced by bone morphogenetic protein-2. J Biol Chem. 2006;281:23246-53.

[358] Jeon O, Song SJ, Kang SW, Putnam AJ, Kim BS. Enhancement of ectopic bone formation by bone morphogenetic protein-2 released from a heparin-conjugated poly(L-lactic-co-glycolic acid) scaffold. Biomaterials. 2007;28:2763-71.

[359] Johnson NR, Wang Y. Controlled Delivery of Heparin-Binding EGF-Like Growth Factor Yields Fast and Comprehensive Wound Healing. J Control Release. 2012.

[360] Peng H, Usas A, Gearhart B, Young B, Olshanski A, Huard J. Development of a self-inactivating tet-on retroviral vector expressing bone morphogenetic protein 4 to achieve regulated bone formation. Mol Ther. 2004;9:885-94.

[361] Li H, Ogle H, Jiang B, Hagar M, Li B. Cefazolin embedded biodegradable polypeptide nanofilms promising for infection prevention: a preliminary study on cell responses. J Orthop Res. 2010;28:992-9.

[362] Katagiri T, Yamaguchi A, Komaki M, Abe E, Takahashi N, Ikeda T, et al. Bone morphogenetic protein-2 converts the differentiation pathway of C2C12 myoblasts into the osteoblast lineage. J Cell Biol. 1994;127:1755-66.

[363] Jiao X, Billings PC, O'Connell MP, Kaplan FS, Shore EM, Glaser DL. Heparan sulfate proteoglycans (HSPGs) modulate BMP2 osteogenic bioactivity in C2C12 cells. J Biol Chem. 2007;282:1080-6.

[364] Zhou H, Qian J, Wang J, Yao W, Liu C, Chen J, et al. Enhanced bioactivity of bone morphogenetic protein-2 with low dose of 2-N, 6-O-sulfated chitosan in vitro and in vivo. Biomaterials. 2009;30:1715-24.

[365] Urish KL, Vella JB, Okada M, Deasy BM, Tobita K, Keller BB, et al. Antioxidant levels represent a major determinant in the regenerative capacity of muscle stem cells. Mol Biol Cell. 2009;20:509-20.

[366] Kruyt MC, de Bruijn JD, Wilson CE, Oner FC, van Blitterswijk CA, Verbout AJ, et al. Viable osteogenic cells are obligatory for tissue-engineered ectopic bone formation in goats. Tissue Eng. 2003;9:327-36.

[367] Kruyt MC, Wilson CE, de Bruijn JD, van Blitterswijk CA, Oner CF, Verbout AJ, et al. The effect of cell-based bone tissue engineering in a goat transverse process model. Biomaterials. 2006;27:5099-106.

[368] Friess W, Uludag H, Foskett S, Biron R, Sargeant C. Characterization of absorbable collagen sponges as recombinant human bone morphogenetic protein-2 carriers. Int J Pharm. 1999;185:51-60.

[369] Martinek V, Latterman C, Usas A, Abramowitch S, Woo SL, Fu FH, et al. Enhancement of tendon-bone integration of anterior cruciate ligament grafts with bone morphogenetic protein-2 gene transfer: a histological and biomechanical study. J Bone Joint Surg Am. 2002;84-A:1123-31.

[370] Lieberman JR, Daluiski A, Einhorn TA. The role of growth factors in the repair of bone. Biology and clinical applications. J Bone Joint Surg Am. 2002;84-A:1032-44.

[371] Takahashi Y, Yamamoto M, Tabata Y. Enhanced osteoinduction by controlled release of bone morphogenetic protein-2 from biodegradable sponge composed of gelatin and beta-tricalcium phosphate. Biomaterials. 2005;26:4856-65.

[372] Helm GA, Sheehan JM, Sheehan JP, Jane JA, Jr., diPierro CG, Simmons NE, et al. Utilization of type I collagen gel, demineralized bone matrix, and bone morphogenetic protein-2 to enhance autologous bone lumbar spinal fusion. J Neurosurg. 1997;86:93-100.

[373] Yang XB, Whitaker MJ, Sebald W, Clarke N, Howdle SM, Shakesheff KM, et al. Human osteoprogenitor bone formation using encapsulated bone morphogenetic protein 2 in porous polymer scaffolds. Tissue engineering. 2004;10:1037-45.

[374] Noshi T, Yoshikawa T, Ikeuchi M, Dohi Y, Ohgushi H, Horiuchi K, et al. Enhancement of the in vivo osteogenic potential of marrow/hydroxyapatite composites by bovine bone morphogenetic protein. J Biomed Mater Res. 2000;52:621-30.

[375] Arnander C, Westermark A, Veltheim R, Docherty-Skogh AC, Hilborn J, Engstrand T. Three-dimensional technology and bone morphogenetic protein in frontal bone reconstruction. J Craniofac Surg. 2006;17:275-9.

[376] Villavicencio AT, Burneikiene S, Nelson EL, Bulsara KR, Favors M, Thramann J. Safety of transforaminal lumbar interbody fusion and intervertebral recombinant human bone morphogenetic protein-2. J Neurosurg Spine. 2005;3:436-43.

[377] Kanayama M, Hashimoto T, Shigenobu K, Yamane S, Bauer TW, Togawa D. A prospective randomized study of posterolateral lumbar fusion using osteogenic protein-1 (OP-1) versus local autograft with ceramic bone substitute: emphasis of surgical exploration and histologic assessment. Spine (Phila Pa 1976). 2006;31:1067-74.

[378] Chen RR, Mooney DJ. Polymeric growth factor delivery strategies for tissue engineering. Pharm Res. 2003;20:1103-12.

[379] Ruppert R, Hoffmann E, Sebald W. Human bone morphogenetic protein 2 contains a heparin-binding site which modifies its biological activity. Eur J Biochem. 1996;237:295-302.

[380] Shimasaki S, Zachow RJ, Li D, Kim H, Iemura S, Ueno N, et al. A functional bone morphogenetic protein system in the ovary. Proc Natl Acad Sci U S A. 1999;96:7282-7.

[381] Takada T, Katagiri T, Ifuku M, Morimura N, Kobayashi M, Hasegawa K, et al. Sulfated polysaccharides enhance the biological activities of bone morphogenetic proteins. J Biol Chem. 2003;278:43229-35.

[382] Pellegrini L. Role of heparan sulfate in fibroblast growth factor signalling: a structural view. Curr Opin Struct Biol. 2001;11:629-34.

[383] Higashiyama S, Abraham JA, Klagsbrun M. Heparin-binding EGF-like growth factor stimulation of smooth muscle cell migration: dependence on interactions with cell surface heparan sulfate. J Cell Biol. 1993;122:933-40.

[384] Friess W, Uludag H, Foskett S, Biron R, Sargeant C. Characterization of absorbable collagen sponges as rhBMP-2 carriers. Int J Pharm. 1999;187:91-9.

[385] Geiger M, Li RH, Friess W. Collagen sponges for bone regeneration with rhBMP-2. Adv Drug Deliv Rev. 2003;55:1613-29.

[386] Carlisle E, Fischgrund JS. Bone morphogenetic proteins for spinal fusion. Spine J. 2005;5:240S-9S.

[387] Gautschi OP, Frey SP, Zellweger R. Bone morphogenetic proteins in clinical applications. ANZ J Surg. 2007;77:626-31.

[388] Gupta MC, Maitra S. Bone grafts and bone morphogenetic proteins in spine fusion. Cell Tissue Bank. 2002;3:255-67.

[389] Robinson Y, Heyde CE, Tschoke SK, Mont MA, Seyler TM, Ulrich SD. Evidence supporting the use of bone morphogenetic proteins for spinal fusion surgery. Expert Rev Med Devices. 2008;5:75-84.

[390] Williams DF. Some Observations on the Role of Cellular Enzymes in the In-Vivo Degradation of Polymers. In: B.C. S, A. A, editors. Corrosion and Degradation of Implant Materials. Baltimore: American Society for Testing and Materials; 1979. p. 61-75.